Frontiers in Bioscience Landmark

Front. Biosci. (Landmark Ed) **2025**; 30(1): 25706
https://doi.org/10.31083/FBL25706

Original Research

Oxidative and Excitatory Neurotoxic Stresses in CRISPR/Cas9-Induced Kynurenine Aminotransferase Knockout Mice: A Novel Model for Despair-Based Depression and Post-Traumatic Stress Disorder

Ágnes Szabó[1,2], Zsolt Galla[3], Eleonóra Spekker[4], Mónika Szűcs[5], Diána Martos[4], Keiko Takeda[6], Kinuyo Ozaki[7], Hiromi Inoue[7], Sayo Yamamoto[7], József Toldi[8], Etsuro Ono[6,7], László Vécsei[1,4,*,†], Masaru Tanaka[4,*,†]

[1]Department of Neurology, Albert Szent-Györgyi Medical School, University of Szeged, H-6725 Szeged, Hungary
[2]Doctoral School of Clinical Medicine, University of Szeged, H-6720 Szeged, Hungary
[3]Department of Pediatrics, Albert Szent-Györgyi Faculty of Medicine, University of Szeged, H-6725 Szeged, Hungary
[4]HUN-REN-SZTE Neuroscience Research Group, Hungarian Research Network, University of Szeged (HUN-REN-SZTE), Danube Neuroscience Research Laboratory, H-6725 Szeged, Hungary
[5]Department of Medical Physics and Informatics, Albert Szent-Györgyi Medical School, Faculty of Science and Informatics, University of Szeged, H-6720 Szeged, Hungary
[6]Department of Biomedicine, Graduate School of Medical Sciences, Kyushu University, 812-8582 Fukuoka, Japan
[7]Center of Biomedical Research, Research Center for Human Disease Modeling, Graduate School of Medical Sciences, Kyushu University, 812-8582 Fukuoka, Japan
[8]Department of Physiology, Anatomy and Neuroscience, Faculty of Science and Informatics, University of Szeged, H-6726 Szeged, Hungary
*Correspondence: vecsei.laszlo@med.u-szeged.hu (László Vécsei); tanaka.masaru.1@med.u-szeged.hu (Masaru Tanaka)
†These authors contributed equally.

Academic Editor: Thomas Heinbockel
Submitted: 15 July 2024 Revised: 24 October 2024 Accepted: 18 November 2024 Published: 20 January 2025

Abstract

Backgrounds: Memory and emotion are especially vulnerable to psychiatric disorders such as post-traumatic stress disorder (PTSD), which is linked to disruptions in serotonin (5-HT) metabolism. Over 90% of the 5-HT precursor tryptophan (Trp) is metabolized via the Trp-kynurenine (KYN) metabolic pathway, which generates a variety of bioactive molecules. Dysregulation of KYN metabolism, particularly low levels of kynurenic acid (KYNA), appears to be linked to neuropsychiatric disorders. The majority of KYNA is produced by the *aadat* (kat2) gene-encoded mitochondrial kynurenine aminotransferase (KAT) isotype 2. Little is known about the consequences of deleting the KYN enzyme gene. **Methods**: In CRISPR/Cas9-induced *aadat* knockout (*kat2*$^{-/-}$) mice, we examined the effects on emotion, memory, motor function, Trp and its metabolite levels, enzyme activities in the plasma and urine of 8-week-old males compared to wild-type mice. **Results**: Transgenic mice showed more depressive-like behaviors in the forced swim test, but not in the tail suspension, anxiety, or memory tests. They also had fewer center field and corner entries, shorter walking distances, and fewer jumping counts in the open field test. Plasma metabolite levels are generally consistent with those of urine: antioxidant KYNs, 5-hydroxyindoleacetic acid, and indole-3-acetic acid levels were lower; enzyme activities in KATs, kynureninase, and monoamine oxidase/aldehyde dehydrogenase were lower, but kynurenine 3-monooxygenase was higher; and oxidative stress and excitotoxicity indices were higher. Transgenic mice displayed depression-like behavior in a learned helplessness model, emotional indifference, and motor deficits, coupled with a decrease in KYNA, a shift of Trp metabolism toward the KYN-3-hydroxykynurenine pathway, and a partial decrease in the gut microbial Trp-indole pathway metabolite. **Conclusions**: This is the first evidence that deleting the *aadat* gene induces depression-like behaviors uniquely linked to experiences of despair, which appear to be associated with excitatory neurotoxic and oxidative stresses. This may lead to the development of a double-hit preclinical model in despair-based depression, a better understanding of these complex conditions, and more effective therapeutic strategies by elucidating the relationship between Trp metabolism and PTSD pathogenesis.

Keywords: post-traumatic stress disorder (PTSD); depression; anxiety; tryptophan; kynurenine; microbiota; oxidative stress; transgenic mice; translational medical research; CRISPR/Cas9

1. Introduction

The interaction between memory and emotion involves a complex interplay of neural, cognitive, and physiological processes involving the amygdala, hippocampus, and prefrontal cortex [1–6]. Orderly function at multi-layered levels is essential to maintaining sound mental well-being [7–10]. The reciprocal interaction between cognitive function and affective states can significantly impact each other. Cognitive impairment can lead to affective disturbances, triggering emotional responses such as frustration, anxiety, and stress, particularly when individuals feel a loss of control over their cognitive abilities [11]. Similarly, emotional disturbances such as depression and anxiety can influence memory function, increasing vulnerability

to cognitive challenges [12–15]. This intricate bidirectional link between cognition and emotions can lead to changes in brain structure, function, behavior, lifestyle, and neurotransmitter systems [15–17]. Memory impairment and emotional disturbance are associated with a wide range of systematic diseases and neuropsychiatric disorders such as Alzheimer's disease (AD), Parkinson's disease, traumatic brain injury, major depressive disorder (MDD), and post-traumatic stress disorder (PTSD) [18–26].

The serotonergic nervous system plays an important role in regulating mood, anxiety, and cognition [27–30]. Serotonin (5-hydroxytryptamine, 5-HT) is involved in cognitive processes such as attention, learning, and memory [31–34]. Studies indicate that 5-HT enhances long-term memory consolidation and improves cognitive flexibility, which is the ability to switch between different cognitive tasks or mental sets [35–44]. 5-HT is implicated in regulating mood and anxiety, influencing cognitive function [45,46]. Mental illnesses like MDD, eating disorders, obsessive-compulsive disorder, schizophrenia (SCZ), and PTSD are associated with dysregulation of 5-HT [47–52]. Selective serotonin reuptake inhibitors (SSRIs) are commonly used for these conditions, targeting the serotonergic nervous system [53–55]. Furthermore, abnormalities in the serotonergic system also affect norepinephrine and dopamine [56–58].

The complex interplay of tryptophan (Trp)-kynurenine (KYN) and 5-HT metabolism is crucial for comprehending the pathogenesis of mental illnesses [59,60]. The Trp-KYN metabolic system, closely associated with 5-HT metabolism, plays a pivotal role in the production of prooxidants and antioxidants, regulation of the immune system, and the balance between neurotoxicity and neuroprotection [61,62]. Approximately 2% of L-Trp undergoes metabolism through the 5-HT metabolic pathway; however, over 90% of Trp is catabolized through the KYN route, which safely to say that it governs Trp metabolism (Fig. 1a,b, Ref. [63–83]) [84]. Various factors, including stress, inflammation, and the gut microbiome, influence this system [85–88]. Dysregulation of the KYN route has been linked to mental health conditions such as MDD, SCZ, and AD [89]. About 5% of dietary Trp is converted by gut bacteria, like *E. coli* and *Clostridium sporogenes*, into indole and its derivatives (e.g., indole-3-acetic acid, indoxyl sulfate) (Fig. 1c) [63,90–98]. Disruptions in this pathway are linked to gastrointestinal and liver conditions (e.g., colorectal cancer, irritable bowel syndrome, non-alcoholic fatty liver disease, hepatic encephalopathy) and affect brain neurotransmitters and communication via the vagus nerve [64,95,99–109]. The gut microbial indole pathway is increasingly recognized for its role in mental health disorders like depression, anxiety, autism, SCZ, and AD [103,110–116].

However, the understanding of the interplay between Trp-KYN, 5-HT, and indole metabolism in the pathogenesis of mental illnesses remains limited. Kynurenine aminotransferases (KATs) are members of the pyridoxal-5′-phosphate-dependent enzyme family involved in the KYN metabolic pathway. The KYN metabolism is responsible for the conversion of L-KYN to kynurenic acid (KYNA), an antioxidant and neuroprotective metabolite with implications for various central nervous system (CNS) diseases [73,117,118]. Among the KAT enzymes, kynurenine/alpha-aminoadipate aminotransferase (KAT/AadAT, aka KAT II) is a mitochondrial enzyme encoded in the gene *aadat* (*kat2*) [119]. KAT II is considered to play the most important role among the four isozymes in the cellular environment due to its highest enzymatic activity close to the physiological pH. Thus, KAT II plays a prominent role in KYNA production in the human brain and is considered a crucial target for managing CNS disorders [120].

Preclinical research has significantly contributed to our understanding of mental illnesses by elucidating the underlying pathomechanisms and identifying potential therapeutic targets [121–129]. Researchers have employed preclinical animal models to examine the causes and effects of mental disorders, thereby attaining a comprehensive understanding of their underlying pathology [130–137]. *In vitro* models, such as cell cultures and organoids, have facilitated the investigation of complex molecular pathways linked to mental disorders [138–141]. Animal models, along with other *in vivo* models, have been instrumental in studying the behavioral, cognitive, and physiological dimensions of mental disorders [142–148]. These models allow researchers to simulate disease conditions, assess symptomatology, and evaluate the efficacy of potential interventions [148,149]. Transgenic animals are vital in biomedical research, enabling the replication of human conditions through gene deletion or the introduction of altered genes into their genome [150]. These animals offer indispensable insights into human diseases, facilitating the exploration of disease mechanisms, experimentation with potential treatments, and assessment of therapeutic effectiveness [151–155]. Moreover, they offer crucial insights into changes in structure and imaging techniques in clinical cases [156–175]. Preclinical and clinical research collaboratively contribute to innovative therapeutics and personalized medicine [176–182].

This study involved manipulating the gene *kat2* in mice to create a knockout (*kat2*$^{-/-}$) model, allowing us to observe the behavioral consequences of KAT II deficiency. By focusing on negative valence in emotional domain, memory acquisition, and motor function, we aimed to gain insights into the role of KAT II in these specific behavioral domains in young adult *kat2*$^{-/-}$ mice. Furthermore, we assess the levels of Trp and its metabolites in three distinct metabolic pathways in both plasma and urine samples, the enzyme activities of Trp metabolism, and the oxidative stress and excitotoxicity indices of KYN metabolites, with

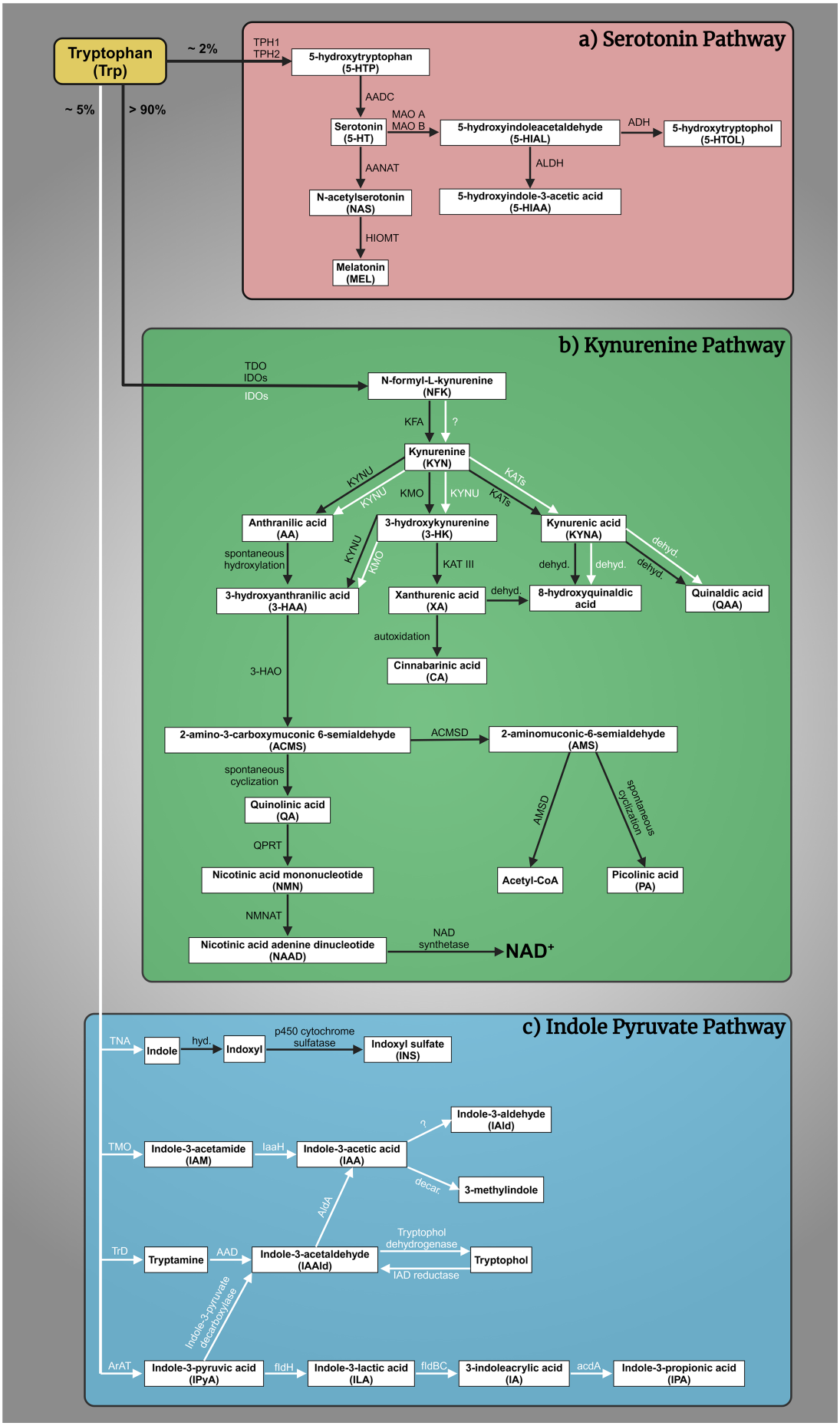
a) Serotonin Pathway
Tryptophan (Trp)
~ 2%
~ 5%
> 90%
TPH1
TPH2
5-hydroxytryptophan (5-HTP)
AADC
Serotonin (5-HT)
MAO A
MAO B
5-hydroxyindoleacetaldehyde (5-HIAL)
ADH
5-hydroxytryptophol (5-HTOL)
AANAT
ALDH
N-acetylserotonin (NAS)
5-hydroxyindole-3-acetic acid (5-HIAA)
HIOMT
Melatonin (MEL)
b) Kynurenine Pathway
TDO
IDOs
IDOs
N-formyl-L-kynurenine (NFK)
KFA
?
Kynurenine (KYN)
KYNU
KYNU
KMO
KYNU
KATs
KATs
Anthranilic acid (AA)
3-hydroxykynurenine (3-HK)
Kynurenic acid (KYNA)
dehyd.
spontaneous hydroxylation
KYNU
KMO
KAT III
dehyd.
dehyd.
dehyd.
3-hydroxyanthranilic acid (3-HAA)
Xanthurenic acid (XA)
dehyd.
8-hydroxyquinaldic acid
Quinaldic acid (QAA)
autoxidation
Cinnabarinic acid (CA)
3-HAO
2-amino-3-carboxymuconic 6-semialdehyde (ACMS)
ACMSD
2-aminomuconic-6-semialdehyde (AMS)
spontaneous cyclization
AMSD
spontaneous cyclization
Quinolinic acid (QA)
QPRT
Acetyl-CoA
Picolinic acid (PA)
Nicotinic acid mononucleotide (NMN)
NMNAT
Nicotinic acid adenine dinucleotide (NAAD)
NAD synthetase
NAD+
c) Indole Pyruvate Pathway
TNA
Indole
hyd.
Indoxyl
p450 cytochrome sulfatase
Indoxyl sulfate (INS)
?
Indole-3-aldehyde (IAld)
TMO
Indole-3-acetamide (IAM)
IaaH
Indole-3-acetic acid (IAA)
decar.
3-methylindole
AldA
TrD
Tryptamine
AAD
Indole-3-acetaldehyde (IAAld)
Tryptophol dehydrogenase
Tryptophol
IAD reductase
Indole-3-pyruvate decarboxylase
ArAT
Indole-3-pyruvic acid (IPyA)
fldH
Indole-3-lactic acid (ILA)
fldBC
3-indoleacrylic acid (IA)
acdA
Indole-3-propionic acid (IPA)

Fig. 1. Tryptophan (Trp) metabolism. (a) The serotonin (5-HT) pathway: A fraction exceeding 2% of L-Trp is metabolized within the 5-HT pathway. The rate-limiting enzyme tryptophan hydroxylase 1 and 2 (TPH1, TPH2) converts Trp to 5-hydroxytryptophan (5-HTP), which is then decarboxylated by aromatic L-amino acid decarboxylase (AADC) to 5-HT. 5-HT is oxidized by monoamine oxidase A and B (MAO A, MAO B) in different tissues to 5-hydroxyindoleacetaldehyde (5-HIAL), which is subsequently further oxidized to 5-hydroxyindoleacetic acid (5-HIAA) by aldehyde dehydrogenase (ALDH) or reduced to 5-hydroxytryptophol (5-HTOL) by alcohol dehydrogenase (ADH). 5-HIAA is the main metabolite and a marker of serotonergic activity, whereas 5-HTOL is a minor pathway of 5-HT degradation [65]. On the other hand, 5-HT synthetizes melatonin (MEL, N-acetyl-5-methoxytryptamine). First, 5-HT is converted into N-acetylserotonin (NAS) by arylalkylamine N-acetyltransferase (AANAT), then hydroxyindole-O-methyltransferase (HIOMT) transform MEL [66–69]. (b) The kynurenine (KYN) pathway: More than 90% of Trp enters the KYN pathway, which produces a variety of biomolecules. The primary metabolites include N-formyl-L-kynurenine (NFK), KYN, kynurenic acid (KYNA), anthranilic acid (AA), 3-hydroxykynurenine (3-HK), xanthurenic acid (XA), 3-hydroxyanthranilic acid (3-HAA), quinolinic acid (QA), picolinic acid (PA), and nicotinamide adenine dinucleotide (NAD^+). These metabolites are produced through the catalytic actions of various enzymes, namely tryptophan 2,3-dioxygenase (TDO), indoleamine 2,3-dioxygenases (IDOs), kynurenine formamidase (KFA), kynurenine 3-monooxygenase (KMO), kynurenine aminotransferases (KATs), kynureninase (KYNU), 3-hydroxyanthranilate oxidase (3-HAO), quinolinate phosphoribosyl transferase (QPRT) [70], nicotinamide mononucleotide adenylyltransferase (NMNAT) [71], NAD synthetase [72], amino-β-carboxymuconate-semialdehyde-decarboxylase (ACMSD) and 2-aminomuconic-6-semialdehyde dehydrogenase (AMSD) [73–75]. KYNA is subsequently metabolized by the gut microbiome to quinaldic acid (QAA) and 8-hydroxyquinaldic acid [76]. 8-hydroxyquinaldic acid can be dehydroxylated from XA [77,78]. (c) The gut microbial indole pyruvate pathway: The metabolism of Trp is accomplished through four distinct pathways, which include the indoxyl sulfate pathway, the indole-3-acetamide (IAM) pathway, the tryptamine pathway, and the indole-3-propionic acid (IPA) pathway. The pyridoxal phosphate-dependent tryptophanase (TNA) enzyme serves as the rate-limiting component of the indoxyl sulfate pathway. Its primary function is to facilitate the transformation of Trp into indole, which is passing through the gut epithelium, then hydroxylated into 3-hydroxyindole (indoxyl) and ultimately transformed into indoxyl sulfate (INS) by p450 cytochrome and sulfanate in the liver [79]. In the IAM pathway, tryptophan-2-monooxygenase (TMO) catalyzes the conversion of Trp to IAM. This is followed by the conversion of IAM to indole-3-acetic acid (IAA) by indole-3-acetamide hydrolase (IaaH), which can then be further metabolized into indole-3-aldehyde (IAld) or decarboxylized into 3-methylindole (skatole) [63,80]. Tryptophan decarboxylase (TrD) catalyzes the conversion of Trp to tryptamine by amino acid decarboxylase (AAD), which subsequently undergoes conversion into indole-3-acetaldehyde (IAAld) [81]. IAAld can be further converted into IAA by indole-3-acetaldehyde dehydrogenase (AldA). It is also worth noting that IAAld can be reversibly converted into indole-3-ethanol (tryptophol) by IAD reductase and tryptophol dehydrogenase [82]. The transformation of Trp into indole-3-pyruvic acid (IPyA) is catalyzed by aromatic amino acid aminotransferase (ArAT), resulting in the formation of either tryptamine, or indole-3-lactic acid (ILA) by phenyllactate dehydrogenase (fldH), then 3-indoleacrylic acid (IA) by phenyllactate dehydratase (fldBC), and ultimately IPA by acyl-coenzim A dehydrogenase (acdA) [64,82,83]. Black arrows: the host pathways, yellow arrows: the gut microbiome pathways. AA, anthranilic acid; acdA, acyl-coenzim A dehydrogenase; AAD, amino acid decarboxylase; AADC, aromatic L-amino acid decarboxylase; AANAT, arylalkylamine N-acetyltransferase; ACMSD, amino-β-carboxymuconate-semialdehyde-decarboxylase; ADH, alcohol dehydrogenase; AldA, indole-3-acetaldehyde dehydrogenase; ALDH, aldehyde dehydrogenase; AMSD, 2-aminomuconic-6-semialdehyde dehydrogenase; ArAT, aromatic amino acid aminotransferase; decar., decarboxylation; dehyd., dehydroxylation; fldBC, phenyllactate dehydratase; fldH, phenyllactate dehydrogenase; 3-HAA, 3-hydroxyanthranilic acid; 3-HAO, 3-hydroxyanthranilate oxidase; 5-HIAA, 5-hydroxyindoleacetic acid; 5-HIAL, 5-hydroxyindoleacetaldehyde; HIOMT, hydroxyindole-O-methyltransferase; 3-HK, 3-hydroxykynurenine; 5-HT, serotonin/5-hydroxytryptamine; 5-HTOL, 5-hydroxytryptophol; 5-HTP, 5-hydroxytryptophan; hyd., hydroxylation; IA, 3-indoleacrylic acid; IAA, indole-3-acetic acid; IaaH, indole-3-acetamide hydrolase; IAAld, indole -3-acetaldehyde; IAld, indole-3-aldehyde; IAA, indole-3-acetic acid; IAM, indole-3-acetamide; IDOs, indoleamine 2,3-dioxygenases 1 and 2; ILA, indole-3-lactic acid; INS, indoxyl sulfate; IPA, indole-3-propionate; IPyA, indole-3-pyruvic acid; KAT III, kynurenine aminotransferase III/cysteine conjugate beta-lyase 2; KATs, kynurenine aminotransferases; KFA, kynurenine formamidase; KMO, kynurenine 3-monooxygenase; KYN, kynurenine; KYNA, kynurenic acid; KYNU, kynureninase; MAO A, monoamine oxidase A; MAO B, monoamine oxidase B; MEL, melatonin/N-acetyl-5-methoxytryptamine; NAAD, nicotinic acid adenine dinucleotide; NAD^+, nicotinamide adenine dinucleotide; NAS, N-acetylserotonin; NFK, N-formyl-L-kynurenine; NMN, nicotinic acid mononucleotide; NMNAT, nicotinamide mononucleotide adenylyltransferase; PA, picolinic acid; QA, quinolinic acid; QAA, quinaldic acid; QPRT, quinolinate phosphoribosyl transferase; TDO, tryptophan-2,3-dioxygenase; TMO, tryptophan-2-monooxygenase; TNA, tryptophanase; TrD, tryptophan decarboxylase; Trp, tryptophan; TPH1/2, tryptophan hydroxylase 1 and 2; XA, xanthurenic acid; ?, unknown. The figure was created with Scientific Image and Illustration Software Biorender.

the aim of elucidating the Trp metabolic profiles that underlie the behavioral phenotype. This research contributes to our understanding of the genetic factors influencing behaviors related to emotional valence, memory, and motor function and Trp catabolism.

2. Materials and Methods

CRISPR/Cas9 was applied on C57BL/6N and CD1 (ICR; Institute for Cancer Reseach) mice to generate knockout *kat2*$^{-/-}$ mice, and Taqman allelic discrimination was used to prove that the gene had been deleted. The emotional domain, including depression-like and anxiety-like behaviors, was evaluated with the modified forced swim test (FST), tail suspension test (TST), elevated plus maze (EPM) test, open field (OF) test, and light dark box (LDB) test; the cognitive domain was evaluated with the passive avoidance test (PAT); and the motor domain was evaluated with the OF test. Furthermore, the levels of Trp and its major metabolites, as well as enzyme activities in plasma and urine samples, were determined, and oxidative stress and excitotoxicity indices were calculated.

2.1 Ethical Approval

Animal experiments were conducted humanely in accordance with the Regulations for Animal Experiments of Kyushu University and the Fundamental Guidelines for Proper Conduct of Animal Experiments and Related Activities in Academic Research Institutions governed by the Ministry of Education, Culture, Sports, Science, and Technology of Japan, and with the approval of the Institutional Animal Experiment Committees of Kyushu University (A29-338-1 (2018), A19-090-1 (2019)). The Department of Nature Conservation of the Ministry of Agriculture has authorized us to use genetically modified organisms in a closed system of the second security isolation level (TMF/43-20/2015). The import of genetically modified animals has been approved by the Department of Biodiversity and Gene Conservation of the Ministry of Agriculture (BGMF/37-5/2020). In accordance with the guidelines of the 8th Edition of the Guide for the Care and Use of Laboratory Animals, the Use of Animals in Research of the International Association for the Study of Pain, and the directive of the European Economic Community (2010/63/EU), the experiments conducted in this study received ethical approval from two committees. The Scientific Ethics Committee for Animal Research of the Protection of Animals Advisory Board (XI./95/2020, CS/I01/170-4/2022) and the Committee of Animal Research at the University of Szeged (I-74-10/2019, I-74-1/2022) both approved the experiments. Furthermore, Directive 2010/63/EU on the protection of animals used for scientific purposes provides guidance for the ethical evaluation of animal use proposals. The directive allows individual institutions to make determinations based on the recommendations of their ethical review committees. These ethical guidelines and regulations ensure that the experiments conducted on animals adhere to the highest standards of animal welfare and scientific integrity. The approval from the Scientific Ethics Committee for Animal Research of the Protection of Animals Advisory Board and the Committee of Animal Research at the University of Szeged demonstrates that the study was conducted in compliance with these ethical principles and regulations.

2.2 Animals

C57BL/6N and CD1 (ICR) mice were purchased from Japan SLC, Inc. (Hamamatsu, Japan) and Charles River Laboratories International, Inc. (Yokohama, Japan), respectively, in order to generate *kat2*$^{-/-}$ mice utilizing the CRISPR/Cas9 technique. After genetic modifications, breeding, and transport from Japan to Hungary, the animals were housed in groups of 4–5 in polycarbonate cages (530 cm^2 floor space) under pathogen-free conditions in the Animal House of the Department of Neurology, University of Szeged, maintained at 24 $\pm$ 1 °C and 45–55% relative humidity under a 12:12-h light:dark cycle. Throughout the duration of the investigation, mice had unrestricted access to standard rodent food and water.

The deletion was introduced into the KATs gene using the CRISPR/Cas9 method. The single guide RNAs (sgRNA) were selected using the CRISPRdirect software [183]. Artificially synthesized sgRNA were purchased from FASMAC (Atsugi, Japan). The 8–12 weeks old female C57BL/6N mice were injected with pregnant mare serum gonadotropin (PMSG) and human chorionic gonadotropin (hCG) with a 48-h interval, and mated with 8–20 weeks old male C57BL/6N mice. The fertilized one-cell embryos were collected from the oviducts. Then, 25 ng/µL of the sgRNA and 75 ng/µL Guide-it™ Recombinant Cas9 protein (TaKaRa, Kusatsu, Japan) were injected into the cytoplasm of these one-cell-stage embryos. The injected two-cell embryos were then transferred into pseudo-pregnant ICR mice (Fig. 2) anesthetized with a combination anesthetic (M/M/B: 0.3/4/5) [184] prepared with 0.3 mg/ kg of medetomidine, 4.0 mg/kg of midazolam, and 5.0 mg/kg of butorphanol by intraperitoneal injection.

The *kat2*$^{-/-}$ mouse line expresses a carboxy-terminal truncated polypeptide consisting of the first 47 amino acids of the intact KAT II with a 2-nucleotide deletion (CCDS nucleotide sequence 32–33) in the mRNA.

2.3 DNA Extraction and Sequencing

Genomic DNA of tails collected from mice was extracted using NucleoSpin Tissue (MACHEREY-NAGEL GmbH&Co, KG, Düren, Germany). Each targeted fragment around the sgRNA targeting site from the extracted genomic DNA as a part of the KATs genes was amplified with TAKARA Ex Taq (Takara Bio, Kusatsu, Japan) and the 1st primers pair and subsequently with 2nd primers pair (Table 1). The polymerase chain reaction (PCR) product was

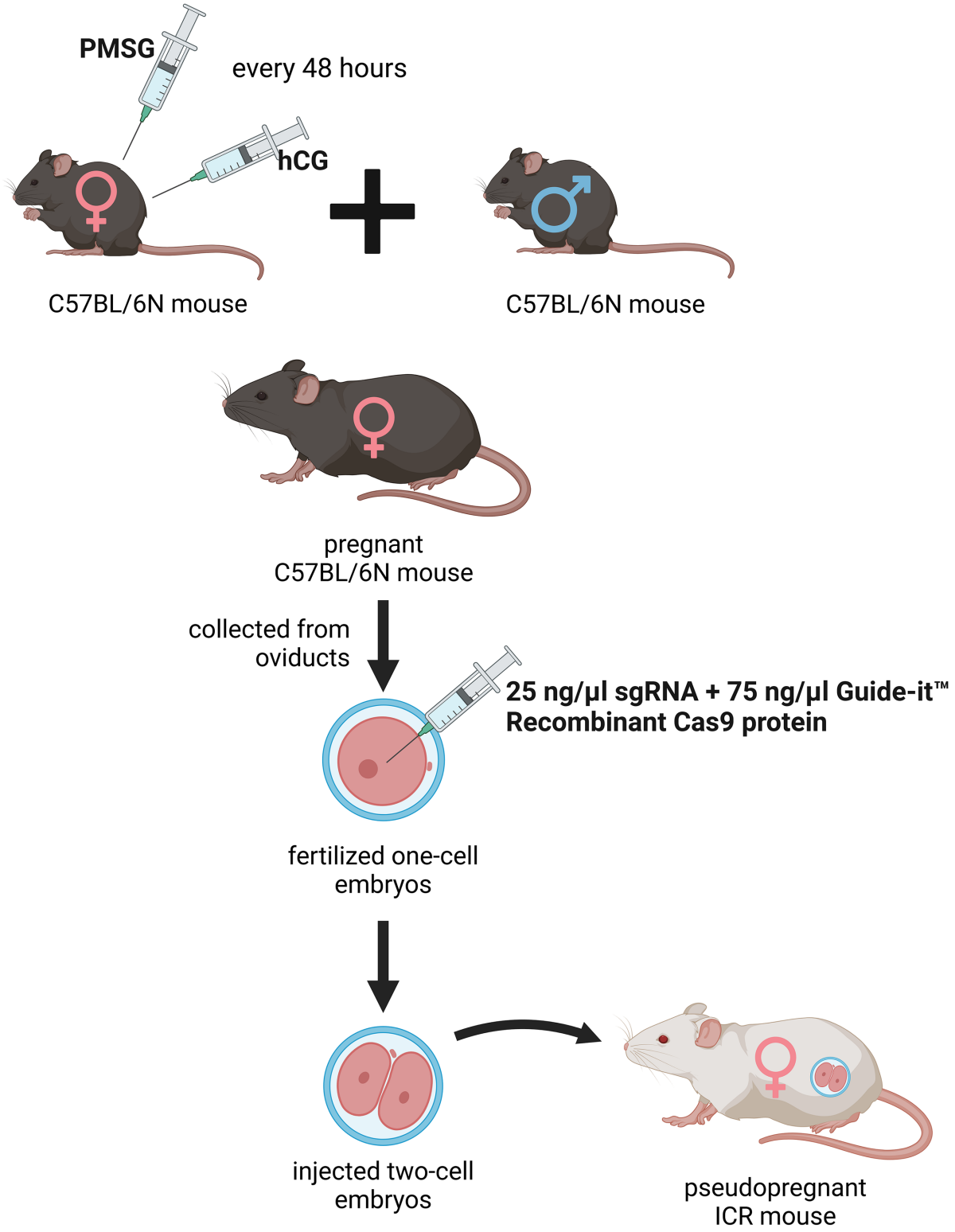

Fig. 2. Generation of the knockout *kat2*$^{-/-}$ mice. Female C57BL/6N mice were treated with pregnant mare serum gonadotropin (PMSG) and human chorionic gonadotropin (hCG) with a 48-hour interval between administrations, then mated with male C57BL/6N mice. From the oviducts, fertilized one-cell embryos were collected and injected with single guide RNA (sgRNA) and Guide-it^{TM} Recombinant Cas9 protein. At the two-cell stage, the embryos were transferred into pseudopregnant Institute for Cancer Research (ICR) mice. PMSG, pregnant mare serum gonadotropin; hCG, human chorionic gonadotropin; sgRNA, single guide RNA. The figure was created with Scientific Image and Illustration Software Biorender.

Table 1. Properties of sgRNA, primers and KAT gene.

Name of sgRNA	Sequence		
M-KAT II-2	GTTCCTCACTGCAACGAGCCguuuuagagcuagaaauagcaaguu-aaaaaaggcuaguccguuaucaacuugaaaaaguggcacggacucggugcuuuu		
Name of primer	Sequence		
M-KAT II_1st_F	CCCTCTGTGGATGGACTTTG		
M-KAT II_1st_R	TTGAAAGATGTGCCTCATGC		
M-KAT II_2nd_F	GGATGGACTTTGTCCCTTCT		
M-KAT II_2nd_R	ATGTGCCTCATGCTTGGCCC		
Name of KAT gene	Transcript ID	CCDS	CCDS Nucleotide Sequence
Aadat-201	ENSMUST00000079472.4	CCDS22320	32–33 (2 nucleotide deletion)

sgRNA, single guide RNA; KAT, kynurenine aminotransferase; KAT II, aminoadipate aminotransferase; CCDS, Consensus Coding Sequence.

purified with a Fast Gene Gel/PCR Extraction Kit (Nippon Genetics Co., Ltd., Tokyo, Japan), and the PCR products were purified by agarose gel electrophoresis and Monarch Gel Extraction Kit (NEW ENGLAND BioLabs Inc., Ipswich, MA, USA). Then, the PCR products were sequenced with M-KAT II_2nd_R (Table 1).

2.4 Western Blotting

For Western blotting, tissue extracts from the liver (20 mg) of the knockout and wild-type (WT) mice were prepared by the Total Protein Extraction Kit for Animal Cultured Cells and Tissues (Invent Biotechnologies, Plymouth, MN, USA) according to the manufacturer's instructions. Subsequently, the tissue extracts were passed through Protein G HP SpinTrap™ (Cytiva, Buckinghamshire, UK) to remove immunoglobulin G. 14 µL of each sample were mixed with 7 µL of SDS Blue Loading Buffer (New England BioLabs Inc.) and separated on a 12% SDS-polyacrylamide gel. Subsequently, the protein was transferred to the membranes. The membranes were blocked and incubated with anti-human KAT II rabbit polyclonal antibody (1:500, Invitrogen, Thermo Fisher Scientific, Waltham, MA, USA) at room temperature for 2 h, followed by combination with alkaline phosphatase-labeled secondary goat anti-rabbit immunoglobulin G (IgG) FC antibody (1:10,000, Sigma-Aldrich Co. LLC, St. Louis, MO, USA) at room temperature for 2 h, followed by visualization of dystrophin and utrophin using Western Blue® Stabilized Substrate for Alkaline Phosphatase (Promega, Madison, WI, USA). The Multicolor Protein Ladder (10–315 kDa) from Nippon Gene Co., Ltd. (Tokyo, Japan) was used as a molecular weight marker for western blotting, allowing visualization and size estimation of target proteins.

2.5 Phenotype Analysis with Modified SHIRPA Test

The 8–48 weeks old male and female mice mated in August 2023 and became pregnant about three to four weeks later. The RIKEN (The Institute of Physical and Chemical Research) modified SHIRPA (SmithKline Beecham, Harwell, Imperial College, Royal London Hospital, phenotype assessment) test was conducted to ascertain the comprehensive phenotypic traits of the mutant rodents. The assessment included the evaluation of diverse behaviors and physical attributes such as motion, bowel movements, urination, locomotor activity, startle response, tactile escape, pinna reflex, trunk curling, limb grasping, contact-righting reflex, grip strength, wire maneuver test, corneal reflex, toe pinching, and overall appearance. The animals were also monitored for vocalization, aggression, head bobbing, jumping, circling, retropulsion, grooming, and tail-wagging [185,186]. The experiment was captured on video using a camera (Basler ace Classic acA1300 - 60gm, Basler AG, Ahrensburg, Germany) and software (EthoVision XT14, Noldus Information Technology BV, Wageningen, the Netherlands).

2.6 Behavioral Tests

The 8–48 weeks old male and female mice mated between April 2021 and April 2022 and became pregnant approximately three to four weeks later. 8-week-old male C57BL/6N and *kat2*$^{-/-}$ mice (n = 10–13) were tested. In order to make the results comparable, all behavioral experiments were performed between 8 a.m. and 12 p.m. The animals were transferred to the laboratory, where the measurements were made, one hour before the start of the experiment, thus they had time to acclimatize to the environmental conditions.

2.6.1 Modified Forced Swim Test (FST)

The modified FST was performed as reported previously. The mice were placed individually in a glass cylinder of 12 cm in diameter and 30 cm in height. Water (25 ± 1 °C) was filled to a height of 20 cm. Fresh water was used for each mouse. A 15-min pretest was carried out 24 hours before the 3-min test session. A time-sampling technique was conducted to count the duration of time spent with climbing, swimming, and immobility [187,188].

2.6.2 Tail Suspension Test (TST)

The mice were placed in a 28 × 28 × 23.5 cm wooden box with three side walls and a clip hanging from the top of the box. The animals were suspended by their tails from the base to the middle two-thirds using a clip and allowed to hang for 6 minutes. We measure the duration of immobility. A cotton swab was pre-attached to the clip's interior to prevent the mice's tails from injuring or severely restricting blood circulation. If the animal is able to climb or falls off the clip, it is removed from the experiment and its results are discarded [189,190]. The experiment was captured on video using a camera (Basler ace Classic acA1300 -60gm, Basler AG, Ahrensburg, Germany) and software (EthoVision XT14, Noldus Information Technology BV, Wageningen, the Netherlands).

2.6.3 Elevated Plus Maze (EPM) Test

The animals were positioned in a plus-shaped apparatus with four arms measuring 35 × 10 cm. Two of the opposite arms are open, while the other two are closed, forming an angle of 90 degrees. The open arms have no side walls, while the closed arms have walls that are 20 cm tall. The entire apparatus is situated 50 cm off the ground. The device is surrounded by a screen that does not display any visual signals. The mouse was placed in the device's center with its nose facing an open arm and allowed it to explore for 5 minutes. We measure the time spent in each part (open arms, closed arms, and central part). The experiment was captured on video using a camera (Basler ace Classic acA1300 -60gm, Basler AG, Ahrensburg, Germany) and software (EthoVision XT14, Noldus Information Technology BV, Wageningen, the Netherlands). Between each animal, the apparatus was disinfected with 70% ethanol and left exposed to the air for 5 minutes [191,192].

2.6.4 Light Dark Box (LDB) Test

The LDB apparatus is comprised of larger illuminated (2/3 of the box) and smaller dark (1/3 of the box) compartments that are connected by a 5 × 5 cm door. The length of time a mouse spent in the lighted compartment during the 5-minute session was determined 5 seconds after a mouse was placed in the bright area. After each session, the box was cleaned with 70% ethanol and allowed to air for 5 minutes [192–194].

2.6.5 Passive Avoidance Test (PAT)

Each mouse was individually placed in a box containing two apparatuses with distinct lighting. The animals began in the bright compartment and had 5 minutes to pass through the 5 × 5 cm door into the dark, smaller portion of the box. As soon as the animals entered the dark compartment, they received a 0.3 mA electroshock through their paws, and the door shut. After 10 seconds, the animals were removed, and the experiment was repeated 24 hours later. Those animals that did not enter the dark area within 5 minutes during the pre-testing phase were omitted from the measurement. The box was cleaned with 70% ethanol and left to air for 5 minutes between mice [195].

2.6.6 Open Field (OF) Test

A standard table lamp illuminated the center of the 48 × 40 cm OF box, while the Conducta 1.0 system (Experimetria Ltd., Budapest, Hungary) monitored the mouse's movements. Each mouse was placed individually in the center of the box. Ambulation distance, time spent in the center zone, and number of entries to the center zone were measured for 10 minutes. After each session, the box was wiped down with 70% ethanol and allowed to for 5 minutes [196,197].

Throughout the experiment, the animals' general physical condition was constantly assessed using a scoring scale, which included body weight, appearance and overall condition, respiration, mobility, and the presence of basic reflexes. Humane endpoints were determined using the scales. If any animal reached the required score for withdrawal from the behavioral assessments, it was euthanized via transcardial perfusion under isoflurane anesthesia, effectively terminating its participation in the evaluation.

2.7 Ultra-High-Performance Liquid Chromatography with Tandem Mass Spectrometry

The 8–48 weeks old male and female mice mated in August 2023 and became pregnant about three to four weeks later. The urine samples were collected before anesthesia, and were immediately stored at –80°C after the sample collection. For plasma collection, the mice were anesthetized with 2% isoflurane, and after exposing their chest, blood samples were taken from the left heart ventricle using a syringe into Eppendorf tubes containing disodium ethylenediaminetetraacetate dihydrate. Plasma was separated by centrifugation (10,300 rpm for 10 minutes at 4 °C). The supernatant plasma samples were pipetted into new Eppendorf tubes. The samples were stored at –80 °C until use. The animals were perfused with artificial cerebrospinal fluid for 5 minutes to remove additional organs for later use. Trp and its metabolites were measured in plasma and urine using previously published protocols [198,199] using ultra-high performance liquid chromatography-tandem mass spectrometry (UHPLC-MS/MS). Picolinic acid multiple reaction monitoring (MRM) showed a change from 124.0 to 106.0 over 1.21 minutes, with 75 V acting as the declustering potential and 13 V acting as the collision energy. All reagents and chemicals were of analytical or liquid chromatography–mass spectrometry grade. Trp and its metabolites, and their deuterated forms: d4-serotonin, d5-tryptophan, d4-kynurenine, d5-kynurenic acid, d4-xanthurenic acid, d5-5-hydroxyindole-acetic acid, d3-3-hydroxyanthranilic acid, d4-picolinic acid, and d3-quinolinic acid were purchased from Toronto Research Chemicals (Toronto, ON, Canada).

d3-3-hydroxykynurenine was obtained from Buchem B. V. (Apeldoorn, The Netherlands). Acetonitrile (ACN) was provided by Molar Chemicals (Halásztelek, Hungary). Methanol (MeOH) was purchased from LGC Standards (Wesel, Germany). Formic acid (FA) and water were obtained from VWR Chemicals (Monroeville, PA, USA). The UHPLC-MS/MS system consisted of a PerkinElmer Flexar UHPLC system (two FX-10 binary pumps, solvent manager, autosampler and thermostatic oven; all PerkinElmer Inc. (Waltham, MA, USA)), coupled to an AB SCIEX QTRAP 5500 MS/MS triple quadrupole mass spectrometer and controlled by Analyst 1.7.1 software (both AB Sciex, Framingham, MA, USA).

2.8 The Enzyme Activities of Tryptophan (Trp) Metabolism

The enzyme activities of each Trp metabolism were determined by dividing the concentration of the product by the concentration of the substrate.

2.9 Oxidative Stress and Excitotoxicity Indices

The oxidative stress index was calculated as the ratios of putative prooxidant metabolite 3-hydroxykynurenine (3-HK) concentrations to the sums of putative antioxidant metabolite concentrations (KYNA, anthranilic acid (AA), and xanthurenic acid (XA)) (Eqn. 1) [200–202].

$$Oxidative\ stress\ index\ =\ [3-Hydroxykynurenine]/ \{[Kynurenic\ acid]\ +\ [Anthranilic\ acid]\ +\ [Xanthurenic\ acid]\} \quad (1)$$

The excitotoxicity index is calculated by dividing the concentration of N-methyl-D-aspartate (NMDA) receptor agonist quinolinic acid (QA) by that of NMDA receptor antagonist KYNA (Eqn. 2) [203–205].

$$Excitotoxicity\ index\ =\ [Quinolinic\ acid]/[Kynurenic\ acid] \quad (2)$$

2.10 Statistical Analysis

We used IBM SPSS Statistics 28.0.0.0 (IBM SPSS statistics, Chicago, IL, USA) for the statistical analysis. The Shapiro–Wilk test was used to determine the distribution of data. In addition, we used a Q-Q plot to find out if two sets of data come from the same distribution. Our data followed a normal distribution. One-way ANOVA test was used to evaluate the results of the behavioral tests and neurochemical measurements followed by the Tamhane post hoc test. Values $p < 0.05$ were considered statistically significant. Our data are reported as means $\pm$ SD for all parameters and groups.

3. Results

3.1 DNA Sequence Analysis and Western Blot

To generate knockout mice of *kat2* gene, 25 ng/µL of sgRNA and 75 ng/µL Cas9 protein were injected into the cytoplasm of the one-cell-stage embryos. Sequencing analyses with their founder mice showed that various deletions and/or insertions were introduced in the target sequence. One of the founders was selected and established the homozygous mouse line for further analyses. KAT II knockout mouse line expresses a carboxy-terminal truncated polypeptide consisting of the first 47 amino acids of the intact KAT II with 2 nucleotides deletion (CCDS nucleotide sequence 32–33) in the mRNA. Western blotting with antibodies against KAT II revealed that the band with approximately 50-kDa supposed to be KAT II was not detected in the knockout mice, while it was detected in the wild-type (WT) counterparts (Fig. 3).

3.2 Phenotype Analysis with SHIRPA Protocol

We did not detect any significant differences between the knockout mice and their wild-type counterparts.

3.3 Behavioral Tests

3.3.1 Forced Swim Test (FST)

The immobility time was significantly longer and the swimming time was significantly shorter in *kat2*$^{-/-}$ mice than in WT mice (Fig. 4a,b; Table 2). There were no significant differences in climbing time (Table 2).

3.3.2 Open Field (OF) Test

The ambulation distance of the *kat2*$^{-/-}$ mice was significantly shorter in the first 10-minute timeframe than that of their WT counterparts (Fig. 4c; Table 2). The number of jumps was significantly fewer in the *kat2*$^{-/-}$ mice than that of their WT counterparts (Fig. 4d; Table 2). There were significantly fewer entries into the center and corner zones compared to their WT counterparts (Fig. 4e; Table 2).

3.3.3 Other Behavioral Tests

There were no statistically significant distinctions observed between the transgenic mice and their WT counterparts in TST, PAT, EPM test, and LDB test (Table 2).

3.4 Ultra-High-Performance Liquid Chromatography with Tandem Mass Spectrometry

Transgenic mice had significantly lower levels of KYN, KYNA, XA, AA, 5-hydroxyindoleacetic acid (5-HIAA), indole-3-acetic acid (IAA), and higher levels of 3-HK in plasma samples than wild-type mice. In urine samples, KYNA, XA, and IAA were significantly lower, whereas KYN, 3-HK, and 5-HT were significantly higher than those of the wild-type counterparts (Fig. 5; Table 3).

3.5 Enzyme Activities in Tryptophan (Trp) Metabolism

The transgenic mice showed significantly lower KATs, kynureninase (KYNU), KAT III, monoamine oxidase (MAO), aldehyde dehydrogenase (ALDH), and tryptophan-2-monooxygenase (TMO) activities and significantly higher kynurenine 3-monooxygenase (KMO) activ-

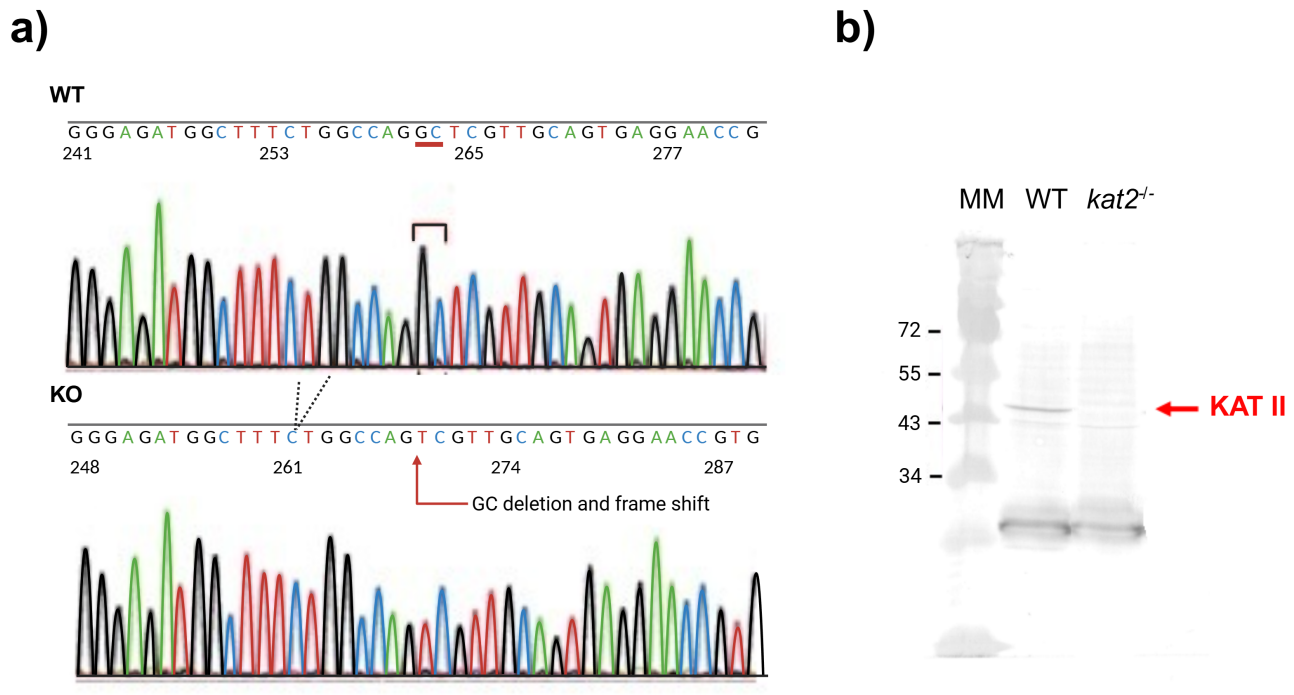

Fig. 3. DNA sequence and western blot analysis of knockout *kat2*$^{-/-}$ mouse line. (a) Genomic sequences around the mutation site of knockout *kat2*$^{-/-}$ mouse strain. (b) Western blot analysis of knockout *kat2*$^{-/-}$ mouse line. MM: molecular weight marker, WT: wild-type mouse. The figure was created with Scientific Image and Illustration Software Biorender.

Table 2. Behaviors of *kat2*$^{-/-}$ mice and the wild-type counterparts.

Test type	Number of animals	Perspectives	Mean ± SD of wild-type	Mean ± SD of *kat2*$^{-/-}$	*p*-value
Modified forced swim test (FST)	WT: n = 12 *kat2*$^{-/-}$: n = 11	Immobility time (s)	157.73 ± 17.23	174.09 ± 6.64	0.022 *
		Swimming time (s)	18.18 ± 15.37	3.18 ± 4.62	0.014 *
		Climbing time (s)	4.09 ± 4.37	1.82 ± 6.03	0.681
Tail suspension test (TST)	WT: n = 10 *kat2*$^{-/-}$: n = 13	Immobility time (s)	194.50 ± 66.76	209.58 ± 67.23	0.625
Passive avoidance test (PAT)	WT: n = 12 *kat2*$^{-/-}$: n = 12	Time spent in the lit box on the training day (s)	48.33 ± 29.24	64.67 ± 55.78	0.979
		Time spent in the lit box on the test day (s)	256.00 ± 76.94	283.75 ± 39.60	0.822
Elevated plus maze (EPM) test	WT: n = 10 *kat2*$^{-/-}$: n = 11	Time spent in the open arms (s)	42.90 ± 61.60	30.64 ± 43.70	0.500
Light dark box (LDB) test	WT: n = 12 *kat2*$^{-/-}$: n = 11	Time spent in the lit box (s)	119.00 ± 31.38	113.91 ± 24.41	0.957
Open field (OF) test	WT: n = 12 *kat2*$^{-/-}$: n = 11	Number of entries to the center zones (times)	281.67 ± 69.13	210.73 ± 65.20	0.011 *
		Number of entries to the corner zones (times)	83.08 ± 26.95	51.27 ± 17.88	0.001 ***
		Ambulation distance (cm)	2191.75 ± 364.45	1609.27 ± 381.96	0.002 **
		Number of jumps (times)	7.33 ± 4.94	2.45 ± 3.08	0.034 *

*, $p < 0.05$; **, $p < 0.01$; ***, $p < 0.001$.

ity in plasma samples than wild-type mice. In the urine samples, the transgenic mice showed significantly lower KATs, KYNU, KAT III, MAO, ALDH, and TMO activities, and significantly higher tryptophan-2,3-dioxygenase (TDO)/indoleamine 2,3-dioxygenases (IDOs) (KFA), KMO, and aromatic L-amino acid decarboxylase (AADC) activities compared to the wild-type counterparts (Fig. 6, Table 4).

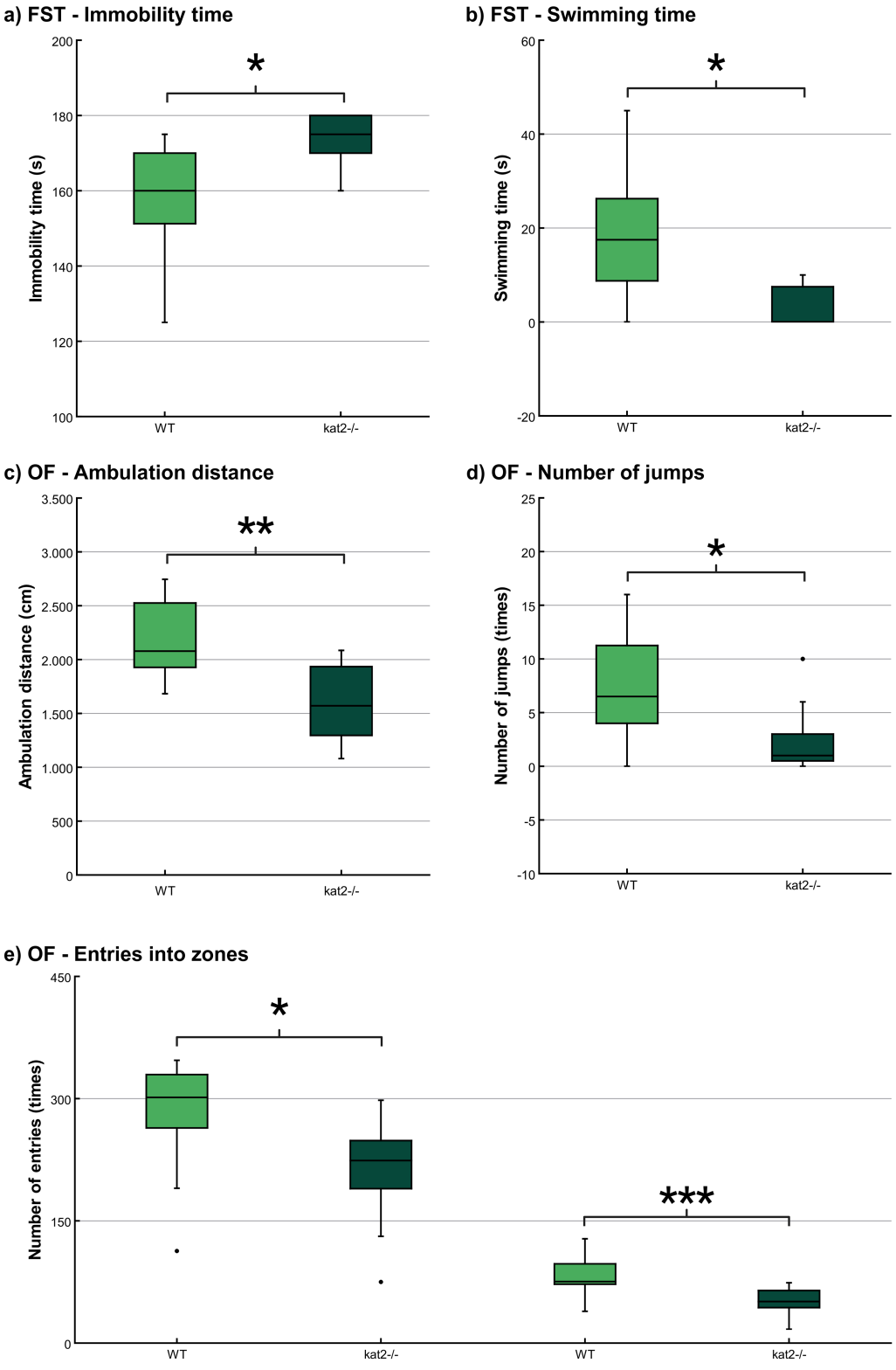

Fig. 4. Behavioral tests. (a) Time spent immobile in the modified forced swim test (FST). (b) Time spent swimming in the modified FST. (c) Ambulation distance in the open field (OF) test. (d) Number of jumps in the OF test; and (e) Number of entries into the center and corner zones in the OF test. Wild-type mice (light green); *kat2*$^{-/-}$ mice (dark green). WT, wild-type; *kat2*$^{-/-}$, kynurenine aminotransferase II knockout mice; FST, forced swim test; OF, open field test; •, outliner. Mean ± SD. *, $p < 0.05$; **, $p < 0.01$; ***, $p < 0.001$. The figure was created with Labplot 2.9.0 (KDE, Berlin, Germany) and Scientific Image and Illustration Software Biorender.

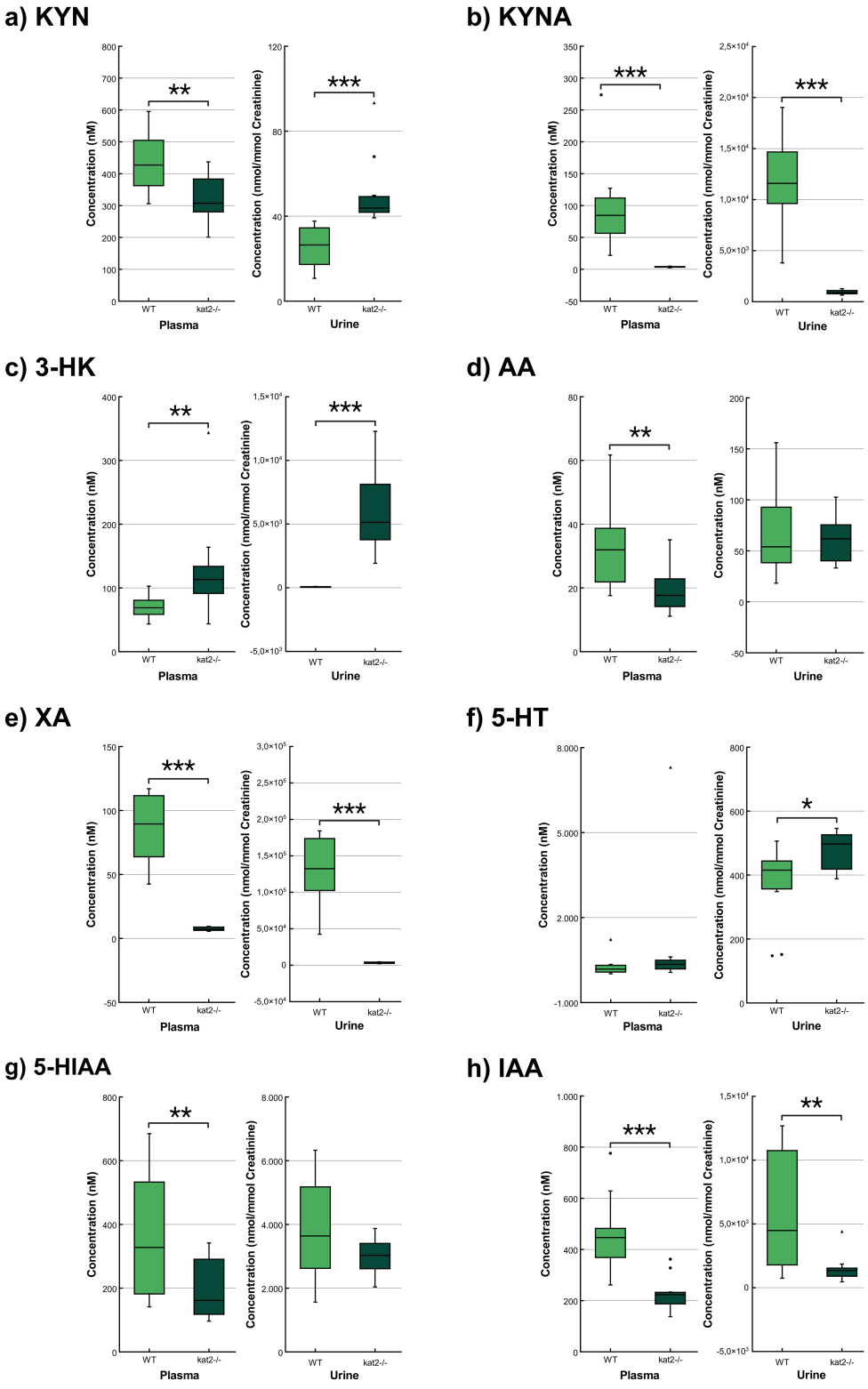

Fig. 5. Concentration level of tryptophan metabolites in plasma and urine. (a) Kynurenine. (b) Kynurenic acid. (c) 3-hydroxykynurenine. (d) Anthranilic acid. (e) Xanthurenic acid. (f) Serotonin/5-hydroxytryptamine. (g) 5-hydroxyanthranilic acid. (h) Indole-3-acetic acid. We marked wild-type mice with light, and *kat2*$^{-/-}$ mice results with dark green boxes. WT, wild-type; *kat2*$^{-/-}$, kynurenine aminotransferase II knockout; 3-HK, 3-hydroxykynurenine; 5-HIAA, 5-hydroxyanthranilic acid; 5-HT, serotonin/5-hydroxytryptamine; AA, anthranilic acid; IAA, indole-3-acetic acid; KYN, kynurenine; KYNA, kynurenic acid; XA, xanthurenic acid; •, outliner; ▲, far out. Mean ± SD; *, $p < 0.05$; **, $p < 0.01$; ***, $p < 0.001$. The figure was created with Labplot 2.9.0 (KDE, Berlin, Germany) and Scientific Image and Illustration Software Biorender.

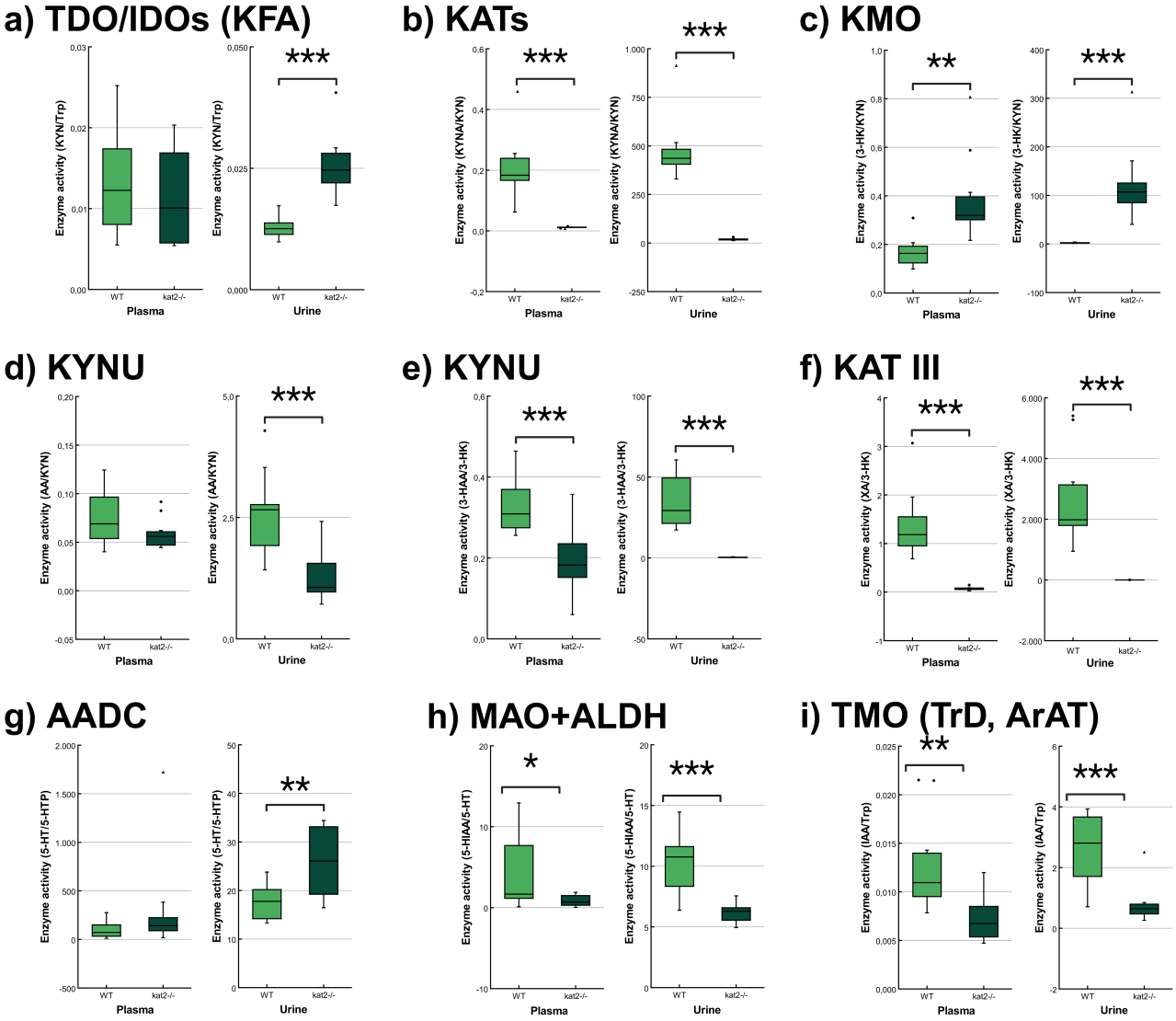

Fig. 6. Tryptophan metabolism's enzyme activity in plasma and urine. (a) Tryptophan 2,3-dioxygenase/indoleamine 2,3-dioxygenases (kynurenine formamidase). (b) Kynurenine aminotransferases. (c) Kynurenine 3-monooxygenase. (d,e) Kynureninase. (f) Kynurenine aminotransferase III/cysteine conjugate beta-lyase 2. (g) Aromatic L-amino acid decarboxylase. (h) Monoamine oxidases + aldehyde dehydrogenase. (i) Tryptophan-2-monooxygenase (tryptophan decarboxylase, aromatic amino acid aminotransferase). We marked wild-type mice with light, and *kat2*$^{-/-}$ mice results with dark green boxes. 3-HAA, 3-hydroxyanthranilic acid; 3-HK, 3-hydroxykynurenine; 5-HIAA, 5-hydroxyindoleacetic acid; 5-HT, serotonin/5-hydroxytryptamine; 5-HTP, 5-hydroxytryptophan; AADC, aromatic L-amino acid decarboxylase; ALDH, aldehyde dehydrogenase; ArAT, aromatic amino acid aminotransferase; IAA, indole-3-acetic acid; IDOs, indoleamine 2,3-dioxygenases; KAT III, kynurenine aminotransferase III/cysteine conjugate beta-lyase 2; *kat2*$^{-/-}$, kynurenine aminotransferase II knockout; KATs, kynurenine aminotransferases; KFA, kynurenine formamidase; KMO, kynurenine 3-monooxygenase; KYNU, kynureninase; MAO, monoamine oxidase; TDO, tryptophan 2,3-dioxygenase; TMO, tryptophan-2-monooxygenase; TrD, tryptophan decarboxylase; Trp, tryptophan; WT, wild-type; XA, xanthurenic acid; KYN, kynurenine; KYNA, kynurenic acid; AA, anthranilic acid; •, outliner; ▲, far out. Mean ± SD; *, $p < 0.05$; **, $p < 0.01$; ***, $p < 0.001$. The figure was created with Labplot 2.9.0 (KDE, Berlin, Germany) and Scientific Image and Illustration Software Biorender.

Table 3. Quality control samples of mouse plasma and urine (runtime 25 h, (mean concentrations, 14-14 replicates of each, the given n is the samples size of the pooled individual samples)).

	Plasma (nM)			Urine (nmol/mmol Creatinine)		
	Mean ± SD		*p* value	Mean ± SD		*p* value
	WT	*kat2*$^{-/-}$		WT	*kat2*$^{-/-}$	
Tryptophan (Trp)	40,901.678 ± 21,056.888	35,543.573 ± 16,203.237	0.532	2022.196 ± 908.643	1972.014 ± 286.954	0.870
Kynurenine (KYN)	440.674 ± 102.886	327.348 ± 76.385	0.012 **	25.238 ± 10.185	50.883 ± 17.134	<0.001 ***
Kynurenic acid (KYNA)	96.960 ± 70.837	3.654 ± 0.860	<0.001 ***	11,783.938 ± 5040.178	920.990 ± 215.223	<0.001 ***
Quinaldic acid (QAA)	6.884 ± 5.397	5.608 ± 1.234	0.476	14.248 ± 9.716	12.014 ± 7.490	0.572
3-hydroxykynurenine (3-HK)	70.714 ± 18.994	130.851 ± 82.199	0.037 **	55.472 ± 31.438	5986.833 ± 3157.255	<0.001 ***
Xanthurenic acid (XA)	93.624 ± 45.637	7.406 ± 1.452	<0.001 ***	127,228.662 ± 52,582.223	3273.334 ±1021.511	<0.001 ***
Anthranilic acid (AA)	32.655 ± 13.114	19.335 ± 7.280	0.012 **	69.112 ± 45.347	60.862 ± 22.368	0.612
3-Hydroxyanthranilic acid (3-HAA)	22.992 ± 6.140	20.920 ± 5.921	0.452	1741.538 ± 824.887	1789.475 ± 454.422	0.874
Quinolinic acid (QA)	132.185 ± 75.409	112.000 ± 41.600	0.468	10,059.485 ± 4601.597	11,718.491 ± 2401.051	0.326
Picolinic acid (PA)	193.797 ± 93.230	154.895 ± 88.753	0.352	190.435 ± 91.394	193.898 ± 113.072	0.941
5-Hydroxytryptophan (5-HTP)	2.790 ± 1.577	2.708 ± 1.297	0.901	21.742 ± 8.520	19.297 ± 3.833	0.419
Serotonin (5-HT)	277.309 ± 353.179	1010.379 ± 2219.355	0.316	371.974 ± 125.489	479.383 ± 63.304	0.027 *
5-hydroxyindoleacetic acid (5-HIAA)	362.241 ± 199.450	201.217 ± 99.184	0.035 **	3774.968 ± 1666.005	2969.725 ± 598.373	0.167
Indole-3-acetic acid (IAA)	457.329 ± 153.046	229.142 ± 68.266	<0.001 ***	6030.306 ± 4737.901	1513.400 ± 1097.122	0.009 **
Indoxyl-sulphate (INS)	6738.111 ± 3559.896	5404.257 ± 2292.535	0.332	400,636.750 ± 185,880.105	497,063.585 ± 190,235.646	0.267

SD, standard deviation; *, $p < 0.05$; **, $p < 0.01$; ***, $p < 0.001$.

Table 4. Enzymes activities in plasma and urine.

Enzyme	Product/Substrate	Plasma			Urine		
		Mean ± SD		*p* value	Mean ± SD		*p* value
		WT	*kat2*$^{-/-}$		WT	*kat2*$^{-/-}$	
TDO/IDOs (KFA)	KYN/Trp	0.013 ± 0.007	0.011 ± 0.006	0.532	0.013 ± 0.002	0.026 ± 0.006	<0.001 ***
KATs	KYNA/KYN	0.205 ± 0.107	0.011 ± 0.002	<0.001 ***	476.464 ± 164.156	18.937 ± 5.057	<0.001 ***
KMO	3-HK/KYN	0.168 ± 0.062	0.386 ± 0.180	0.002 **	2.219 ± 0.827	122.983 ± 75.543	<0.001 ***
KYNU	AA/KYN	0.075 ± 0.028	0.059 ± 0.016	0.120	2.593 ± 0.862	1.253 ± 0.529	<0.001 ***
KYNU	3-HAA/3-HK	0.330 ± 0.070	0.194 ± 0.080	<0.001 ***	35.177 ± 16.776	0.372 ± 0.182	<0.001 ***
KAT III	XA/3-HK	1.374 ± 0.714	0.070 ± 0.033	<0.001 ***	2702.990 ± 1524.430	0.629 ± 0.229	<0.001 ***
3-HAO	QA/3-HAA	5.1771 ± 2.978	5.486 ± 1.994	0.804	6.240 ± 2.487	6.856 ± 1.779	0.532
3-HAO + ACMSD	PA/3-HAA	8.797 ± 4.263	7.681 ± 4.872	0.592	0.123 ± 0.071	0.119 ± 0.085	0.906
TPHs	5-HTP/Trp	<0.001 ± <0.001	<0.001 ± <0.001	0.128	0.011 ± 0.002	0.010 ± 0.003	0.410
AADC	5-HT/5-HTP	97.585 ± 87.384	307.233 ± 509.276	0.216	17.608 ± 3.583	25.997 ± 7.185	0.004 **
MAOs + ALDH	5-HIAA/5-HT	4.217 ± 4.818	0.905 ± 0.712	0.045 *	10.209 ± 2.530	6.181 ± 0.859	<0.001 ***
TMO (TrD, ArAT)	IAA/Trp	0.013 ± 0.005	0.007 ± 0.002	0.005 **	2.570 ± 1.243	0.786 ± 0.636	<0.001 ***
TNA	INS/Trp	0.208 ± 0.178	0.170 ± 0.089	0.555	215.671 ± 100.757	248.916 ± 81.413	0.428

*, $p < 0.05$; **, $p < 0.01$; ***, $p < 0.001$.

Table 5. The oxidative stress and excitotoxicity indices in the plasma and urine.

Oxidative stress index						
Oxidant/antioxidant metabolites	Plasma (nM)			Urine (nmol/mmol Creatinine)		
	Mean ± SD		*p* value	Mean ± SD		*p* value
	WT	*kat2*$^{-/-}$		WT	*kat2*$^{-/-}$	
3-HK/KYNA+AA+XA	0.378 ± 0.163	4.090 ± 1.478	<0.001 ***	0.085 ± 0.011	1.352 ± 0.473	<0.001 ***

Excitotoxicity index						
NMDA agonist/antagonist metabolites	Plasma (nM)			Urine (nmol/mmol Creatinine)		
	Mean ± SD		*p* value	Mean ± SD		*p* value
	WT	*kat2*$^{-/-}$		WT	*kat2*$^{-/-}$	
QA/KYNA	1.648 ± 0.810	30.514 ± 8.618	<0.001 ***	0.884 ± 0.320	13.092 ± 2.833	<0.001 ***

***, $p < 0.001$.

3.6 Oxidative stress and Excitotoxicity indices

Transgenic mice had higher levels of oxidative stress and excitotoxicity in both plasma and urine than wild-type mice (Fig. 7, Table 5).

4. Discussion

Dysregulation of 5-HT metabolism is a key factor in mental symptom development, with attention focused on its imbalance with neurotransmitters like dopamine, norepinephrine, and biosystems such as substance P [206–210]. Alterations in 5-HT precursor Trp metabolism are noted in mental illnesses, but their connection with the Trp-KYN metabolic system remains poorly understood [211–213]. Growing evidence suggests that the gut microbial indole pyruvate pathway can influence the microbiome-gut-brain axis, implying that intestinal Trp metabolism may play a significant role in psychological health. The microbiome-gut-brain axis is responsible for regulating mood, cognition, stress response, and behavior [101]. As a result, the gut-microbial indole pyruvate pathway can influence the microbiome-gut-brain axis by controlling the production and availability of neurotransmitters, hormones, cytokines, and bioactive metabolites involved in neuropsychiatric conditions.

KATs are cytosolic and mitochondrial aminotransferases that convert KYN to KYNA [74,214–216]. The mitochondrial isoform KAT II exclusively influences cellular bioenergetics due to its exclusive location in the mitochondria [117,205]. CRISPR/Cas9 was employed to knock out the *kat2* gene, creating *kat2*$^{-/-}$ mice. This study aimed to examine the negative emotional aspects and evaluate any behavioral alterations caused by the knockout of the *kat2* gene in young adults aged 8 weeks. *kat2*$^{-/-}$ mice, studied in 8-week-old adults, induce a unique depression-like phenotype marked by increased immobility in FST, likely linked to serotonergic pathways. TST did not show significant differences, possibly due to FST conditioning. The results that the PAT did not show a significant difference may suggest that depression-like behavior is more likely to be related to depression-like behavior caused by despair experiences than to aversive-conditioned memory. Anxiety-like behaviors (EPM and LDB) showed no difference, but the OF test revealed shorter ambulation distance, fewer jumping counts, and fewer entries into both center field and corners, suggesting a la belle indifference-like trait. *kat2*$^{-/-}$ mice exhibited despair-based depression-like behavior without anxiety-like traits, demonstrating motor deficits. The study suggests the *kat2* gene deletion potentially leads to a PTSD-like phenotype, including a la belle indifference trait, indicative of complex PTSD with emotional dysregulation [217–219].

The gene knockout significantly alters Trp metabolism in both 5-HT, KYN, and indole pathways in plasma and urine. A major 5-HT metabolite, 5-HIAA, is markedly reduced, possibly explained by scarce mitochondrial enzyme activity. Lower levels of KYNA and antioxidant KYNs indicate decreased production in peripheral tissues of *kat2*$^{-/-}$ mice. Conversely, 3-HK is significantly elevated. The levels of the gut microbial metabolite IAA, an antioxidant and anti-inflammatory molecule, were reduced. The disruption of the KAT II gene may lead to a reduction in the levels of IAA in the indole pathway of the gut microbiota, as the enzyme plays a role in controlling Trp metabolism. KAT II has an impact on the availability of Trp and its subsequent metabolic pathways, including the production of IAA. In the absence of KAT II, the Trp metabolite balance may shift, resulting in less IAA synthesis by gut bacteria. This change may disrupt the gut-brain axis and have an impact on intestinal health, as IAA is required for immune response regulation, intestinal barrier integrity, and modulating the production of other indole derivatives. Furthermore, gene knockout affects enzyme activity, puts organisms under oxidative stress, imposes high excitotoxicity and neurotoxicity, and alters immune responses. The study demonstrates that the deletion of the *kat2* gene leads to a specific set of characteristics, including behavior similar to depression, impaired

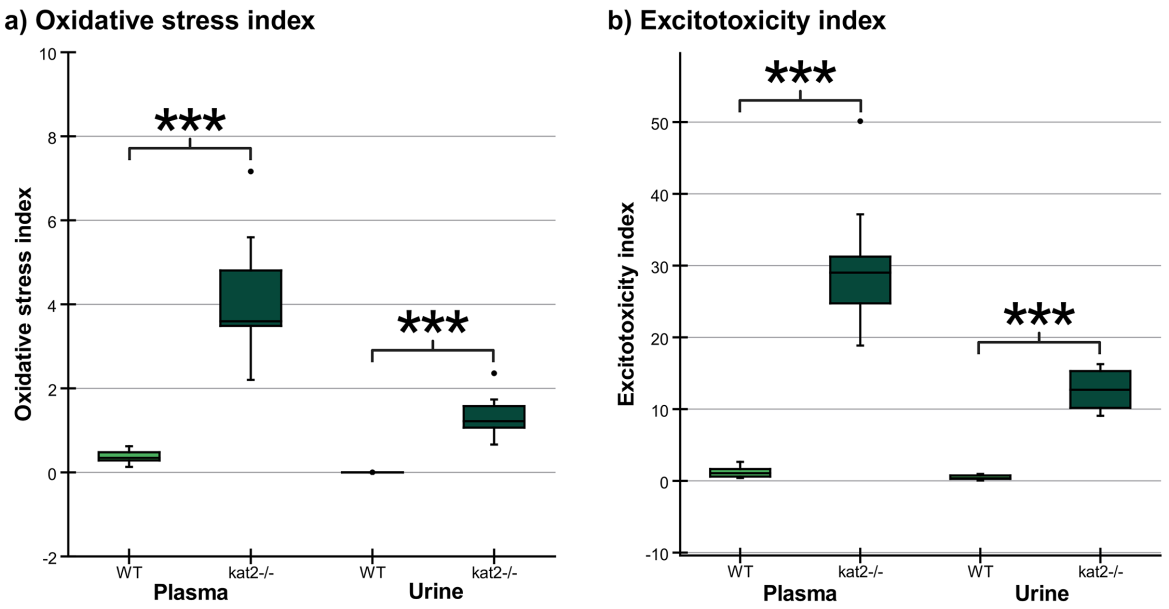

Fig. 7. Oxidative stress and excitotoxicity indices in plasma and urine. (a) The oxidative stress indices in *kat2*$^{-/-}$ mice's plasma and urine samples are significantly higher than those in the wild-type. (b) The excitotoxicity indices in *kat2*$^{-/-}$ mice's plasma and urine samples are significantly higher than those in the wild-type. We marked wild-type with light, and *kat2*$^{-/-}$ mice results with dark green boxes. WT, wild-type; *kat2*$^{-/-}$, kynurenine aminotransferase II knockout; •, outliner. Mean ± SD; ***, $p < 0.001$. The figure was created with Labplot 2.9.0 (KDE, Berlin, Germany) and Scientific Image and Illustration Software Biorender.

motor function, decreased levels of KYNA, and a change in the way Trp is metabolized towards the KYN pathway. This phenotype exhibits similarities to PTSD in humans, potentially indicating the presence of complex PTSD due to the observed belle indifference-like trait.

The amygdala encodes and stores fear memory after receiving sensory input from the thalamus, which also consolidates and retrieves memories from the initial stimuli that induce fear [220–222]. Fear memory is associated with the release of stress hormones such as adrenaline and cortisol, which stimulate the sympathetic nervous system and the hypothalamic-pituitary-adrenal axis [46,223–227]. This study does not show evidence of fear memory acquisition. In contrast, the encoding and storage of memories associated with despair occur in the prefrontal cortex, which plays a crucial role in the cognitive and emotional processing of negative experiences [228]. Recalling distressing memories, triggered by cues linked to the initial negative encounter, results in the disruption of 5-HT, norepinephrine, and dopamine regulation. Although fear and despair memories have similarities in terms of encoding and retrieval processes, they are associated with different brain regions, neurotransmitters, and neural circuits [229,230].

Furthermore, despair memory and despair experience differ. The latter pertains to an instantaneous, personal feeling of despair or hopelessness, prompted by present circumstances, as opposed to a remembrance of past experiences [231]. Despair memory involves the consolidation and retrieval of long-term memories, influenced by stress and emotion [232]. In contrast, a despair experience entails immediate emotional responses influenced by factors like cognitive assessments, environmental cues, and physiological states [233]. Additionally, la belle indifference arises from a discrepancy between cognitive and emotional symptom processing, including altered emotional processing in the amygdala and insula, changed self-awareness in the medial prefrontal cortex, and adjusted activity in the somatosensory cortex influenced by dopamine and 5-HT [234]. Thus, *kat2*$^{-/-}$ mice show more despair-based depression-like behavior involving a change in 5-HT metabolism.

Approximately 60% of individuals on antidepressants, including SSRIs, for two months experience a 50% reduction in depression symptoms [235]. The observation aligns with the monoamine hypothesis, suggesting depression's pathogenesis is linked to low 5-HT levels. Transgenic models are used to study 5-HT dysmetabolism behaviors, with a focus on the *Tph* gene, which encodes tryptophan hydroxylase, a key enzyme in 5-HT synthesis [236]. Preclinical studies found normal 5-HT levels with no behavioral changes in *Tph1*$^{-/-}$ mice, while *Tph2*$^{-/-}$ mice's behaviors are inconclusive [237,238]. The knock-in mice of the TPH2 variant (R439H) showed depression-like behavior in TST [239]. Intriguingly, *Tph1/Tph2*$^{-/-}$ mice exhibited contrasting behaviors: antidepressant-like in FST, depressive in TST, and anxious in the MB test, accompanied by low 5-HT levels in the brain and periphery [240]. 5-HT1A receptor knockout (*5-HT1AR*$^{-/-}$) mice display heightened fear memory to contextual cues, suggesting a role for 5-HT re-

ceptors in PTSD-like phenotype [241]. 5-HT 2C receptor knockout *5-HT2CR*$^{-/-}$ mice attenuates fear responses in contextual or cued but not compound context-cue fear conditioning [242]. Knockout of the 5-HTT gene in mice (*5-HTT*$^{-/-}$) leads to impaired stress response, fear extinction, and abnormal corticolimbic structure [243].

Over 90% of 5-HT precursor Trp undergoes catabolism in the Trp-KYN metabolic system, generating a variety of bioactive molecules including prooxidants, antioxidants, inflammation suppressants, neurotoxins, neuroprotectants, and/or immunomodulators [244]. Growing evidence indicates disrupted KYN metabolism in MDD, bipolar disorder, and SCZ [245–247]. Earlier, KYN metabolites were suggested to be either neuroprotective or neurotoxic [248]. However, increasing evidence suggests that KYN metabolites exhibit versatile actions, potentially influenced by concentrations and the microenvironment [249]. Previously, cognitive and motor functions of 129/SvEv *kat2*$^{-/-}$ mice were reported. These transgenic mice exhibited transient hyperlocomotive activity and motor coordination issues at postnatal day 21. However, from postnatal day 17 to 26, they demonstrated notable improvements in cognitive functions, particularly in object exploration and recognition tasks in PAT and T-maze tests [250,251].

Other biosystems play an important role in the pathogenesis of PTSD, including dopaminergic and gamma-aminobutyric acid (GABA)ergic, and cannabinoid systems. Catechol-*O*-methyltransferase (COMT) degrades dopamine. *COMT*$^{-/-}$ mice exhibited an increased response to repeated stress exposures [252]. Glutamic acid decarboxylase (GAD) synthesizes GABA [253]. *GAD6*$^{-/-}$ mice shows increased generalized fear and impaired extinction of cued fear [254]. GABA receptor subunit B1a knockout *GABAB1a*$^{-/-}$ mice showed a generalization of conditioned fear to nonconditioned stimuli [255]. Cannabinoid 1 receptor (CBIR) knockout *CB1R*$^{-/-}$ mice showed an increased response to repeated stress exposures [256].

The potential of this study is to characterize the negative valence of emotional domain in context with aversive-conditioned memory and despair experience in the young adult (8 week) of *kat2*$^{-/-}$ mice. The findings complement the previous studies of *kat2*$^{-/-}$ mice in the early adolescence (2 and 1/2 to 4 weeks) to reveal that, toward adulthood, there is a dynamic change in emotional susceptibility and motor function derived from despair experience in adjunct to Trp metabolism. Furthermore, urinary Trp metabolite levels were generally consistent with plasma levels, suggesting that urinary samples may serve as non-invasive biomarkers for Trp metabolism status. This study may shed new light on the deletion of the *kat2* gene as a new avenue toward understanding a KYN metabolite as an oxidative stressor, a potential barrier between aversive-conditioned memory and despair experience, a distinction between memory and experience, their mechanism for the formation of intrusive memories, and the pathogenesis of PTSD. The ultimate goal is to probe a potential interventionable stage in age where the progression of PTSD is preventable and to identify targets which drugs or psychotherapy can relieve symptoms of PTSD. The greatest challenge lies in preclinical animal models that are difficult to simulate and interpolate to mental illnesses to achieve high model validity.

This research on transgenic mice offers great potential for future studies. By examining the link between behavioral changes and variations in Trp and its metabolites in plasma and urine, scientists can gain insights into Trp metabolism's role in emotional and cognitive functions. Additionally, assessing enzyme activities related to Trp metabolism and their effects on oxidative stress and neurochemical imbalances may uncover mechanisms behind observed behavioral differences. This thorough approach could reveal causal or parallel relationships, shedding light on how altered Trp metabolism impacts neurochemical imbalances and oxidative stress, contributing to conditions like depression and PTSD. The results may help identify specific biomarkers and therapeutic targets, opening new pathways for precision medicine and more effective treatments for neuropsychiatric disorders. The study's findings could lead to the development of customized therapies, enhancing mental health by focusing on unique metabolic pathways and genetic factors. This research highlights the importance of combining metabolic, behavioral, and genetic data to deepen our understanding of complex psychiatric disorders [257].

This study suggests that behavioral sampling in rodents can distinguish between fear-, memory-, and despair-based depression-like behavior associated with Trp metabolism gene deletions. Further research incorporating neurochemical, neurogenetic, and electrophysiological biomarkers may reinforce this finding. Additionally, using inhibitory RNA or antisense RNA on neurotransmitters in specific brain regions could elucidate the precise mechanisms underlying emotional behaviors. Preclinical research drives advances in clinical applications like precision medicine and drug discovery [258–260]. The study acknowledges weaknesses, noting distinctions in interpreting animal behaviors and drug responses compared to humans. Recent perspectives consider depression-like behavior in FST as related to different stages of stress-coping behaviors [261]. Consequently, Translational research has limitations that necessitate careful interpretation [262–264]. This study employed animal models with standard protocols, focusing on the negative valence of the emotional domain and motor function in *kat2*$^{-/-}$ mice. Further exploration with diverse models such as sucrose preference tests, fear condition tests, and those using non-standard protocols is crucial for a more accurate characterization of *kat2*$^{-/-}$ mouse behavior. Notably, the Diagnostic and Statistical Manual of Mental Disorders, Fifth Edition, emphasizes four symptom clusters in PTSD diagnosis [265–267]. The transgenic mice

in this study did not exhibit signs related to negative cognitions and mood, and arousal state and reactivity were not investigated.

5. Conclusions

Psychiatric disorders, including PTSD, have a significant impact on memory and emotion, and disruptions in 5-HT metabolism have been associated with these disorders. The Trp-KYN metabolic pathway plays a crucial role in metabolizing over 95% of the 5-HT precursor Trp. To investigate the effects of gene deletion on negative valence in emotion, memory, and motor function, transgenic *kat2*$^{-/-}$ mice were created and compared to WT mice. The *kat2*$^{-/-}$ mice exhibited depression-like behavior characterized by despair experiences, diminished motor functions, and la belle indifference-like characteristics without anxiety-like behavior. This study provides insights into the negative valence of the emotional domain in the context of aversive-conditioned memory and despair experiences in 8-week-old *kat2*$^{-/-}$ mice. Understanding the complex interplay between memory, emotion, and genetic factors is crucial for advancing our knowledge of psychiatric disorders [268,269]. By elucidating the specific effects of gene deletion on negative valence and related behaviors, this research contributes to our understanding of the underlying mechanisms and potential interventions.

Declaration of AI and AI-assisted Technologies in the Writing

During preparation for this work, the authors used QuillBot for gingrammar and style checks in the main text. After using this tool, the authors reviewed and edited the content as needed and took full responsibility for the content of the publication.

Abbreviations

3-HAA, 3-hydroxyanthranilic acid; 3-HAO, 3-hydroxyanthranilate oxidase; 3-HK, 3-hydroxykynurenine; 5-HIAA, 5-hydroxyindoleacetic acid; 5-HT, serotonin/5-hydroxytryptamine; 5-HTP, 5-hydroxytryptophan; AA, anthranilic acid; AADC, aromatic L-amino acid decarboxylase; ACMSD, amino-β-carboxymuconate-semialdehyde-decarboxylase; AD, Alzheimer's disease; ALDH, aldehyde dehydrogenase; ArAT, aromatic amino acid aminotransferase; CBIR, cannabinoid 1 receptor; CNS, central nervous system; COMT, catechol-O-methyltransferase; EPM, elevated plus maze; FST, forced swim test; GABA, gamma-aminobutyric acid; GAD, glutamic acid decarboxylase; hCG, human chorionic gonadotropin; IAA, indole-3-acetic acid; ICR: Institute of Cancer Research; IDOs, indoleamine 2,3-dioxygenases; IgG, immunoglobulin G; INS, indoxyl sulfate; KAT II, α-aminoadipate aminotransferase/kynurenine aminotransferase II; KAT III, kynurenine aminotransferase III/cysteine conjugate beta-lyase 2; KATs, kynurenine aminotransferases; KFA, kynurenine formamidase; KMO, kynurenine 3-monooxygenase; KYN, kynurenine; KYNA, kynurenic acid; KYNU, kynureninase; LDB, light dark box; MAO, monoamine oxidase; MDD, major depressive disorder; MRM, multiple reaction monitoring; NMDA, N-methyl-D-aspartate; OF, open field; PA, picolinic acid; PAT, passive avoidance test; PCR, polymerase chain reaction; PMSG, pregnant mare serum gonadotropin; PTSD, post-traumatic stress disorder; QA, quinolinic acid; SCZ, schizophrenia; sgRNA, single guide RNA; SSRI, selective serotonin reuptake inhibitor; TDO, tryptophan 2,3-dioxygenase; TMO, tryptophan-2-monooxygenase; TNA, tryptophanase; TPHs, tryptophan hydroxylases; TrD, tryptophan decarboxylase; Trp, tryptophan; TST, tail suspension test; UHPLC-MS, ultra-high performance liquid chromatography-tandem mass spectrometry; WT, wild-type; XA, xanthurenic acid.

Availability of Data and Materials

The data presented in this study are available on request from the corresponding author.

Author Contributions

Conceptualization, ÁS, JT, EO, LV, and MT; methodology, ÁS, ZG, ES, MS, DM, KT, KO, HI, SY, and MT; software, ÁS, ES, MS, KO; validation, ÁS, ZG, ES, MS, KT, KO, and MT; formal analysis, ÁS, ZG, ES, MS, KO, and MT; investigation, ÁS, ZG, ES, MS, DM, KT, KO, and MT; resources, ÁS and EO; data curation, ÁS, ZG, ES, MS, KO; writing—original draft preparation, ÁS, ZG, MT; writing—review and editing, ÁS, ZG, ES, MS, DM, JT, EO, LV, and MT; visualization, ÁS, KO; supervision, JT, EO, LV, and MT; project administration, JT, EO, and LV; funding acquisition, JT, EO, LV, and MT. All authors have read and agreed to the published version of the manuscript. All authors contributed to editorial changes in the manuscript. All authors read and approved the final manuscript. All authors have participated sufficiently in the work and agreed to be accountable for all aspects of the work.

Ethics Approval and Consent to Participate

The study was conducted in accordance with the Regulations for Animal Experiments of Kyushu University, the Fundamental Guidelines for Proper Conduct of Animal Experiments and Related Activities in Academic Research Institutions governed by the Ministry of Education, Culture, Sports, Science, and Technology of Japan, and with the approval of the Institutional Animal Experiment Committees of Kyushu University (A29-338-1 (2018), A19-090-1 (2019)), and approved by the National Food Chain Safety Office (XI./95/2020, CS/I01/170-4/2022) and the Committee of Animal Research at the University of Szeged (I-74-10/2019, I-74-1/2022).

Acknowledgment

The authors express their gratitude to Dr. Nikolett Nánási for her chemical analysis. The figures are created with biorender.com.

Funding

This work was supported by the National Research, Development, and Innovation Office—NKFIH K138125, SZTE SZAOK-KKA No:2022/5S729, the HUN-REN Hungarian Research Network, and JSPS Joint Research Projects under Bilateral Programs Grant Number JPJSBP120203803.

Conflict of Interest

Given his role as a Guest Editor, Masaru Tanaka had no involvement in the peer-review of this article and has no access to information regarding its peer review. Full responsibility for the editorial process for this article was delegated to Thomas Heinbockel. The authors declare no conflict of interest.

References

[1] Tyng CM, Amin HU, Saad MNM, Malik AS. The Influences of Emotion on Learning and Memory. Frontiers in Psychology. 2017; 8: 1454. https://doi.org/10.3389/fpsyg.2017.01454.

[2] Battaglia S, Garofalo S, di Pellegrino G, Starita F. Revaluing the Role of vmPFC in the Acquisition of Pavlovian Threat Conditioning in Humans. The Journal of Neuroscience: the Official Journal of the Society for Neuroscience. 2020; 40: 8491–8500. https://doi.org/10.1523/JNEUROSCI.0304-20.2020.

[3] Battaglia S, Harrison BJ, Fullana MA. Does the human ventromedial prefrontal cortex support fear learning, fear extinction or both? A commentary on subregional contributions. Molecular Psychiatry. 2022; 27: 784–786. https://doi.org/10.1038/s41380-021-01326-4.

[4] Sumsuzzman DM, Choi J, Jin Y, Hong Y. Neurocognitive effects of melatonin treatment in healthy adults and individuals with Alzheimer's disease and insomnia: A systematic review and meta-analysis of randomized controlled trials. Neuroscience and Biobehavioral Reviews. 2021; 127: 459–473. https://doi.org/10.1016/j.neubiorev.2021.04.034.

[5] Borgomaneri S, Battaglia S, Sciamanna G, Tortora F, Laricchiuta D. Memories are not written in stone: Re-writing fear memories by means of non-invasive brain stimulation and optogenetic manipulations. Neuroscience and Biobehavioral Reviews. 2021; 127: 334–352. https://doi.org/10.1016/j.neubiorev.2021.04.036.

[6] Matias JN, Achete G, Campanari GSDS, Guiguer ÉL, Araújo AC, Buglio DS, *et al*. A systematic review of the antidepressant effects of curcumin: Beyond monoamines theory. The Australian and New Zealand Journal of Psychiatry. 2021; 55: 451–462. https://doi.org/10.1177/0004867421998795.

[7] Hasson U, Chen J, Honey CJ. Hierarchical process memory: memory as an integral component of information processing. Trends in Cognitive Sciences. 2015; 19: 304–313. https://doi.org/10.1016/j.tics.2015.04.006.

[8] Clewett D, Sakaki M, Nielsen S, Petzinger G, Mather M. Noradrenergic mechanisms of arousal's bidirectional effects on episodic memory. Neurobiology of Learning and Memory. 2017; 137: 1–14. https://doi.org/10.1016/j.nlm.2016.10.017.

[9] Battaglia S, Nazzi C, Thayer JF. Fear-induced bradycardia in mental disorders: Foundations, current advances, future perspectives. Neuroscience and Biobehavioral Reviews. 2023; 149: 105163. https://doi.org/10.1016/j.neubiorev.2023.105163.

[10] Battaglia S, Di Fazio C, Vicario CM, Avenanti A. Neuropharmacological Modulation of N-methyl-D-aspartate, Noradrenaline and Endocannabinoid Receptors in Fear Extinction Learning: Synaptic Transmission and Plasticity. International Journal of Molecular Sciences. 2023; 24: 5926. https://doi.org/10.3390/ijms24065926.

[11] Hayes JP, Vanelzakker MB, Shin LM. Emotion and cognition interactions in PTSD: a review of neurocognitive and neuroimaging studies. Frontiers in Integrative Neuroscience. 2012; 6: 89. https://doi.org/10.3389/fnint.2012.00089.

[12] Dillon DG, Pizzagalli DA. Mechanisms of Memory Disruption in Depression. Trends in Neurosciences. 2018; 41: 137–149. https://doi.org/10.1016/j.tins.2017.12.006.

[13] Mathews A, MacLeod C. Cognitive vulnerability to emotional disorders. Annual Review of Clinical Psychology. 2005; 1: 167–195. https://doi.org/10.1146/annurev.clinpsy.1.102803.143916.

[14] de Oliveira Zanuso B, de Oliveira Dos Santos AR, Miola VFB, Guissoni Campos LM, Spilla CSG, Barbalho SM. Panax ginseng and aging related disorders: A systematic review. Experimental Gerontology. 2022; 161: 111731. https://doi.org/10.1016/j.exger.2022.111731.

[15] Darcet F, Mendez-David I, Tritschler L, Gardier AM, Guilloux JP, David DJ. Learning and memory impairments in a neuroendocrine mouse model of anxiety/depression. Frontiers in Behavioral Neuroscience. 2014; 8: 136. https://doi.org/10.3389/fnbeh.2014.00136.

[16] Hasebe K, Kendig MD, Morris MJ. Mechanisms Underlying the Cognitive and Behavioural Effects of Maternal Obesity. Nutrients. 2021; 13: 240. https://doi.org/10.3390/nu13010240.

[17] Junges VM, Closs VE, Nogueira GM, Gottlieb MGV. Crosstalk between Gut Microbiota and Central Nervous System: A Focus on Alzheimer's Disease. Current Alzheimer Research. 2018; 15: 1179–1190. https://doi.org/10.2174/1567205015666180904155908.

[18] Guzmán-Vélez E, Feinstein JS, Tranel D. Feelings without memory in Alzheimer disease. Cognitive and Behavioral Neurology: Official Journal of the Society for Behavioral and Cognitive Neurology. 2014; 27: 117–129. https://doi.org/10.1097/WNN.0000000000000020.

[19] Mack J, Marsh L. Parkinson's Disease: Cognitive Impairment. Focus (American Psychiatric Publishing). 2017; 15: 42–54. https://doi.org/10.1176/appi.focus.20160043.

[20] Mckee AC, Daneshvar DH. The neuropathology of traumatic brain injury. Handbook of Clinical Neurology. 2015; 127: 45–66. https://doi.org/10.1016/B978-0-444-52892-6.00004-0.

[21] Li M, Feng L, Liu X, Zhang M, Fu B, Wang G, *et al*. Emotional working memory in patients with major depressive disorder. The Journal of International Medical Research. 2018; 46: 1734–1746. https://doi.org/10.1177/0300060518758225.

[22] Samuelson KW. Post-traumatic stress disorder and declarative memory functioning: a review. Dialogues in Clinical Neuroscience. 2011; 13: 346–351. https://doi.org/10.31887/DCNS.2011.13.2/ksamuelson.

[23] Dere E, Pause BM, Pietrowsky R. Emotion and episodic memory in neuropsychiatric disorders. Behavioural Brain Research. 2010; 215: 162–171. https://doi.org/10.1016/j.bbr.2010.03.017.

[24] Buglio DS, Marton LT, Laurindo LF, Guiguer EL, Araújo AC, Buchaim RL, *et al*. The Role of Resveratrol in Mild Cognitive Impairment and Alzheimer's Disease: A Systematic Review. Journal of Medicinal Food. 2022; 25: 797–806. https://doi.org/10.1089/jmf.2021.0084.

[25] Barbalho SM, Direito R, Laurindo LF, Marton LT, Guiguer EL, Goulart RDA, *et al*. *Ginkgo biloba* in the Aging Process: A

Narrative Review. Antioxidants (Basel, Switzerland). 2022; 11: 525. https://doi.org/10.3390/antiox11030525.

[26] Tanaka M, Vécsei L. Revolutionizing our understanding of Parkinson's disease: Dr. Heinz Reichmann's pioneering research and future research direction. Journal of Neural Transmission (Vienna, Austria: 1996). 2024; 10.1007/s00702–10.1007/s00702–024–02812–z. https://doi.org/10.1007/s00702-024-02812-z.

[27] Berger M, Gray JA, Roth BL. The expanded biology of serotonin. Annual Review of Medicine. 2009; 60: 355–366. https://doi.org/10.1146/annurev.med.60.042307.110802.

[28] Ressler KJ, Nemeroff CB. Role of serotonergic and noradrenergic systems in the pathophysiology of depression and anxiety disorders. Depression and Anxiety. 2000; 12 Suppl 1: 2–19. https://doi.org/10.1002/1520-6394(2000)12:1+<2::AID-DA2>3.0.CO;2-4.

[29] Bacqué-Cazenave J, Bharatiya R, Barrière G, Delbecque JP, Bouguiyoud N, Di Giovanni G, *et al*. Serotonin in Animal Cognition and Behavior. International Journal of Molecular Sciences. 2020; 21: 1649. https://doi.org/10.3390/ijms21051649.

[30] Meneses A, Liy-Salmeron G. Serotonin and emotion, learning and memory. Reviews in the Neurosciences. 2012; 23: 543–553. https://doi.org/10.1515/revneuro-2012-0060.

[31] Švob Štrac D, Pivac N, Mück-Šeler D. The serotonergic system and cognitive function. Translational Neuroscience. 2016; 7: 35–49. https://doi.org/10.1515/tnsci-2016-0007.

[32] Schmitt JAJ, Wingen M, Ramaekers JG, Evers EAT, Riedel WJ. Serotonin and human cognitive performance. Current Pharmaceutical Design. 2006; 12: 2473–2486. https://doi.org/10.2174/138161206777698909.

[33] Buhot MC, Martin S, Segu L. Role of serotonin in memory impairment. Annals of Medicine. 2000; 32: 210–221. https://doi.org/10.3109/07853890008998828.

[34] Battaglia S, Avenanti A, Vécsei L, Tanaka M. Neural Correlates and Molecular Mechanisms of Memory and Learning. International Journal of Molecular Sciences. 2024; 25: 2724. https://doi.org/10.3390/ijms25052724.

[35] Battaglia S, Cardellicchio P, Di Fazio C, Nazzi C, Fracasso A, Borgomaneri S. Stopping in (e)motion: Reactive action inhibition when facing valence-independent emotional stimuli. Frontiers in Behavioral Neuroscience. 2022; 16: 998714. https://doi.org/10.3389/fnbeh.2022.998714.

[36] Cowen P, Sherwood AC. The role of serotonin in cognitive function: evidence from recent studies and implications for understanding depression. Journal of Psychopharmacology (Oxford, England). 2013; 27: 575–583. https://doi.org/10.1177/0269881113482531.

[37] Battaglia S, Cardellicchio P, Di Fazio C, Nazzi C, Fracasso A, Borgomaneri S. The Influence of Vicarious Fear-Learning in "In-fecting" Reactive Action Inhibition. Frontiers in Behavioral Neuroscience. 2022; 16: 946263. https://doi.org/10.3389/fnbeh.2022.946263.

[38] Battaglia S, Thayer JF. Functional interplay between central and autonomic nervous systems in human fear conditioning. Trends in Neurosciences. 2022; 45: 504–506. https://doi.org/10.1016/j.tins.2022.04.003.

[39] Battaglia S, Orsolini S, Borgomaneri S, Barbieri R, Diciotti S, di Pellegrino G. Characterizing cardiac autonomic dynamics of fear learning in humans. Psychophysiology. 2022; 59: e14122. https://doi.org/10.1111/psyp.14122.

[40] Di Gregorio F, La Porta F, Petrone V, Battaglia S, Orlandi S, Ippolito G, *et al*. Accuracy of EEG Biomarkers in the Detection of Clinical Outcome in Disorders of Consciousness after Severe Acquired Brain Injury: Preliminary Results of a Pilot Study Using a Machine Learning Approach. Biomedicines. 2022; 10: 1897. https://doi.org/10.3390/biomedicines10081897.

[41] Borgomaneri S, Battaglia S, Avenanti A, Pellegrino GD. Don't Hurt Me No More: State-dependent Transcranial Magnetic Stimu-lation for the treatment of specific phobia. Journal of Affective Disorders. 2021; 286: 78–79. https://doi.org/10.1016/j.jad.2021.02.076.

[42] Khalil R, Godde B, Karim AA. The Link Between Creativity, Cognition, and Creative Drives and Underlying Neural Mechanisms. Frontiers in Neural Circuits. 2019; 13: 18. https://doi.org/10.3389/fncir.2019.00018.

[43] Borgomaneri S, Battaglia S, Garofalo S, Tortora F, Avenanti A, di Pellegrino G. State-Dependent TMS over Prefrontal Cortex Disrupts Fear-Memory Reconsolidation and Prevents the Return of Fear. Current Biology: CB. 2020; 30: 3672–3679.e4. https://doi.org/10.1016/j.cub.2020.06.091.

[44] Battaglia S, Garofalo S, di Pellegrino G. Context-dependent extinction of threat memories: influences of healthy aging. Scientific Reports. 2018; 8: 12592. https://doi.org/10.1038/s41598-018-31000-9.

[45] Albert PR, Vahid-Ansari F, Luckhart C. Serotonin-prefrontal cortical circuitry in anxiety and depression phenotypes: pivotal role of pre- and post-synaptic 5-HT1A receptor expression. Frontiers in Behavioral Neuroscience. 2014; 8: 199. https://doi.org/10.3389/fnbeh.2014.00199.

[46] Tortora F, Hadipour AL, Battaglia S, Falzone A, Avenanti A, Vicario CM. The Role of Serotonin in Fear Learning and Memory: A Systematic Review of Human Studies. Brain Sciences. 2023; 13: 1197. https://doi.org/10.3390/brainsci13081197.

[47] Brewerton TD. Toward a unified theory of serotonin dysregulation in eating and related disorders. Psychoneuroendocrinology. 1995; 20: 561–590. https://doi.org/10.1016/0306-4530(95)00001-5.

[48] Savitz J, Lucki I, Drevets WC. 5-HT(1A) receptor function in major depressive disorder. Progress in Neurobiology. 2009; 88: 17–31. https://doi.org/10.1016/j.pneurobio.2009.01.009.

[49] Nutt DJ. Neurobiological mechanisms in generalized anxiety disorder. The Journal of Clinical Psychiatry. 2001; 62 Suppl 11: 22–27; discussion 28.

[50] Steiger H. Eating disorders and the serotonin connection: state, trait and developmental effects. Journal of Psychiatry & Neuroscience: JPN. 2004; 29: 20–29.

[51] Meltzer HY, Li Z, Kaneda Y, Ichikawa J. Serotonin receptors: their key role in drugs to treat schizophrenia. Progress in Neuro-psychopharmacology & Biological Psychiatry. 2003; 27: 1159–1172. https://doi.org/10.1016/j.pnpbp.2003.09.010.

[52] Kelmendi B, Adams TG, Yarnell S, Southwick S, Abdallah CG, Krystal JH. PTSD: from neurobiology to pharmacological treatments. European Journal of Psychotraumatology. 2016; 7: 31858. https://doi.org/10.3402/ejpt.v7.31858.

[53] Chu A, Wadhwa R. Selective Serotonin Reuptake Inhibitors. [Updated 2022 May 8]. StatPearls [Internet] Treasure Island (FL): StatPearls Publishing. 2022.

[54] Alvares GA, Quintana DS, Hickie IB, Guastella AJ. Autonomic nervous system dysfunction in psychiatric disorders and the impact of psychotropic medications: a systematic review and meta-analysis. Journal of Psychiatry & Neuroscience: JPN. 2016; 41: 89–104. https://doi.org/10.1503/jpn.140217.

[55] Stahl SM, Lee-Zimmerman C, Cartwright S, Morrissette DA. Serotonergic drugs for depression and beyond. Current Drug Targets. 2013; 14: 578–585. https://doi.org/10.2174/1389450111314050007.

[56] Teleanu RI, Niculescu AG, Roza E, Vladâcenco O, Grumezescu AM, Teleanu DM. Neurotransmitters-Key Factors in Neurological and Neurodegenerative Disorders of the Central Nervous System. International Journal of Molecular Sciences. 2022; 23: 5954. https://doi.org/10.3390/ijms23115954.

[57] Liu Y, Zhao J, Guo W. Emotional Roles of Mono-Aminergic

Neurotransmitters in Major Depressive Disorder and Anxiety Dis-orders. Frontiers in Psychology. 2018; 9: 2201. https://doi.org/10.3389/fpsyg.2018.02201.

[58] Nutt DJ. The role of dopamine and norepinephrine in depression and antidepressant treatment. The Journal of Clinical Psychiatry. 2006; 67 Suppl 6: 3–8.

[59] Muneer A. Kynurenine Pathway of Tryptophan Metabolism in Neuropsychiatric Disorders: Pathophysiologic and Therapeutic Considerations. Clinical Psychopharmacology and Neuroscience: the Official Scientific Journal of the Korean College of Neuropsycho-pharmacology. 2020; 18: 507–526. https://doi.org/10.9758/cpn.2020.18.4.507.

[60] Tanaka M, Szabó Á, Vécsei L. Redefining Roles: A Paradigm Shift in Tryptophan–Kynurenine Metabolism for Inno-vative Clinical Applications. International Journal of Molecular Sciences. 2024; 25: 12767. https://doi.org/10.3390/ijms252312767

[61] Huang Y, Zhao M, Chen X, Zhang R, Le A, Hong M, *et al*. Tryptophan Metabolism in Central Nervous System Diseases: Pathophysiology and Potential Therapeutic Strategies. Aging and Disease. 2023; 14: 858–878. https://doi.org/10.14336/AD.2022.0916.

[62] Polyák H, Galla Z, Nánási N, Cseh EK, Rajda C, Veres G, *et al*. The Tryptophan-Kynurenine Metabolic System Is Suppressed in Cuprizone-Induced Model of Demyelination Simulating Progressive Multiple Sclerosis. Biomedicines. 2023; 11: 945. https://doi.org/10.3390/biomedicines11030945.

[63] Ye X, Li H, Anjum K, Zhong X, Miao S, Zheng G, *et al*. Dual Role of Indoles Derived From Intestinal Microbiota on Human Health. Frontiers in Immunology. 2022; 13: 903526. https://doi.org/10.3389/fimmu.2022.903526.

[64] Li X, Zhang B, Hu Y, Zhao Y. New Insights Into Gut-Bacteria-Derived Indole and Its Derivatives in Intestinal and Liver Diseases. Frontiers in Pharmacology. 2021; 12: 769501. https://doi.org/10.3389/fphar.2021.769501.

[65] Jones AW. Brief history of the alcohol biomarkers CDT, EtG, EtS, 5-HTOL, and PEth. Drug Testing and Analysis. 2024; 16: 570–587. https://doi.org/10.1002/dta.3584.

[66] Höglund E, Øverli Ø, Winberg S. Tryptophan Metabolic Pathways and Brain Serotonergic Activity: A Comparative Review. Frontiers in Endocrinology. 2019; 10: 158. https://doi.org/10.3389/fendo.2019.00158.

[67] Jayamohananan H, Manoj Kumar MK, T P A. 5-HIAA as a Potential Biological Marker for Neurological and Psychiatric Disorders. Advanced Pharmaceutical Bulletin. 2019; 9: 374–381. https://doi.org/10.15171/apb.2019.044.

[68] Hardeland R. Melatonin metabolism in the central nervous system. Current Neuropharmacology. 2010; 8: 168–181. https://doi.org/10.2174/157015910792246244.

[69] Granado MDJ, Pinato L, Santiago J, Barbalho SM, Parmezzan JEL, Suzuki LM, *et al*. Melatonin receptors and Per1 expression in the inferior olivary nucleus of the *Sapajus apella* monkey. Frontiers in Neuroscience. 2022; 16: 1072772. https://doi.org/10.3389/fnins.2022.1072772.

[70] Ishidoh K, Kamemura N, Imagawa T, Oda M, Sakurai J, Katunuma N. Quinolinate phosphoribosyl transferase, a key enzyme in de novo NAD(+) synthesis, suppresses spontaneous cell death by inhibiting overproduction of active-caspase-3. Biochimica et Biophysica Acta. 2010; 1803: 527–533. https://doi.org/10.1016/j.bbamcr.2010.02.007.

[71] Raffaelli N, Sorci L, Amici A, Emanuelli M, Mazzola F, Magni G. Identification of a novel human nicotinamide mononucleotide adenylyltransferase. Biochemical and Biophysical Research Communications. 2002; 297: 835–840. https://doi.org/10.1016/s0006-291x(02)02285-4.

[72] Jauch R, Humm A, Huber R, Wahl MC. Structures of Escherichia coli NAD synthetase with substrates and products reveal mechanistic rearrangements. The Journal of Biological Chemistry. 2005; 280: 15131–15140. https://doi.org/10.1074/jbc.M413195200.

[73] Tanaka M, Tóth F, Polyák H, Szabó Á, Mándi Y, Vécsei L. Immune Influencers in Action: Metabolites and Enzymes of the Tryptophan-Kynurenine Metabolic Pathway. Biomedicines. 2021; 9: 734. https://doi.org/10.3390/biomedicines9070734.

[74] Tanaka M, Szabó Á, Spekker E, Polyák H, Tóth F, Vécsei L. Mitochondrial Impairment: A Common Motif in Neuropsychiatric Presentation? The Link to the Tryptophan-Kynurenine Metabolic System. Cells. 2022; 11: 2607. https://doi.org/10.3390/cells11162607.

[75] Fila M, Chojnacki J, Pawlowska E, Szczepanska J, Chojnacki C, Blasiak J. Kynurenine Pathway of Tryptophan Metabolism in Migraine and Functional Gastrointestinal Disorders. International Journal of Molecular Sciences. 2021; 22: 10134. https://doi.org/10.3390/ijms221810134.

[76] Wirthgen E, Hoeflich A, Rebl A, Günther J. Kynurenic Acid: The Janus-Faced Role of an Immunomodulatory Tryptophan Metabolite and Its Link to Pathological Conditions. Frontiers in Immunology. 2018; 8: 1957. https://doi.org/10.3389/fimmu.2017.01957.

[77] Takahashi H, Price JM. Dehydroxylation of xanthurenic acid to 8-hydroxy-quinaldic acid. The Journal of Biological Chemistry. 1958; 233: 150–153.

[78] Walczak K, Langner E, Szalast K, Makuch-Kocka A, Pożarowski P, Plech T. A Tryptophan Metabolite, 8-Hydroxyquinaldic Acid, Exerts Antiproliferative and Anti-Migratory Effects on Colorectal Cancer Cells. Molecules (Basel, Switzerland). 2020; 25: 1655. https://doi.org/10.3390/molecules25071655.

[79] Espi M, Koppe L, Fouque D, Thaunat O. Chronic Kidney Disease-Associated Immune Dysfunctions: Impact of Protein-Bound Uremic Retention Solutes on Immune Cells. Toxins. 2020; 12: 300. https://doi.org/10.3390/toxins12050300.

[80] Mishra P, Kaur S, Sharma AN, Jolly RS. Characterization of an Indole-3-Acetamide Hydrolase from Alcaligenes faecalis subsp. parafaecalis and Its Application in Efficient Preparation of Both Enantiomers of Chiral Building Block 2,3-Dihydro-1,4-Benzodioxin-2-Carboxylic Acid. PloS One. 2016; 11: e0159009. https://doi.org/10.1371/journal.pone.0159009.

[81] Mousseau DD. Tryptamine: a metabolite of tryptophan implicated in various neuropsychiatric disorders. Metabolic Brain Disease. 1993; 8: 1–44. https://doi.org/10.1007/BF01000528.

[82] Brydges CR, Fiehn O, Mayberg HS, Schreiber H, Dehkordi SM, Bhattacharyya S, *et al*. Indoxyl sulfate, a gut micro-biome-derived uremic toxin, is associated with psychic anxiety and its functional magnetic resonance imaging-based neurologic signature. Scientific Reports. 2021; 11: 21011. https://doi.org/10.1038/s41598-021-99845-1.

[83] Hou Y, Li J, Ying S. Tryptophan Metabolism and Gut Microbiota: A Novel Regulatory Axis Integrating the Microbiome, Immunity, and Cancer. Metabolites. 2023; 13: 1166. https://doi.org/10.3390/metabo13111166.

[84] Hubková B, Valko-Rokytovská M, Čižmárová B, Zábavníková M, Mareková M, Birková A. Tryptophan: Its Metabolism along the Kynurenine, Serotonin, and Indole Pathway in Malignant Melanoma. International Journal of Molecular Sciences. 2022; 23: 9160. https://doi.org/10.3390/ijms23169160.

[85] Mor A, Tankiewicz-Kwedlo A, Krupa A, Pawlak D. Role of Kynurenine Pathway in Oxidative Stress during Neurodegenerative Disorders. Cells. 2021; 10: 1603. https://doi.org/10.3390/cells10071603.

[86] Bosi A, Banfi D, Bistoletti M, Giaroni C, Baj A. Tryptophan Metabolites Along the Microbiota-Gut-Brain Axis: An Interkingdom Communication System Influencing the Gut in Health

and Disease. International Journal of Tryptophan Research: IJTR. 2020; 13: 1178646920928984. https://doi.org/10.1177/1178646920928984.

[87] Roth W, Zadeh K, Vekariya R, Ge Y, Mohamadzadeh M. Tryptophan metabolism and gut-brain homeostasis. Inter-national journal of molecular sciences. 2021; 22: 2973. https://doi.org/10.3390/ijms22062973.

[88] Laurindo LF, Santos ARDOD, Carvalho ACAD, Bechara MD, Guiguer EL, Goulart RDA, *et al*. Phytochemicals and Regulation of NF-kB in Inflammatory Bowel Diseases: An Overview of In Vitro and In Vivo Effects. Metabolites. 2023; 13: 96. https://doi.org/10.3390/metabo13010096.

[89] Réus GZ, Jansen K, Titus S, Carvalho AF, Gabbay V, Quevedo J. Kynurenine pathway dysfunction in the pathophysiology and treatment of depression: Evidences from animal and human studies. Journal of Psychiatric Research. 2015; 68: 316–328. https://doi.org/10.1016/j.jpsychires.2015.05.007.

[90] Gao J, Xu K, Liu H, Liu G, Bai M, Peng C, *et al*. Impact of the Gut Microbiota on Intestinal Immunity Mediated by Tryptophan Metabolism. Frontiers in Cellular and Infection Microbiology. 2018; 8: 13. https://doi.org/10.3389/fcimb.2018.00013.

[91] Ranhotra HS. Discrete interplay of gut microbiota L-tryptophan metabolites in host biology and disease. Molecular and Cellular Biochemistry. 2024; 479: 2273–2290. https://doi.org/10.1007/s11010-023-04867-0.

[92] Hyland NP, Cavanaugh CR, Hornby PJ. Emerging effects of tryptophan pathway metabolites and intestinal microbiota on metabolism and intestinal function. Amino Acids. 2022; 54: 57–70. https://doi.org/10.1007/s00726-022-03123-x.

[93] Kumar P, Lee JH, Lee J. Diverse roles of microbial indole compounds in eukaryotic systems. Biological Reviews of the Cambridge Philosophical Society. 2021; 96: 2522–2545. https://doi.org/10.1111/brv.12765.

[94] Su X, Gao Y, Yang R. Gut Microbiota-Derived Tryptophan Metabolites Maintain Gut and Systemic Homeostasis. Cells. 2022; 11: 2296. https://doi.org/10.3390/cells11152296.

[95] Gasaly N, de Vos P, Hermoso MA. Impact of Bacterial Metabolites on Gut Barrier Function and Host Immunity: A Focus on Bacterial Metabolism and Its Relevance for Intestinal Inflammation. Frontiers in Immunology. 2021; 12: 658354. https://doi.org/10.3389/fimmu.2021.658354.

[96] Hubbard TD, Murray IA, Perdew GH. Indole and Tryptophan Metabolism: Endogenous and Dietary Routes to Ah Receptor Activation. Drug Metabolism and Disposition: the Biological Fate of Chemicals. 2015; 43: 1522–1535. https://doi.org/10.1124/dmd.115.064246.

[97] Fu Y, Lyu J, Wang S. The role of intestinal microbes on intestinal barrier function and host immunity from a metabolite perspective. Frontiers in Immunology. 2023; 14: 1277102. https://doi.org/10.3389/fimmu.2023.1277102.

[98] Fornari Laurindo L, Aparecido Dias J, Cressoni Araújo A, Torres Pomini K, Machado Galhardi C, Rucco Penteado Detregiachi C, *et al*. Immunological dimensions of neuroinflammation and microglial activation: exploring innovative immunomodulatory ap-proaches to mitigate neuroinflammatory progression. Frontiers in Immunology. 2024; 14: 1305933. https://doi.org/10.3389/fimmu.2023.1305933.

[99] Madella AM, Van Bergenhenegouwen J, Garssen J, Masereeuw R, Overbeek SA. Microbial-Derived Tryptophan Catabolites, Kidney Disease and Gut Inflammation. Toxins. 2022; 14: 645. https://doi.org/10.3390/toxins14090645.

[100] Barbalho SM, Goulart RDA, Araújo AC, Guiguer ÉL, Bechara MD. Irritable bowel syndrome: a review of the general aspects and the potential role of vitamin D. Expert Review of Gastroenterology & Hepatology. 2019; 13: 345–359. https://doi.org/10.1080/17474124.2019.1570137.

[101] Carpi RZ, Barbalho SM, Sloan KP, Laurindo LF, Gonzaga HF, Grippa PC, *et al*. The Effects of Probiotics, Prebiotics and Synbiotics in Non-Alcoholic Fat Liver Disease (NAFLD) and Non-Alcoholic Steatohepatitis (NASH): A Systematic Review. International Journal of Molecular Sciences. 2022; 23: 8805. https://doi.org/10.3390/ijms23158805.

[102] Marton LT, Goulart RDA, Carvalho ACAD, Barbalho SM. Omega Fatty Acids and Inflammatory Bowel Diseases: An Overview. International Journal of Molecular Sciences. 2019; 20: 4851. https://doi.org/10.3390/ijms20194851.

[103] Laurindo LF, Direito R, Bueno Otoboni AM, Goulart RA, Quesada K, Barbalho SM. Grape processing waste: effects on inflammatory bowel disease and colorectal cancer. Food Reviews International. 2024; 40: 336–369.

[104] Sun LJ, Li JN, Nie YZ. Gut hormones in microbiota-gut-brain cross-talk. Chinese Medical Journal. 2020; 133: 826–833. https://doi.org/10.1097/CM9.0000000000000706.

[105] Mittal R, Debs LH, Patel AP, Nguyen D, Patel K, O'Connor G, *et al*. Neurotransmitters: The Critical Modulators Regulating Gut-Brain Axis. Journal of Cellular Physiology. 2017; 232: 2359–2372. https://doi.org/10.1002/jcp.25518.

[106] Tran SMS, Mohajeri MH. The Role of Gut Bacterial Metabolites in Brain Development, Aging and Disease. Nutrients. 2021; 13: 732. https://doi.org/10.3390/nu13030732.

[107] Han Y, Wang B, Gao H, He C, Hua R, Liang C, *et al*. Vagus Nerve and Underlying Impact on the Gut Microbiota-Brain Axis in Behavior and Neurodegenerative Diseases. Journal of Inflammation Research. 2022; 15: 6213–6230. https://doi.org/10.2147/JIR.S384949.

[108] Gershon MD, Margolis KG. The gut, its microbiome, and the brain: connections and communications. The Journal of Clinical Investigation. 2021; 131: e143768. https://doi.org/10.1172/JCI143768.

[109] Caspani G, Swann J. Small talk: microbial metabolites involved in the signaling from microbiota to brain. Current Opinion in Pharmacology. 2019; 48: 99–106. https://doi.org/10.1016/j.coph.2019.08.001.

[110] Zhou Y, Chen Y, He H, Peng M, Zeng M, Sun H. The role of the indoles in microbiota-gut-brain axis and potential therapeutic targets: A focus on human neurological and neuropsychiatric diseases. Neuropharmacology. 2023; 239: 109690. https://doi.org/10.1016/j.neuropharm.2023.109690.

[111] Caspani G, Kennedy S, Foster JA, Swann J. Gut microbial metabolites in depression: understanding the biochemical mechanisms. Microbial Cell (Graz, Austria). 2019; 6: 454–481. https://doi.org/10.15698/mic2019.10.693.

[112] Chernikova MA, Flores GD, Kilroy E, Labus JS, Mayer EA, Aziz-Zadeh L. The Brain-Gut-Microbiome System: Pathways and Implications for Autism Spectrum Disorder. Nutrients. 2021; 13: 4497. https://doi.org/10.3390/nu13124497.

[113] Ju S, Shin Y, Han S, Kwon J, Choi TG, Kang I, *et al*. The Gut-Brain Axis in Schizophrenia: The Implications of the Gut Microbiome and SCFA Production. Nutrients. 2023; 15: 4391. https://doi.org/10.3390/nu15204391.

[114] Pappolla MA, Perry G, Fang X, Zagorski M, Sambamurti K, Poeggeler B. Indoles as essential mediators in the gut-brain axis. Their role in Alzheimer's disease. Neurobiology of Disease. 2021; 156: 105403. https://doi.org/10.1016/j.nbd.2021.105403.

[115] Direito R, Barbalho SM, Sepodes B, Figueira ME. Plant-Derived Bioactive Compounds: Exploring Neuroprotective, Metabolic, and Hepatoprotective Effects for Health Promotion and Disease Prevention. Pharmaceutics. 2024; 16: 577. https://doi.org/10.3390/pharmaceutics16050577.

[116] Valotto Neto LJ, Reverete de Araujo M, Moretti Junior RC, Mendes Machado N, Joshi RK, Dos Santos Buglio D, *et al*. Investigating the Neuroprotective and Cognitive-Enhancing Ef-

fects of *Bacopa monnieri*: A Systematic Review Focused on Inflammation, Oxidative Stress, Mitochondrial Dysfunction, and Apoptosis. Antioxidants (Basel, Switzerland). 2024; 13: 393. https://doi.org/10.3390/antiox13040393.

[117] Tanaka M, Bohár Z, Martos D, Telegdy G, Vécsei L. Antidepressant-like effects of kynurenic acid in a modified forced swim test. Pharmacological Reports: PR. 2020; 72: 449–455. https://doi.org/10.1007/s43440-020-00067-5.

[118] Martos D, Tuka B, Tanaka M, Vécsei L, Telegdy G. Memory Enhancement with Kynurenic Acid and Its Mechanisms in Neuro-transmission. Biomedicines. 2022; 10: 849. https://doi.org/10.3390/biomedicines10040849.

[119] Goh DLM, Patel A, Thomas GH, Salomons GS, Schor DSM, Jakobs C, *et al*. Characterization of the human gene encoding alpha-aminoadipate aminotransferase (AADAT). Molecular Genetics and Metabolism. 2002; 76: 172–180. https://doi.org/10.1016/s1096-7192(02)00037-9.

[120] Modoux M, Rolhion N, Mani S, Sokol H. Tryptophan Metabolism as a Pharmacological Target. Trends in Pharmacological Sciences. 2021; 42: 60–73. https://doi.org/10.1016/j.tips.2020.11.006.

[121] Machado-Vieira R, Zarate Jr CA. Proof of concept trials in bipolar disorder and major depressive disorder: a transla-tional per-spective in the search for improved treatments. Depression and anxiety. 2011; 28: 267–281.https://doi.org/10.1002/da.20800.

[122] Tanaka M, Telegdy G. Involvement of adrenergic and serotonergic receptors in antidepressant-like effect of urocortin 3 in a modified forced swimming test in mice. Brain Research Bulletin. 2008; 77: 301–305. https://doi.org/10.1016/j.brainresbull.2008.08.012.

[123] Tanaka M, Schally AV, Telegdy G. Neurotransmission of the antidepressant-like effects of the growth hormone-releasing hormone antagonist MZ-4-71. Behavioural Brain Research. 2012; 228: 388–391. https://doi.org/10.1016/j.bbr.2011.12.022.

[124] Kaiser T, Feng G. Modeling psychiatric disorders for developing effective treatments. Nature medicine. 2015; 21: 979–988. https://doi.org/10.1038/nm.3935.

[125] Zucker NL, Strauss GP, Smyth JM, Scherf KS, Brotman MA, Boyd RC, *et al*. Experimental therapeutics: Opportunities and challenges stemming from the national institute of mental health workshop on novel target discovery and psychosocial intervention devel-opment. Perspectives on Psy-chological Science. 2023; 24: 17456916231197980. https://doi.org/10.1177/17456916231197980.

[126] Rákosi K, Masaru T, Zarándia M, Telegdy G, Tóth GK. Short analogs and mimetics of human urocortin 3 display antidepressant effects in vivo. Peptides. 2014; 62: 59–66. https://doi.org/10.1016/j.peptides.2014.09.023.

[127] Tanaka M, Vécsei L. Editorial of Special Issue 'Dissecting Neurological and Neuropsychiatric Diseases: Neurodegeneration and Neuroprotection'. International Journal of Molecular Sciences. 2022; 23: 6991. https://doi.org/10.3390/ijms23136991.

[128] Uliana DL, Zhu X, Gomes FV, Grace AA. Using animal models for the studies of schizophrenia and depression: The value of translational models for treatment and prevention. Frontiers in Behavioral Neuroscience. 2022; 16: 935320. https://doi.org/10.3389/fnbeh.2022.935320.

[129] Tanaka M, Szabó Á, Vécsei L. Integrating Armchair, Bench, and Bedside Research for Behavioral Neurology and Neuropsychiatry: Editorial. Biomedicines. 2022; 10: 2999. https://doi.org/10.3390/biomedicines10122999.

[130] Tanaka M, Kádár K, Tóth G, Telegdy G. Antidepressant-like effects of urocortin 3 fragments. Brain Research Bulletin. 2011; 84: 414–418. https://doi.org/10.1016/j.brainresbull.2011.01.016.

[131] Telegdy G, Adamik A, Tanaka M, Schally AV. Effects of the LHRH antagonist Cetrorelix on affective and cognitive functions in rats. Regulatory Peptides. 2010; 159: 142–147. https://doi.org/10.1016/j.regpep.2009.08.005.

[132] Milton AL. Editorial introduction: animal models relevant to mental health disorders. Emerging Topics in Life Sci-ences. 2022; 6: 441–443. https://doi.org/10.1042/ETLS20220094.

[133] Song J, Kim YK. Animal models for the study of depressive disorder. CNS neuroscience & therapeutics. 2021; 27: 633–642. https://doi.org/10.1111/cns.13622.

[134] Bale TL, Abel T, Akil H, Carlezon Jr WA, Moghaddam B, Nestler EJ, Ressler KJ, Thompson SM. The critical im-portance of basic animal research for neuropsychiatric disorders. Neuropsychopharmacology. 2019; 44: 1349–1353. https://doi.org/10.1038/s41386-019-0405-9.

[135] Bueno CRDS, Tonin MCC, Buchaim DV, Barraviera B, Ferreira Junior RS, Santos PSDS, *et al*. Morphofunctional Improvement of the Facial Nerve and Muscles with Repair Using Heterologous Fibrin Biopolymer and Photobiomodulation. Pharmaceuticals (Basel, Switzerland). 2023; 16: 653. https://doi.org/10.3390/ph16050653.

[136] Białoń M, Wąsik A. Advantages and limitations of animal schizophrenia models. International Journal of Molecular Sciences. 2022; 23: 5968. https://doi.org/10.3390/ijms23115968.

[137] Tanaka M, Szabó Á, Vécsei L, Giménez-Llort L. Emerging Translational Research in Neurological and Psychiatric Diseases: From In Vitro to In Vivo Models. International Journal of Molecular Sciences. 2023; 24: 15739. https://doi.org/10.3390/ijms242115739.

[138] Datki Z, Sinka R. Translational biomedicine-oriented exploratory research on bioactive rotifer-specific biopolymers. Advances in Clinical and Experimental Medicine: Official Organ Wroclaw Medical University. 2022; 31: 931–935. https://doi.org/10.17219/acem/152430.

[139] Villanueva R. Advances in the knowledge and therapeutics of schizophrenia, major depression disorder, and bipolar disorder from human brain organoid research. Frontiers in Psychiatry. 2023; 14: 1178494. https://doi.org/10.3389/fpsyt.2023.1178494.

[140] Chen B, Hasan MM, Zhang H, Zhai Q, Waliullah ASM, Ping Y, *et al*. UBL3 Interacts with Alpha-Synuclein in Cells and the Interaction Is Downregulated by the EGFR Pathway Inhibitor Osimertinib. Biomedicines. 2023; 11: 1685. https://doi.org/10.3390/biomedicines11061685.

[141] Song A, Cho GW, Vijayakumar KA, Moon C, Ang MJ, Kim J, *et al*. Neuroprotective Effect of Valproic Acid on Salic-ylate-Induced Tinnitus. International Journal of Molecular Sciences. 2021; 23: 23. https://doi.org/10.3390/ijms23010023.

[142] Ibos KE, Bodnár É, Bagosi Z, Bozsó Z, Tóth G, Szabó G, *et al*. Kisspeptin-8 Induces Anxiety-Like Behavior and Hy-polocomotion by Activating the HPA Axis and Increasing GABA Release in the Nucleus Accumbens in Rats. Biomedicines. 2021; 9: 112. https://doi.org/10.3390/biomedicines9020112.

[143] Puri S, Kenyon BM, Hamrah P. Immunomodulatory Role of Neuropeptides in the Cornea. Biomedicines. 2022; 10: 1985. https://doi.org/10.3390/biomedicines10081985.

[144] Mirchandani-Duque M, Barbancho MA, López-Salas A, Alvarez-Contino JE, García-Casares N, Fuxe K, *et al*. Galanin and Neuropeptide Y Interaction Enhances Proliferation of Granule Precursor Cells and Expression of Neuroprotective Factors in the Rat Hip-pocampus with Consequent Augmented Spatial Memory. Biomedicines. 2022; 10: 1297. https://doi.org/10.3390/biomedicines10061297.

[145] Taschereau-Dumouchel V, Michel M, Lau H, Hofmann SG,

LeDoux JE. Putting the “mental” back in “mental disorders”: a perspective from research on fear and anxiety. Molecular Psychiatry. 2022; 27: 1322–1330. https://doi.org/10.1038/s41380-021-01395-5.

[146] Li J, Li C, Subedi P, Tian X, Lu X, Miriyala S, *et al*. Light Alcohol Consumption Promotes Early Neurogenesis Following Ischemic Stroke in Adult C57BL/6J Mice. Biomedicines. 2023; 11: 1074. https://doi.org/10.3390/biomedicines11041074.

[147] Petković A, Chaudhury D. Encore: Behavioural animal models of stress, depression and mood disorders. Frontiers in Behavioral Neuroscience. 2022; 16: 931964. https://doi.org/10.3389/fnbeh.2022.931964.

[148] Bahor Z, Nunes-Fonseca C, Thomson LDG, Sena ES, Macleod MR. Improving our understanding of the *in vivo* modelling of psychotic disorders: A protocol for a systematic review and meta-analysis. Evidence-based Preclinical Medicine. 2016; 3: e00022. https://doi.org/10.1002/ebm2.22.

[149] Tanaka M, Spekker E, Szabó Á, Polyák H, Vécsei L. Modelling the neurodevelopmental pathogenesis in neuropsychiatric disorders. Bioactive kynurenines and their analogues as neuroprotective agents-in celebration of 80th birthday of Professor Peter Riederer. Journal of Neural Transmission (Vienna, Austria: 1996). 2022; 129: 627–642. https://doi.org/10.1007/s00702-022-02513-5.

[150] Sobolewska-Nowak J, Wachowska K, Nowak A, Orzechowska A, Szulc A, Płaza O, *et al*. Exploring the Heart-Mind Connection: Unraveling the Shared Pathways between Depression and Cardiovascular Diseases. Biomedicines. 2023; 11: 1903. https://doi.org/10.3390/biomedicines11071903.

[151] Tug E, Fidan I, Bozdayi G, Yildirim F, Tunccan OG, Lale Z, *et al*. The relationship between the clinical course of SARS-CoV-2 infections and ACE2 and TMPRSS2 expression and polymorphisms. Advances in Clinical and Experimental Medicine: Official Organ Wroclaw Medical University. 2024; 33: 39–51. https://doi.org/10.17219/acem/163409.

[152] Fan P, Miranda O, Qi X, Kofler J, Sweet RA, Wang L. Unveiling the Enigma: Exploring Risk Factors and Mechanisms for Psychotic Symptoms in Alzheimer’s Disease through Electronic Medical Records with Deep Learning Models. Pharmaceuticals (Basel, Switzerland). 2023; 16: 911. https://doi.org/10.3390/ph16070911.

[153] Festa F, Medori S, Macrì M. Move Your Body, Boost Your Brain: The Positive Impact of Physical Activity on Cognition across All Age Groups. Biomedicines. 2023; 11: 1765. https://doi.org/10.3390/biomedicines11061765.

[154] Alhaddad A, Radwan A, Mohamed NA, Mehanna ET, Mostafa YM, El-Sayed NM, *et al*. Rosiglitazone Mitigates Dexamethasone-Induced Depression in Mice via Modulating Brain Glucose Metabolism and AMPK/mTOR Signaling Pathway. Biomedi-cines. 2023; 11: 860. https://doi.org/10.3390/biomedicines11030860.

[155] Statsenko Y, Habuza T, Smetanina D, Simiyu GL, Meribout S, King FC, *et al*. Unraveling Lifelong Brain Morphometric Dynamics: A Protocol for Systematic Review and Meta-Analysis in Healthy Neurodevelopment and Ageing. Biomedicines. 2023; 11: 1999. https://doi.org/10.3390/biomedicines11071999.

[156] Dang J, Tao Q, Niu X, Zhang M, Gao X, Yang Z, *et al*. Meta-Analysis of Structural and Functional Brain Abnormalities in Cocaine Addiction. Frontiers in Psychiatry. 2022; 13: 927075. https://doi.org/10.3389/fpsyt.2022.927075.

[157] Okanda Nyatega C, Qiang L, Jajere Adamu M, Bello Kawuwa H. Altered striatal functional connectivity and structural dysconnectivity in individuals with bipolar disorder: A resting state magnetic resonance imaging study. Frontiers in Psychiatry. 2022; 13: 1054380. https://doi.org/10.3389/fpsyt.2022.1054380.

[158] Du H, Yang B, Wang H, Zeng Y, Xin J, Li X. The non-linear correlation between the volume of cerebral white matter lesions and incidence of bipolar disorder: A secondary analysis of data from a cross-sectional study. Frontiers in Psychiatry. 2023; 14: 1149663. https://doi.org/10.3389/fpsyt.2023.1149663.

[159] Chen Y, Yu R, DeSouza JFX, Shen Y, Zhang H, Zhu C, *et al*. Differential responses from the left postcentral gyrus, right middle frontal gyrus, and precuneus to meal ingestion in patients with functional dyspepsia. Frontiers in Psychiatry. 2023; 14: 1184797. https://doi.org/10.3389/fpsyt.2023.1184797.

[160] Adamu MJ, Qiang L, Nyatega CO, Younis A, Kawuwa HB, Jabire AH, *et al*. Unraveling the pathophysiology of schizophrenia: insights from structural magnetic resonance imaging studies. Frontiers in Psychiatry. 2023; 14: 1188603. https://doi.org/10.3389/fpsyt.2023.1188603.

[161] Chang CH, Wang WL, Shieh YH, Peng HY, Ho CS, Tsai HC. Case Report: Low-Frequency Repetitive Transcranial Magnetic Stimulation to Dorsolateral Prefrontal Cortex and Auditory Cortex in a Patient With Tinnitus and Depression. Frontiers in Psychiatry. 2022; 13: 847618. https://doi.org/10.3389/fpsyt.2022.847618.

[162] Zakia H, Iskandar S. Case report: Depressive disorder with peripartum onset camouflages suspected intracranial tuberculoma. Frontiers in Psychiatry. 2022; 13: 932635. https://doi.org/10.3389/fpsyt.2022.932635.

[163] Nyatega CO, Qiang L, Adamu MJ, Kawuwa HB. Gray matter, white matter and cerebrospinal fluid abnormalities in Parkinson’s disease: A voxel-based morphometry study. Frontiers in Psychiatry. 2022; 13: 1027907. https://doi.org/10.3389/fpsyt.2022.1027907.

[164] Rymaszewska J, Wieczorek T, Fila-Witecka K, Smarzewska K, Weiser A, Piotrowski P, *et al*. Various neuromodulation methods including Deep Brain Stimulation of the medial forebrain bundle combined with psychopharmacotherapy of treatment-resistant depression-Case report. Frontiers in Psychiatry. 2023; 13: 1068054. https://doi.org/10.3389/fpsyt.2022.1068054.

[165] Kim BH, Kim SH, Han C, Jeong HG, Lee MS, Kim J. Antidepressant-induced mania in panic disorder: a single-case study of clinical and functional connectivity characteristics. Frontiers in Psychiatry. 2023; 14: 1205126. https://doi.org/10.3389/fpsyt.2023.1205126.

[166] Zhou J, Cao Y, Deng G, Fang J, Qiu C. Transient splenial lesion syndrome in bipolar-II disorder: a case report highlighting reversible brain changes during hypomanic episodes. Frontiers in Psychiatry. 2023; 14: 1219592. https://doi.org/10.3389/fpsyt.2023.1219592.

[167] Veldema J. Non-Invasive Brain Stimulation and Sex/Polypeptide Hormones in Reciprocal Interactions: A Systematic Review. Biomedicines. 2023; 11: 1981. https://doi.org/10.3390/biomedicines11071981.

[168] Manuello J, Costa T, Cauda F, Liloia D. Six actions to improve detection of critical features for neuroimaging coordinate-based meta-analysis preparation. Neuroscience and Biobehavioral Reviews. 2022; 137: 104659. https://doi.org/10.1016/j.neubiorev.2022.104659.

[169] Nani A, Manuello J, Mancuso L, Liloia D, Costa T, Vercelli A, *et al*. The pathoconnectivity network analysis of the insular cortex: A morphometric fingerprinting. NeuroImage. 2021; 225: 117481. https://doi.org/10.1016/j.neuroimage.2020.117481.

[170] Liloia D, Crocetta A, Cauda F, Duca S, Costa T, Manuello J. Seeking Overlapping Neuroanatomical Alterations between Dyslexia and Attention-Deficit/Hyperactivity Disorder: A Meta-Analytic Replication Study. Brain Sciences. 2022; 12: 1367. https://doi.org/10.3390/brainsci12101367.

[171] Liloia D, Cauda F, Uddin LQ, Manuello J, Mancuso L, Keller R, *et al*. Revealing the Selectivity of Neuroanatomical Alteration

in Autism Spectrum Disorder via Reverse Inference. Biological Psychiatry. Cognitive Neuroscience and Neuroimaging. 2023; 8: 1075–1083. https://doi.org/10.1016/j.bpsc.2022.01.007.

[172] Tanaka M, Chen C. Editorial: Towards a mechanistic understanding of depression, anxiety, and their comorbidity: perspectives from cognitive neuroscience. Frontiers in Behavioral Neuroscience. 2023; 17: 1268156. https://doi.org/10.3389/fnbeh.2023.1268156.

[173] Battaglia S, Schmidt A, Hassel S, Tanaka M. Editorial: Case reports in neuroimaging and stimulation. Frontiers in Psychiatry. 2023; 14: 1264669. https://doi.org/10.3389/fpsyt.2023.1264669.

[174] Cauda F, Nani A, Liloia D, Manuello J, Premi E, Duca S, *et al*. Finding specificity in structural brain alterations through Bayesian reverse inference. Human Brain Mapping. 2020; 41: 4155–4172. https://doi.org/10.1002/hbm.25105.

[175] Liloia D, Zamfira DA, Tanaka M, Manuello J, Crocetta A, Keller R, *et al*. Disentangling the role of gray matter volume and concentration in autism spectrum disorder: A meta-analytic investigation of 25 years of voxel-based morphometry research. Neuroscience and Biobehavioral Reviews. 2024; 164: 105791. https://doi.org/10.1016/j.neubiorev.2024.105791.

[176] Balogh L, Tanaka M, Török N, Vécsei L, Taguchi S. Crosstalk between Existential Phenomenological Psychotherapy and Neu-rological Sciences in Mood and Anxiety Disorders. Biomedicines. 2021; 9: 340. https://doi.org/10.3390/biomedicines9040340.

[177] Di Gregorio F, Battaglia S. Advances in EEG-based functional connectivity approaches to the study of the central nervous system in health and disease. Advances in Clinical and Experimental Medicine: Official Organ Wroclaw Medical University. 2023; 32: 607–612. https://doi.org/10.17219/acem/166476.

[178] Hakamata Y, Hori H, Mizukami S, Izawa S, Yoshida F, Moriguchi Y, *et al*. Blunted diurnal interleukin-6 rhythm is associated with amygdala emotional hyporeactivity and depression: a modulating role of gene-stressor interactions. Frontiers in Psychiatry. 2023; 14: 1196235. https://doi.org/10.3389/fpsyt.2023.1196235.

[179] Rassler B, Blinowska K, Kaminski M, Pfurtscheller G. Analysis of Respiratory Sinus Arrhythmia and Directed Information Flow between Brain and Body Indicate Different Management Strategies of fMRI-Related Anxiety. Biomedicines. 2023; 11: 1028. https://doi.org/10.3390/biomedicines11041028.

[180] Vasiliu O. Efficacy, Tolerability, and Safety of Toludesvenlafaxine for the Treatment of Major Depressive Disorder-A Narrative Review. Pharmaceuticals (Basel, Switzerland). 2023; 16: 411. https://doi.org/10.3390/ph16030411.

[181] Tanaka M, Szabó Á, Körtési T, Szok D, Tajti J, Vécsei L. From CGRP to PACAP, VIP, and Beyond: Unraveling the Next Chapters in Migraine Treatment. Cells. 2023; 12: 2649. https://doi.org/10.3390/cells12222649.

[182] Battaglia S, Avenanti A, Vécsei L, Tanaka M. Neurodegeneration in Cognitive Impairment and Mood Disorders for Experimental, Clinical and Translational Neuropsychiatry. Biomedicines. 2024; 12: 574. https://doi.org/10.3390/biomedicines12030574.

[183] Naito Y, Hino K, Bono H, Ui-Tei K. CRISPRdirect: software for designing CRISPR/Cas guide RNA with reduced off-target sites. Bioinformatics. 2015; 31: 1120–1123. https://doi.org/10.1093/bioinformatics/btu743.

[184] Kawai S, Takagi Y, Kaneko S, Kurosawa T. Effect of three types of mixed anesthetic agents alternate to ketamine in mice. Ex-perimental Animal. 2011; 60: 481–487. https://doi:10.1538/expanim.60.481.

[185] Masuya H, Inoue M, Wada Y, Shimizu A, Nagano J, Kawai A, *et al*. Implementation of the modified-SHIRPA protocol for screening of dominant phenotypes in a large-scale ENU mutagenesis program. Mammalian Genome: Official Journal of the International Mammalian Genome Society. 2005; 16: 829–837. https://doi.org/10.1007/s00335-005-2430-8.

[186] Mandillo S, Tucci V, Hölter SM, Meziane H, Banchaabouchi MA, Kallnik M, *et al*. Reliability, robustness, and reproducibility in mouse behavioral phenotyping: a cross-laboratory study. Physiological Genomics. 2008; 34: 243–255. https://doi.org/10.1152/physiolgenomics.90207.2008.

[187] Detke MJ, Rickels M, Lucki I. Active behaviors in the rat forced swimming test differentially produced by serotonergic and noradrenergic antidepressants. Psychopharmacology. 1995; 121: 66–72. https://doi.org/10.1007/BF02245592.

[188] Khisti RT, Chopde CT, Jain SP. Antidepressant-like effect of the neurosteroid 3alpha-hydroxy-5alpha-pregnan-20-one in mice forced swim test. Pharmacology, Biochemistry, and Behavior. 2000; 67: 137–143. https://doi.org/10.1016/s0091-3057(00)00300-2.

[189] Steru L, Chermat R, Thierry B, Simon P. The tail suspension test: a new method for screening antidepressants in mice. Psycho-pharmacology. 1985; 85: 367–370. https://doi.org/10.1007/BF00428203.

[190] Cryan JF, Mombereau C, Vassout A. The tail suspension test as a model for assessing antidepressant activity: review of phar-macological and genetic studies in mice. Neuroscience and Biobehavioral Reviews. 2005; 29: 571–625. https://doi.org/10.1016/j.neubiorev.2005.03.009.

[191] Lister RG. The use of a plus-maze to measure anxiety in the mouse. Psychopharmacology. 1987; 92: 180–185. https://doi.org/10.1007/BF00177912.

[192] Pellow S, Chopin P, File SE, Briley M. Validation of open:closed arm entries in an elevated plus-maze as a measure of anxiety in the rat. Journal of Neuroscience Methods. 1985; 14: 149–167. https://doi.org/10.1016/0165-0270(85)90031-7.

[193] Costall B, Coughlan J, Horovitz ZP, Kelly ME, Naylor RJ, Tomkins DM. The effects of ACE inhibitors captopril and SQ29,852 in rodent tests of cognition. Pharmacology, Biochemistry, and Behavior. 1989; 33: 573–579. https://doi.org/10.1016/0091-3057(89)90390-0.

[194] Onaivi ES, Martin BR. Neuropharmacological and physiological validation of a computer-controlled two-compartment black and white box for the assessment of anxiety. Progress in Neuropsychopharmacology & Biological Psychiatry. 1989; 13: 963–976. https://doi.org/10.1016/0278-5846(89)90047-x.

[195] van der Poel AM. Ethological study of the behaviour of the albino rat in a passive-avoidance test. Acta Physiologica et Pharma-cologica Neerlandica. 1967; 14: 503–505.

[196] Stanford SC. The Open Field Test: reinventing the wheel. Journal of Psychopharmacology (Oxford, England). 2007; 21: 134–135. https://doi.org/10.1177/0269881107073199.

[197] Walsh RN, Cummins RA. The Open-Field Test: a critical review. Psychological Bulletin. 1976; 83: 482–504.

[198] Galla Z, Rajda C, Rácz G, Grecsó N, Baráth Á, Vécsei L, *et al*. Simultaneous determination of 30 neurologically and metabolically important molecules: A sensitive and selective way to measure tyrosine and tryptophan pathway metabolites and other bi-omarkers in human serum and cerebrospinal fluid. Journal of Chromatography. a. 2021; 1635: 461775. https://doi.org/10.1016/j.chroma.2020.461775.

[199] Galla Z, Rácz G, Grecsó N, Baráth Á, Kósa M, Bereczki C, *et al*. Improved LC-MS/MS method for the determination of 42 neurologically and metabolically important molecules in urine. Journal of Chromatography. B, Analytical Technologies in the Biomedical and Life Sciences. 2021; 1179: 122846. https://doi.org/10.1016/j.jchromb.2021.122846.

[200] Kabadayi Sahin E, Caykoylu A, Senat A, Erel O. A com-

prehensive study of oxidative stress in patients with somatic symptom disorder. Acta Neuropsychiatrica. 2019; 31: 100–105. https://doi.org/10.1017/neu.2018.33.

[201] Polat N, Beyaztas H, Aktas S, Maden O, Metin Guler E. Comparison of oxidative stress parameters, thiol-disulfide homeostasis, and pro-inflammatory cytokines levels in patients with bipolar disorder and their first-degree relatives. Journal of Psychiatric Research. 2023; 162: 103–112. https://doi.org/10.1016/j.jpsychires.2023.05.022.

[202] Juchnowicz D, Dzikowski M, Rog J, Waszkiewicz N, Zalewska A, Maciejczyk M, *et al*. Oxidative Stress Biomarkers as a Predictor of Stage Illness and Clinical Course of Schizophrenia. Frontiers in Psychiatry. 2021; 12: 728986. https://doi.org/10.3389/fpsyt.2021.728986.

[203] Savitz J, Drevets WC, Smith CM, Victor TA, Wurfel BE, Bellgowan PSF, *et al*. Putative neuroprotective and neurotoxic kynurenine pathway metabolites are associated with hippocampal and amygdalar volumes in subjects with major depressive disorder. Neuropsychopharmacology: Official Publication of the American College of Neuropsychopharmacology. 2015; 40: 463–471. https://doi.org/10.1038/npp.2014.194.

[204] Barone P. The 'Yin' and the 'Yang' of the kynurenine pathway: excitotoxicity and neuroprotection imbalance in stress-induced disorders. Behavioural Pharmacology. 2019; 30: 163–186. https://doi.org/10.1097/FBP.0000000000000477.

[205] Globus MY, Ginsberg MD, Busto R. Excitotoxic index–a biochemical marker of selective vulnerability. Neuroscience Letters. 1991; 127: 39–42. https://doi.org/10.1016/0304-3940(91)90889-2.

[206] Schwarz MJ, Ackenheil M. The role of substance P in depression: therapeutic implications. Dialogues in Clinical Neuroscience. 2002; 4: 21–29. https://doi.org/10.31887/DCNS.2002.4.1/mschwarz.

[207] Tanaka M, Török N, Vécsei L. Are 5-HT_1 receptor agonists effective anti-migraine drugs? Expert Opinion on Pharma-cotherapy. 2021; 22: 1221–1225. https://doi.org/10.1080/14656566.2021.1910235.

[208] Kindler J, Lim CK, Weickert CS, Boerrigter D, Galletly C, Liu D, *et al*. Dysregulation of kynurenine metabolism is related to proinflammatory cytokines, attention, and prefrontal cortex volume in schizophrenia. Molecular Psychiatry. 2020; 25: 2860–2872. https://doi.org/10.1038/s41380-019-0401-9.

[209] van Praag HM, Kahn RS, Asnis GM, Wetzler S, Brown SL, Bleich A, *et al*. Denosologization of biological psychiatry or the specificity of 5-HT disturbances in psychiatric disorders. Journal of Affective Disorders. 1987; 13: 1–8. https://doi.org/10.1016/0165-0327(87)90067-x.

[210] Tanaka M, Tuka B, Vécsei L. Navigating the Neurobiology of Migraine: From Pathways to Potential Therapies. Cells. 2024; 13: 1098. https://doi.org/10.3390/cells13131098.

[211] Li D, Yu S, Long Y, Shi A, Deng J, Ma Y, *et al*. Tryptophan metabolism: Mechanism-oriented therapy for neurological and psychiatric disorders. Frontiers in Immunology. 2022; 13: 985378. https://doi.org/10.3389/fimmu.2022.985378.

[212] Miura H, Ozaki N, Sawada M, Isobe K, Ohta T, Nagatsu T. A link between stress and depression: shifts in the balance between the kynurenine and serotonin pathways of tryptophan metabolism and the etiology and pathophysiology of depression. Stress (Amsterdam, Netherlands). 2008; 11: 198–209. https://doi.org/10.1080/10253890701754068.

[213] Correia AS, Vale N. Tryptophan Metabolism in Depression: A Narrative Review with a Focus on Serotonin and Kynurenine Pathways. International Journal of Molecular Sciences. 2022; 23: 8493. https://doi.org/10.3390/ijms23158493.

[214] Han Q, Cai T, Tagle DA, Li J. Structure, expression, and function of kynurenine aminotransferases in human and rodent brains. Cellular and Molecular Life Sciences: CMLS. 2010; 67: 353–368. https://doi.org/10.1007/s00018-009-0166-4.

[215] Okada K, Angkawidjaja C, Koga Y, Kanaya S. Structural and mechanistic insights into the kynurenine aminotransferase-mediated excretion of kynurenic acid. Journal of Structural Biology. 2014; 185: 257–266. https://doi.org/10.1016/j.jsb.2014.01.009.

[216] Kucukkarapinar M, Yay-Pence A, Yildiz Y, Buyukkoruk M, Yaz-Aydin G, Deveci-Bulut TS, *et al*. Psychological out-comes of COVID-19 survivors at sixth months after diagnose: the role of kynurenine pathway metabolites in depression, anxiety, and stress. Journal of Neural Transmission (Vienna, Austria: 1996). 2022; 129: 1077–1089. https://doi.org/10.1007/s00702-022-02525-1.

[217] Ford JD, Courtois CA. Complex PTSD and borderline personality disorder. Borderline Personality Disorder and Emotion Dysregulation. 2021; 8: 16. https://doi.org/10.1186/s40479-021-00155-9.

[218] Lanius RA, Vermetten E, Loewenstein RJ, Brand B, Schmahl C, Bremner JD, *et al*. Emotion modulation in PTSD: Clinical and neurobiological evidence for a dissociative subtype. American journal of psychiatry. 2010; 167: 640–647. https://doi.org/10.1176/appi.ajp.2009.09081168.

[219] Powers A, Cross D, Fani N, Bradley B. PTSD, emotion dysregulation, and dissociative symptoms in a highly traumatized sample. Journal of psychiatric research. 2015; 61: 174–179. https://doi.org/10.1016/j.jpsychires.2014.12.011.

[220] Ehrlich I, Humeau Y, Grenier F, Ciocchi S, Herry C, Lüthi A. Amygdala inhibitory circuits and the control of fear memory. Neuron. 2009; 62: 757–771. https://doi.org/10.1016/j.neuron.2009.05.026.

[221] Hartley CA, Phelps EA. Changing fear: the neurocircuitry of emotion regulation. Neuropsychopharmacology: Official Publication of the American College of Neuropsychopharmacology. 2010; 35: 136–146. https://doi.org/10.1038/npp.2009.121.

[222] Cowansage KK, Shuman T, Dillingham BC, Chang A, Golshani P, Mayford M. Direct reactivation of a coherent neocortical memory of context. Neuron. 2014; 84: 432–441. https://doi.org/10.1016/j.neuron.2014.09.022.

[223] Barsy B, Kocsis K, Magyar A, Babiczky Á, Szabó M, Veres JM, *et al*. Associative and plastic thalamic signaling to the lateral amygdala controls fear behavior. Nature Neuroscience. 2020; 23: 625–637. https://doi.org/10.1038/s41593-020-0620-z.

[224] Tsigos C, Chrousos GP. Hypothalamic-pituitary-adrenal axis, neuroendocrine factors and stress. Journal of Psychosomatic Research. 2002; 53: 865–871. https://doi.org/10.1016/s0022-3999(02)00429-4.

[225] Rodrigues SM, LeDoux JE, Sapolsky RM. The influence of stress hormones on fear circuitry. Annual Review of Neuroscience. 2009; 32: 289–313. https://doi.org/10.1146/annurev.neuro.051508.135620.

[226] Battaglia S, Di Fazio C, Mazzà M, Tamietto M, Avenanti A. Targeting Human Glucocorticoid Receptors in Fear Learning: A Multiscale Integrated Approach to Study Functional Connectivity. International Journal of Molecular Sciences. 2024; 25: 864. https://doi.org/10.3390/ijms25020864.

[227] Jászberényi M, Thurzó B, Bagosi Z, Vécsei L, Tanaka M. The Orexin/Hypocretin System, the Peptidergic Regulator of Vigilance, Orchestrates Adaptation to Stress. Biomedicines. 2024; 12: 448. https://doi.org/10.3390/biomedicines12020448.

[228] Spielberg JM, Stewart JL, Levin RL, Miller GA, Heller W. Prefrontal Cortex, Emotion, and Approach/Withdrawal Motivation. Social and Personality Psychology Compass. 2008; 2: 135–153. https://doi.org/10.1111/j.1751-9004.2007.00064.x.

[229] Frankland PW, Josselyn SA, Köhler S. The neurobiological foundation of memory retrieval. Nature Neuroscience. 2019; 22:

1576–1585. https://doi.org/10.1038/s41593-019-0493-1.
[230] Grace AA. Dysregulation of the dopamine system in the pathophysiology of schizophrenia and depression. Nature Reviews. Neuroscience. 2016; 17: 524–532. https://doi.org/10.1038/nrn.2016.57.
[231] Westerhof GJ, Bohlmeijer ET, McAdams DP. The Relation of Ego Integrity and Despair to Personality Traits and Mental Health. The Journals of Gerontology. Series B, Psychological Sciences and Social Sciences. 2017; 72: 400–407. https://doi.org/10.1093/geronb/gbv062.
[232] Jing L, Duan TT, Tian M, Yuan Q, Tan JW, Zhu YY, *et al*. Despair-associated memory requires a slow-onset CA1 long-term potentiation with unique underlying mechanisms. Scientific Reports. 2015; 5: 15000. https://doi.org/10.1038/srep15000.
[233] van der Kolk BA. The body keeps the score: memory and the evolving psychobiology of posttraumatic stress. Harvard Review of Psychiatry. 1994; 1: 253–265. https://doi.org/10.3109/10673229409017088.
[234] van Meerkerk-Aanen PJ, de Vroege L, Khasho D, Foruz A, van Asseldonk JT, van der Feltz-Cornelis CM. La belle indifférence revisited: a case report on progressive supranuclear palsy misdiagnosed as conversion disorder. Neuropsychiatric Disease and Treatment. 2017; 13: 2057–2067. https://doi.org/10.2147/NDT.S130475.
[235] Reid S, Barbui C. Long term treatment of depression with selective serotonin reuptake inhibitors and newer antidepressants. BMJ (Clinical Research Ed.). 2010; 340: c1468. https://doi.org/10.1136/bmj.c1468.
[236] Raison S, Weissmann D, Rousset C, Pujol JF, Descarries L. Changes in steady-state levels of tryptophan hydroxylase protein in adult rat brain after neonatal 6-hydroxydopamine lesion. Neuroscience. 1995; 67: 463–475. https://doi.org/10.1016/0306-4522(95)00064-p.
[237] Jacobsen JPR, Medvedev IO, Caron MG. The 5-HT deficiency theory of depression: perspectives from a naturalistic 5-HT deficiency model, the tryptophan hydroxylase 2Arg439His knockin mouse. Philosophical Transactions of the Royal Society of London. Series B, Biological Sciences. 2012; 367: 2444–2459. https://doi.org/10.1098/rstb.2012.0109.
[238] Xu CJ, Wang JL, Jing-Pan, Min-Liao. Tph2 Genetic Ablation Contributes to Senile Plaque Load and Astrogliosis in APP/PS1 Mice. Current Alzheimer Research. 2019; 16: 219–232. https://doi.org/10.2174/1567205016666190301110110.
[239] Angoa-Pérez M, Kane MJ, Briggs DI, Herrera-Mundo N, Sykes CE, Francescutti DM, *et al*. Mice genetically depleted of brain serotonin do not display a depression-like behavioral phenotype. ACS Chemical Neuroscience. 2014; 5: 908–919. https://doi.org/10.1021/cn500096g.
[240] Sbrini G, Hanswijk SI, Brivio P, Middelman A, Bader M, Fumagalli F, *et al*. Peripheral Serotonin Deficiency Affects Anxiety-like Behavior and the Molecular Response to an Acute Challenge in Rats. International Journal of Molecular Sciences. 2022; 23: 4941. https://doi.org/10.3390/ijms23094941.
[241] Klemenhagen KC, Gordon JA, David DJ, Hen R, Gross CT. Increased fear response to contextual cues in mice lacking the 5-HT1A receptor. Neuropsychopharmacology: Official Publication of the American College of Neuropsychopharmacology. 2006; 31: 101–111. https://doi.org/10.1038/sj.npp.1300774.
[242] Bouchekioua Y, Nebuka M, Sasamori H, Nishitani N, Sugiura C, Sato M, *et al*. Serotonin 5-HT_{2C} receptor knockout in mice attenuates fear responses in contextual or cued but not compound context-cue fear conditioning. Translational Psychiatry. 2022; 12: 58. https://doi.org/10.1038/s41398-022-01815-2.
[243] Wellman CL, Izquierdo A, Garrett JE, Martin KP, Carroll J, Millstein R, *et al*. Impaired stress-coping and fear extinction and abnormal corticolimbic morphology in serotonin transporter knock-out mice. The Journal of Neuroscience: the Official Journal of the Society for Neuroscience. 2007; 27: 684–691. https://doi.org/10.1523/JNEUROSCI.4595-06.2007.
[244] Sorgdrager FJH, Naudé PJW, Kema IP, Nollen EA, Deyn PPD. Tryptophan Metabolism in Inflammaging: From Biomarker to Therapeutic Target. Frontiers in Immunology. 2019; 10: 2565. https://doi.org/10.3389/fimmu.2019.02565.
[245] Myint AM. Kynurenines: from the perspective of major psychiatric disorders. The FEBS Journal. 2012; 279: 1375–1385. https://doi.org/10.1111/j.1742-4658.2012.08551.x.
[246] Battaglia MR, Di Fazio C, Battaglia S. Activated Tryptophan-Kynurenine metabolic system in the human brain is associated with learned fear. Frontiers in Molecular Neuroscience. 2023; 16: 1217090. https://doi.org/10.3389/fnmol.2023.1217090.
[247] Skorobogatov K, Autier V, Foiselle M, Richard JR, Boukouaci W, Wu CL, *et al*. Kynurenine pathway abnormalities are state-specific but not diagnosis-specific in schizophrenia and bipolar disorder. Brain, Behavior, & Immunity - Health. 2023; 27: 100584. https://doi.org/10.1016/j.bbih.2022.100584.
[248] Liang Y, Xie S, He Y, Xu M, Qiao X, Zhu Y, *et al*. Kynurenine Pathway Metabolites as Biomarkers in Alzheimer's Disease. Disease Markers. 2022; 2022: 9484217. https://doi.org/10.1155/2022/9484217.
[249] Marszalek-Grabska M, Walczak K, Gawel K, Wicha-Komsta K, Wnorowska S, Wnorowski A, *et al*. Kynurenine emerges from the shadows - Current knowledge on its fate and function. Pharmacology & Therapeutics. 2021; 225: 107845. https://doi.org/10.1016/j.pharmthera.2021.107845.
[250] Yu P, Di Prospero NA, Sapko MT, Cai T, Chen A, Melendez-Ferro M, *et al*. Biochemical and phenotypic abnormalities in kynurenine aminotransferase II-deficient mice. Molecular and Cellular Biology. 2004; 24: 6919–6930. https://doi.org/10.1128/MCB.24.16.6919-6930.2004.
[251] Potter MC, Elmer GI, Bergeron R, Albuquerque EX, Guidetti P, Wu HQ, *et al*. Reduction of endogenous kynurenic acid formation enhances extracellular glutamate, hippocampal plasticity, and cognitive behavior. Neuropsychopharmacology: Official Publication of the American College of Neuropsychopharmacology. 2010; 35: 1734–1742. https://doi.org/10.1038/npp.2010.39.
[252] Desbonnet L, Tighe O, Karayiorgou M, Gogos JA, Waddington JL, O'Tuathaigh CMP. Physiological and behavioural responsivity to stress and anxiogenic stimuli in COMT-deficient mice. Behavioural Brain Research. 2012; 228: 351–358. https://doi.org/10.1016/j.bbr.2011.12.014.
[253] Kash SF, Tecott LH, Hodge C, Baekkeskov S. Increased anxiety and altered responses to anxiolytics in mice deficient in the 65-kDa isoform of glutamic acid decarboxylase. Proceedings of the National Academy of Sciences of the United States of America. 1999; 96: 1698–1703. https://doi.org/10.1073/pnas.96.4.1698.
[254] Sangha S, Narayanan RT, Bergado-Acosta JR, Stork O, Seidenbecher T, Pape HC. Deficiency of the 65 kDa isoform of glutamic acid decarboxylase impairs extinction of cued but not contextual fear memory. The Journal of Neuroscience: the Official Journal of the Society for Neuroscience. 2009; 29: 15713–15720. https://doi.org/10.1523/JNEUROSCI.2620-09.2009.
[255] Zhang WH, Zhou J, Pan HQ, Wang XY, Liu WZ, Zhang JY, *et al*. δ Subunit-containing $GABA_A$ receptor prevents overgeneralization of fear in adult mice. Learning & Memory (Cold Spring Harbor, N.Y.). 2017; 24: 381–384. https://doi.org/10.1101/lm.045856.117.
[256] Sideris A, Piskoun B, Russo L, Norcini M, Blanck T, Recio-Pinto E. Cannabinoid 1 receptor knockout mice display cold allodynia, but enhanced recovery from spared-

nerve injury-induced mechanical hypersensitivity. Molecular Pain. 2016; 12: 1744806916649191. https://doi.org/10.1177/1744806916649191.

[257] de Lima EP, Tanaka M, Lamas CB, Quesada K, Detregiachi CRP, Araújo AC, *et al*. Vascular Impairment, Muscle Atrophy, and Cognitive Decline: Critical Age-Related Conditions. Biomedicines. 2024; 12: 2096. https://doi.org/10.3390/biomedicines12092096.

[258] Martos D, Lőrinczi B, Szatmári I, Vécsei L, Tanaka M. The Impact of C-3 Side Chain Modifications on Kynurenic Acid: A Behavioral Analysis of Its Analogs in the Motor Domain. International Journal of Molecular Sciences. 2024; 25: 3394. https://doi.org/10.3390/ijms25063394.

[259] Pagotto GLDO, Santos LMOD, Osman N, Lamas CB, Laurindo LF, Pomini KT, *et al*. *Ginkgo biloba*: A Leaf of Hope in the Fight against Alzheimer's Dementia: Clinical Trial Systematic Review. Antioxidants (Basel, Switzerland). 2024; 13: 651. https://doi.org/10.3390/antiox13060651.

[260] Nunes YC, Mendes NM, Pereira de Lima E, Chehadi AC, Lamas CB, Haber JFS, *et al*. Curcumin: A Golden Approach to Healthy Aging: A Systematic Review of the Evidence. Nutrients. 2024; 16: 2721. https://doi.org/10.3390/nu16162721.

[261] de Kloet ER, Molendijk ML. Coping with the Forced Swim Stressor: Towards Understanding an Adaptive Mechanism. Neural Plasticity. 2016; 2016: 6503162. https://doi.org/10.1155/2016/6503162.

[262] Tanaka M, Vécsei L. From Lab to Life: Exploring Cutting-Edge Models for Neurological and Psychiatric Disorders. Biomedicines. 2024; 12: 613. https://doi.org/10.3390/biomedicines12030613.

[263] Tanaka M, Battaglia S, Giménez-Llort L, Chen C, Hepsomali P, Avenanti A, *et al*. Innovation at the Intersection: Emerging Translational Research in Neurology and Psychiatry. Cells. 2024; 13: 790. https://doi.org/10.3390/cells13100790.

[264] Tanaka M, Vécsei L. A Decade of Dedication: Pioneering Perspectives on Neurological Diseases and Mental Illnesses. Biomed-icines. 2024; 12: 1083. https://doi.org/10.3390/biomedicines12051083.

[265] Lee DJ, Bovin MJ, Weathers FW, Palmieri PA, Schnurr PP, Sloan DM, *et al*. Latent factor structure of DSM-5 post-traumatic stress disorder: Evaluation of method variance and construct validity of novel symptom clusters. Psychological Assessment. 2019; 31: 46–58. https://doi.org/10.1037/pas0000642.

[266] McSweeney LB, Koch EI, Saules KK, Jefferson S. Exploratory Factor Analysis of Diagnostic and Statistical Manual, 5th Edition, Criteria for Posttraumatic Stress Disorder. The Journal of Nervous and Mental Disease. 2016; 204: 9–14. https://doi.org/10.1097/NMD.0000000000000390.

[267] Seligowski AV, Rogers AP, Orcutt HK. Relations among emotion regulation and DSM-5 symptom clusters of PTSD. Personality and Individual Differences. 2016; 92: 104–108.

[268] Di Gregorio F, Steinhauser M, Maier ME, Thayer JF, Battaglia S. Error-related cardiac deceleration: Functional interplay between error-related brain activity and autonomic nervous system in performance monitoring. Neuroscience and Biobehavioral Reviews. 2024; 157: 105542. https://doi.org/10.1016/j.neubiorev.2024.105542.

[269] Battaglia S, Nazzi C, Thayer JF. Genetic differences associated with dopamine and serotonin release mediate fear-induced bradycardia in the human brain. Translational Psychiatry. 2024; 14: 24. https://doi.org/10.1038/s41398-024-02737-x.

cells

MDPI

Article

Behavioral Balance in Tryptophan Turmoil: Regional Metabolic Rewiring in Kynurenine Aminotransferase II Knockout Mice

Ágnes Szabó [1,2,3], Zsolt Galla [4], Eleonóra Spekker [1,5], Diána Martos [1,3], Mónika Szűcs [6], Annamária Fejes-Szabó [1,7], Ágnes Fehér [8], Keiko Takeda [9], Kinuyo Ozaki [10], Hiromi Inoue [10], Sayo Yamamoto [10], Péter Monostori [4], József Toldi [11], Etsuro Ono [9,10], László Vécsei [1,2,*,†] and Masaru Tanaka [1,*,†]

1 HUN-REN-SZTE Neuroscience Research Group, Hungarian Research Network, University of Szeged, Danube Neuroscience Research Laboratory, H-6725 Szeged, Hungary; szabo.agnes.4@med.u-szeged.hu (Á.S.)
2 Department of Neurology, Albert Szent-Györgyi Medical School, University of Szeged, H-6725 Szeged, Hungary
3 Doctoral School of Clinical Medicine, University of Szeged, H-6720 Szeged, Hungary
4 Metabolic and Newborn Screening Laboratory, Department of Pediatrics, Albert Szent-Györgyi Faculty of Medicine, University of Szeged, H-6725 Szeged, Hungary
5 Competence Center for Drug Development and Clinical Trials, Directorate-General for Strategy and Development, University of Szeged, H-6720 Szeged, Hungary
6 Department of Medical Physics and Informatics, Albert Szent-Györgyi Medical School, Faculty of Science and Informatics, University of Szeged, H-6720 Szeged, Hungary
7 Competence Centre for Drug Development and Clinical Trials, Centre of Excellence for Interdisciplinary Research, Development and Innovation, University of Szeged, H-6722 Szeged, Hungary
8 Department of Physiology, Albert Szent-Györgyi Medical School, University of Szeged, H-6720 Szeged, Hungary
9 Department of Biomedicine, Graduate School of Medical Sciences, Kyushu University, Fukuoka 812-8582, Japan
10 Center of Biomedical Research, Research Center for Human Disease Modeling, Graduate School of Medical Sciences, Kyushu University, Fukuoka 812-8582, Japan
11 Department of Physiology, Anatomy and Neuroscience, Faculty of Science and Informatics, University of Szeged, H-6726 Szeged, Hungary
* Correspondence: vecsei.laszlo@med.u-szeged.hu (L.V.); tanaka.masaru.1@med.u-szeged.hu (M.T.); Tel.: +36-62-545-351 (L.V.); +36-62-342-847 (M.T.)
† These authors contributed equally to this work.

check for updates

Academic Editors: Korrapati V. Sathyasaikumar, Sarah Beggiato and Verónica Pérez de la Cruz

Received: 17 September 2025
Revised: 23 October 2025
Accepted: 29 October 2025
Published: 31 October 2025

Citation: Szabó, Á.; Galla, Z.; Spekker, E.; Martos, D.; Szűcs, M.; Fejes-Szabó, A.; Fehér, Á.; Takeda, K.; Ozaki, K.; Inoue, H.; et al. Behavioral Balance in Tryptophan Turmoil: Regional Metabolic Rewiring in Kynurenine Aminotransferase II Knockout Mice. *Cells* **2025**, *14*, 1711. https://doi.org/10.3390/cells14211711

Abstract

Background: Cognitive, emotional, and social impairments are pervasive across neuropsychiatric conditions, where alterations in the tryptophan (Trp)–kynurenine pathway and its product kynurenic acid (KYNA) from kynurenine aminotransferases (KATs) have been linked to Alzheimer's disease, Parkinson's disease, depression, and post-traumatic stress disorder. In novel CRISPR/Cas9-engineered KAT II knockout (*aadat*$^{-/-}$ also known as *kat2*$^{-/-}$) mice, we observed despair-linked depression-like behavior with peripheral excitotoxicity and oxidative stress. KAT II's role and its crosstalk with serotonin, indole-pyruvate, and tyrosine–dopamine remain unclear. It is unknown whether deficits extend to cognitive, emotional, motor, and social domains or whether brain tissues mirror peripheral stress. Objectives: Delineate domain-wide behaviors, brain oxidative/excitotoxic profiles, and pathway interactions attributable to KAT II. Results: Behavior was unchanged across strains. *kat2*$^{-/-}$ deletion remodeled Trp metabolic pathways: 3-hydroxykynurenine increased, xanthurenic acid decreased, KYNA fell in cortex and hippocampus but rose in striatum, quinaldic acid decreased in cerebellum and brainstem. These region-specific changes indicate metabolic stress across the brain and align with higher oxidative load and signs of excitotoxic pressure. Conclusions: Here, we show that KAT II deletion reshapes regional Trp metabolism and amplifies oxidative and excitotoxic imbalance. Although domain-wide behavioral measures, spanning cognition, sociability, and motor coordination,

remained largely unchanged, these neurochemical alterations signify a latent emotional bias rather than overt depressive-like behavior. This work, therefore, refines prior findings by delineating KAT II–linked biochemical vulnerability as a potential substrate for stress-reactive affective dysregulation.

Keywords: tryptophan metabolism; kynurenine; serotonin; dopamine; kynurenine aminotransferase (KAT); oxidative stress; excitotoxicity; gut microbiota; transgenic mice; behavioral test; emotional bias; affective vulnerability

1. Introduction

Cognitive dysfunction, emotional dysregulation, motor impairment, and atypical social behavior represent core clinical features across a broad spectrum of neuropsychiatric and neurodegenerative disorders, including Alzheimer's disease, Parkinson's disease, schizophrenia (SCZ), and autism spectrum disorder (ASD) [1–5]. As the incidence of these conditions continues to rise globally, their cumulative impact on public health infrastructure, caregivers, and society becomes increasingly profound [2,3,6–8]. These growing challenges underscore the urgent need for elucidating the molecular and cellular mechanisms that drive these complex disorders [1,4,9,10]. Among the neurobiological systems under investigation, the metabolism of tryptophan (Trp)—an essential amino acid and a biochemical precursor to numerous neuroactive compounds—has garnered substantial attention in recent years [9,11–14].

Trp metabolism plays a pivotal role in modulating central nervous system (CNS) functions, particularly those related to cognitive abilities, mood regulation, and social behavior [15–19]. Dysregulation within these metabolic pathways has been increasingly linked to the pathophysiology of diseases marked by cognitive decline and deficits in social functioning [15–17,20,21]. The kynurenine (KYN) pathway is the principal route for Trp catabolism, accounting for approximately 90% of total metabolic flux [15,16,21–23] (Figure 1). This pathway produces a variety of bioactive metabolites with diverse effects on CNS function [15,16,18,24,25]. Among these, kynurenic acid (KYNA) stands out due to its ability to modify excitatory neurotransmission through its action on multiple receptors, including N-methyl-D-aspartate (NMDA), α7-nicotinic acetylcholine, α-amino-3-hydroxy-5-methyl-4-isoxazolepropionic acid (AMPA), and kainate receptors [24,26–30]. KYNA is synthesized via the irreversible transamination of KYN by kynurenine aminotransferase enzymes (KATs), with the KAT II isoform being particularly prominent in the brain [19,25,28,31,32]. In contrast, another KYN pathway metabolite, 3-hydroxykynurenine (3-HK), contributes to neurotoxicity by promoting oxidative stress through the generation of reactive oxygen species [17,20,22,33,34]. While historically KYNA and 3-HK were categorized as strictly neuroprotective and neurotoxic, respectively, emerging evidence reveals more complex, context-dependent functions that vary based on concentration, receptor expression patterns, and disease-specific factors [15,24,33,35,36].

In addition to the KYN pathway, several alternative routes for Trp metabolism significantly influence CNS homeostasis [15,37–40]. One such pathway is the 5-HT–melatonin (MEL) system [15,37,40–42]. 5-HT, synthesized from Trp, is a critical neurotransmitter involved in mood regulation, affective balance, and social cognition. Its downstream metabolite, MEL, regulates circadian rhythms and sleep architecture—factors integrally linked to learning, memory consolidation, and executive functioning [39,42–44]. Perturbations in this pathway are associated with a wide range of psychiatric disorders, including major depressive disorder (MDD), generalized anxiety disorder (GAD), and disturbances

in sleep and circadian regulation [12,39,41,45,46]. Here, we quantify regional 5-HT and 5-hydroxyindoleacetic acid (5-HIAA) to estimate serotonergic turnover in vivo and relate these indices to KYN-pathway shifts.

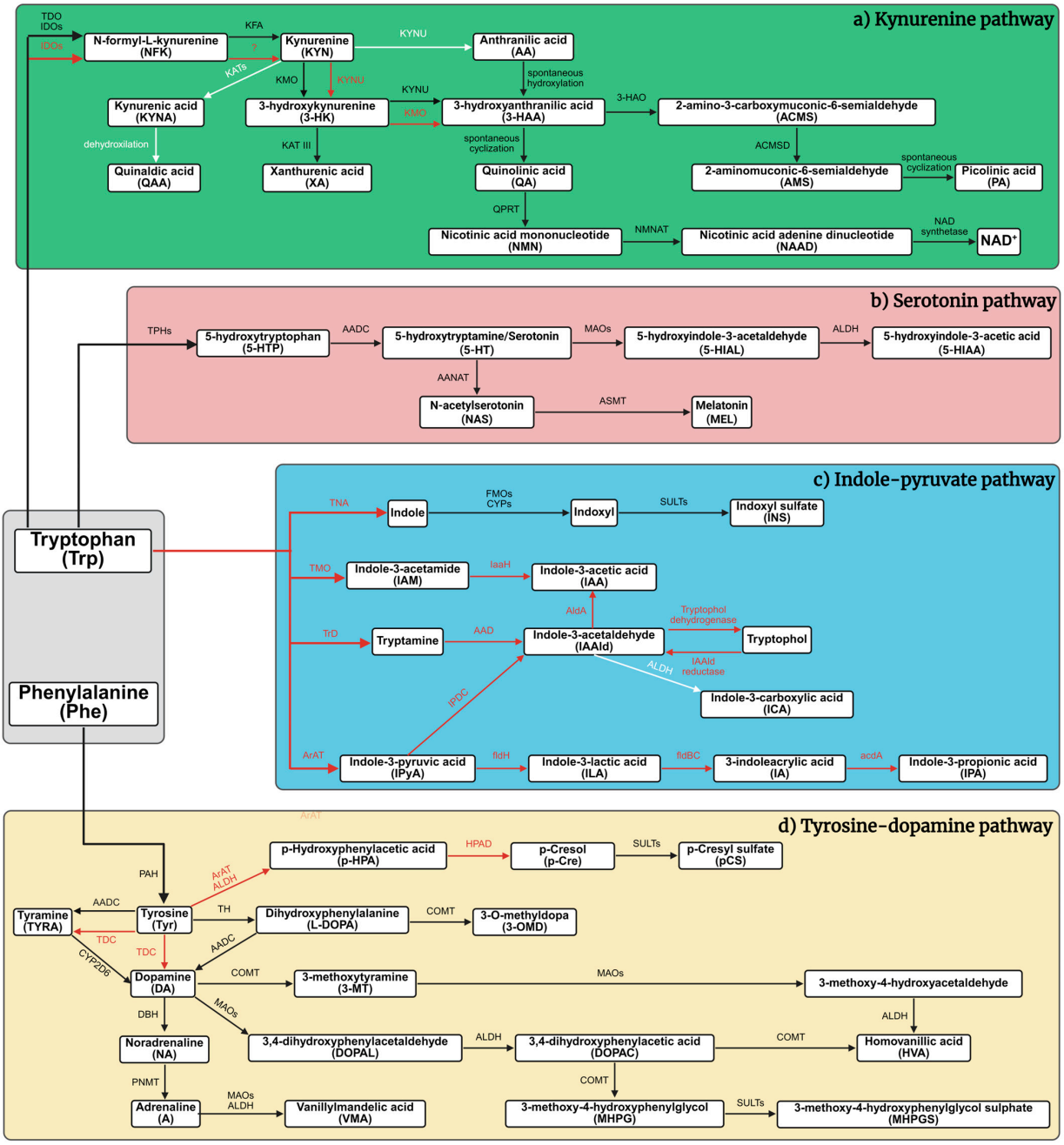

Figure 1. Host–microbiota co-metabolism of aromatic amino acids: tryptophan (Trp) and phenylalanine routes to neuroactive and redox-active metabolites. (**a**) Kynurenine pathway (green): tryptophan enters the kynurenine axis via TDO/IDOs to *N*-formyl-L-kynurenine → kynurenine, branching through KMO to 3-hydroxykynurenine and 3-hydroxyanthranilic acid (→ quinolinic acid) or through KATs to kynurenic acid. 2-amino-3-carboxymuconic-6-semialdehyde cyclizes/oxidizes toward quinolinic acid, which is converted by QPRT → nicotinic acid mononucleotide and onward to NAD^+ (via NMNAT/NAD synthetase). This pathway balances neurotoxic (3-hydroxykynurenine, quinolinic acid) and neuroprotective (kynurenic acid) signals while supplying cellular NAD^+. (**b**) Serotonin pathway (rose): tryptophan is hydroxylated by TPHs to 5-hydroxytryptophan and decarboxylated by aromatic L-amino acid decarboxylase (AADC) to serotonin. Serotonin is catabolized by MAOs/ALDH

to 5-hydroxyindole-3-acetic acid, or acetylated/methylated by AANAT → N-acetylserotonin and HIOMT/ASMT → melatonin. This route links gut/brain serotonin tone with circadian signaling. (**c**) Indole-pyruvate pathway (blue; microbiota–host): bacterial TNA converts tryptophan to indole, which is oxidized to indoxyl and sulfated in the host to indoxyl sulfate. Parallel microbial transamination/reduction/oxidation steps yield indole-3-pyruvic acid → indole-3-lactic acid/indole-3-acetic acid, indole-3-acetaldehyde, 3-indoleacrylic acid, and indole-3-propionic acid. These ligands engage AhR, fortify epithelial barriers, and shape systemic immunity. Note: microbiome composition/function was not assessed here; indole readouts are interpreted as central metabolic signatures rather than direct measures of microbial activity. (**d**) Tyrosine (Tyr)–dopamine (DA) pathway (yellow): phenylalanine → tyrosine (PAH) → levodopa (TH) → dopamine (AADC) → noradrenaline (DBH) → adrenaline (PNMT), with COMT/MAOs/ALDH producing 3,4-dihydroxyphenylacetic acid, 3-methoxytyramine, homovanillic acid, vanyllilmandelic acid, and 3-methoxy-4-hydroxyphenylglycol. In parallel, microbial fermentation of phenylalanine/tyrosine generates p-Hydroxyphenylacetic acid and p-Cresol, further host-conjugated to p-Cresyl sulfate—an impactful uremic/toxic metabolite. The enzymes AADC, ArAT, MAOs, ALDH, and SULTs are involved not only in the Tyr–DA pathway but also participate in the 5-HT or indole–pyruvate metabolic pathways. Black arrows: the host routes; red arrows: the gut microbiota routes; white arrows: host and microbiota routes with the same enzyme. 3-HAA, 3-hydroxyanthranilic acid; 3-HAO, 3-hydroxyanthranilate oxidase; 3-HK, 3-hydroxykynurenine; 3-MT, 3-methoxytyramine; 3-OMD, 3-O-methyldopa; 5-HIAA, 5-hydroxyindole-3-acetic acid; 5-HIAL, 5-hydroxyindole-3-acetaldehyde; 5-HT, 5-hydroxytryptamine/serotonin; 5-HTP, 5-hydroxytryptophan; A, adrenaline; AA, anthranilic acid; AAD, amino acid decarboxylase; AADC, aromatic L-amino acid decarboxylase; AANAT, arylalkylamine N-acetyltransferase; acdA, acyl-CoA dehydrogenase; ACMS, 2-amino-3-carboxymuconic-6-semialdehyde; ACMSD, amino-β-carboxymuconate-semialdehyde-decarboxylase; AldA, indole-3-acetaldehyde dehydrogenase; ALDH, aldehyde dehydrogenase; AMS, 2-aminomuconic-6-semialdehyde; ArAT, aromatic amino acid aminotransferase; ASMT, acetylserotonin-O-methyltransferase; COMT, catechol-O-methyltransferase; CYP2D6, cytochrome P450 2D6; CYPs, cytochrome P450 monooxygenases; DA, dopamine; DBH, dopamine β-hydroxylase; DOPAC, 3,4-dihydroxyphenylacetic acid; DOPAL, 3,4-dihydroxyphenylacetaldehyde; fldBC, phenyllactate dehydratase; fldH, indole-3-pyruvate ferredoxin oxidoreductase; FMOs, flavin-containing monooxygenases; HPAD, 4-hydroxyphenylacetate decarboxylase; HVA, homovanillic acid; IA, 3-indoleacrylic acid; IAA, indole-3-acetic acid; IaaH, indole-3-acetamide hydrolase; IAAld, indole-3-acetaldehyde; IAM, indole-3-acetamide; ICA, indole-3-carboxylic acid; IDOs, indoleamine 2,3-dioxygenases (IDO1 and IDO2); ILA, indole-3-lactic acid; INS, indoxyl sulfate; IPA, indole-3-propionic acid; IPDC, indole-3-pyruvate decarboxylase; IPyA, indole-3-pyruvic acid; KAT III, kynurenine aminotransferase III; KATs, kynurenine aminotransferases (KAT I, II, III, and IV); KFA, kynurenine formamidase; KMO, kynurenine-3-monooxygenase; KYN, kynurenine; KYNA, kynurenic acid; KYNU, kynureninase; L-DOPA, dihydroxyphenylalanine/levodopa; MAOs, monoamine oxidases (MAO-A and MAO-B); MEL, melatonin; MHPG, 3-methoxy-4-hydroxyphenylglycol; MHPGS, 3-methoxy-4-hydroxyphenylglycol sulfate; NA, noradrenaline; NAD^+, nicotinamide adenine dinucleotide; NAAD, nicotinic acid adenine dinucleotide; NAS, N-acetylserotonin; NFK, N-formyl-L-kynurenine; NMN, nicotinic acid mononucleotide; NMNAT, nicotinamide mononucleotide adenylyltransferase; p-Cre, p-Cresol; p-HPA, para-hydroxyphenylacetic acid; pCS, p-Cresyl sulfate; PA, picolinic acid; PAH, phenylalanine hydroxylase; Phe, phenylalanine; PNMT, phenylethanolamine N-methyltransferase; QA, quinolinic acid; QAA, quinaldic acid; QPRT, quinolinate phosphoribosyl transferase; SULTs, sulfotransferases; TDC, tyrosine decarboxylase; TDO, tryptophan-2,3-dioxygenase; TH, tyrosine hydroxylase; TMO, tryptophan-2-monooxygenase; TNA, tryptophanase; TPHs, tryptophan hydroxylases (TPH1 and TPH2); TrD, tryptophan decarboxylase; Trp, tryptophan; Tyr, tyrosine; TYRA, tyramine; VMA, vanyllilmandelic acid; XA, xanthurenic acid; ?, unknown.

Another prominent route is the indole–pyruvate pathway, primarily driven by the gut microbiota [47–51]. In this pathway, microbial enzymes convert Trp into several indole derivatives through distinct enzymatic reactions [47–49,51,52]. These indole metabolites are capable of crossing the intestinal barrier and influencing the CNS by modulating neuroinflammatory processes, maintaining gut epithelial integrity, and regulating blood–brain

barrier (BBB) permeability [47,48,51,53,54]. This bidirectional communication along the gut–brain axis has been implicated in the pathophysiology of mood disorders, ASD, and other conditions characterized by social and emotional dysregulation [48,52,55–57]. We therefore profile brain-region levels of indole-3-acetic acid (IAA) and indole-3-carboxaldehyde (ICA) as sentinel markers of gut–brain indole signaling in KAT II knockout mice. ICA, IAA, and indoxyl sulfate (INS) are established readouts of microbiota-derived indole flux, but microbiome profiling was not performed here; thus, brain-region values represent neurochemical correlates rather than direct measures of microbial composition or function.

Additionally, Trp metabolism exerts regulatory effects on dopaminergic neurotransmission via its influence on the tyrosine (Tyr)–dopamine (DA) pathway [37,58–61]. Specifically, Trp availability impacts the synthesis of tetrahydrobiopterin (BH4), a critical cofactor required by tyrosine hydroxylase—the rate-limiting enzyme in DA production [37,58,59,62,63]. Given DA's fundamental role in mediating reward processing, attentional control, and social engagement, this intersection further emphasizes the extensive reach of Trp metabolism in orchestrating complex behavioral and cognitive outcomes [39,59,64–66]. To capture this crosstalk, we quantify Tyr, levodopa (L-DOPA), DA, and downstream metabolites alongside the pterin pool (BH4, dihydrobiopterin [BH2], and biopterin [BIO]).

In earlier research, we examined the interrelationships between affective disorders—such as MDD, GAD, and post-traumatic stress disorder—and systemic alterations in Trp and its downstream metabolites in the *kat2*$^{-/-}$ mice model [67]. Although traditionally conceptualized as mood disorders, these conditions also encompass profound cognitive impairments, including deficits in memory, sustained attention, and executive functioning [68–72]. Such impairments frequently manifest early in the course of illness and may persist independently of affective symptoms [68,70,72–74]. Notably, MDD has emerged as a significant risk factor for the subsequent development of neurodegenerative conditions like AD [68,70,75–77]. In parallel, individuals suffering from MDD and GAD often exhibit marked social dysfunction, including social withdrawal, blunted affect, and reduced empathic capacity [68,69,71,72,78]. These features closely parallel behavioral phenotypes observed in ASD and SCZ, further complicating differential diagnosis and therapeutic decision-making [68,71,78–81]. A mechanistic understanding of the molecular pathways that underlie these shared features is therefore of paramount importance [68,75,81–83].

To probe the contributions of Trp metabolic dysregulation to these behavioral phenotypes, we utilized a genetically engineered mouse model deficient in KAT II (*kat2*$^{-/-}$) [67]. This knockout model disrupts the biosynthetic pathway for KYNA, allowing for detailed investigation of downstream metabolic consequences. Targeted metabolomic profiling of urine and plasma revealed a pronounced decrease in KYNA levels, accompanied by elevated concentrations of 3-HK. These findings reinforce the essential role of KAT II in modulating the balance between neuroprotective and neurotoxic metabolites within the KYN pathway. Building directly on this peripheral signature, the current study extends metabolomics to five brain regions (striatum [STR], cortex [CTX], hippocampus [HIPP], cerebellum [CER], brainstem [STEM]) to resolve central, region-specific consequences of KAT II deletion.

Despite inherent limitations in modeling human psychiatric and neurodegenerative diseases in rodents—especially with regard to complex cognitive processes and nuanced social behaviors—this genetic model affords a valuable platform for dissecting the neurochemical substrates of behavior [84–88]. In the present study, we aimed to systematically evaluate cognitive function and social behavior in *kat2*$^{-/-}$ mutant mice, with a particular focus on mapping these behavioral parameters to region-specific changes in the concentrations of Trp and its metabolites within the brain. To avoid overreach, links to depression

and post-traumatic stress disorder are framed at the pathway level rather than the disorder level, recognizing that this model does not reproduce full clinical syndromes. To enhance cross-domain alignment, behavioral endpoints are mapped to region-specific metabolic indices using shared labels and synchronized panel order across figures and tables, with NORT and 3CT panels cross-referenced to cortical and hippocampal KYNA, 3 HK, and XA, and Rotarod aligned to striatal metrics. This integrative approach offers a robust framework for uncovering potential neurochemical signatures that underlie cognitive and social impairments. Accordingly, our prespecified objectives were to (i) map region-resolved Trp metabolism across the KYN, 5-HT, and indole axes; (ii) quantify the Tyr to L-DOPA to DA cascade and its enzymatic and cofactor milieu (BH4, BH2, BIO); (iii) infer pathway activities using product-substrate ratios (for example, KMO and KAT fluxes, monoamine oxidase [MAO] and aldehyde dehydrogenase [ALDH] turnover) and derive oxidative-stress and excitotoxicity indices; (iv) link these neurochemical states to a broadened behavioral battery encompassing cognition (novel object recognition [NORT], object-based attention [OBAT], Y-maze test), motor coordination (rotarod test), emotion (marble burying test [MBT]), and sociability (three-chamber test [3CT]); and (v) test concordance between brain and peripheral metabolic signatures. By coupling this expanded behavioral panel with multi-region neurochemical profiling, we aim to delineate how KAT II loss reshapes a KYN-tilted, cofactor-constrained, and indole-modulated milieu, and to determine whether such biochemical disequilibria necessarily generalize to global cognitive or social dysfunction, thereby informing pathway-targeted therapeutic strategies across neuropsychiatric spectra [89]. We therefore consider whether regionally divergent KYN remodeling could preserve baseline performance through circuit-level buffering while predisposing selected behavioral domains to failure under cognitive load or stress.

In our previous investigation [67], *kat2*$^{-/-}$ mice exhibited despair-like responses under stress-inducing paradigms such as the forced swim test, suggesting enhanced affective vulnerability. The present study, however, was specifically designed to determine whether these affective alterations persist under non-stressful baseline conditions and extend to cognitive, social, and motor domains. The absence of significant behavioral divergence observed here indicates that KAT II deficiency alone does not elicit broad behavioral dysfunction but may instead confer a latent predisposition that becomes evident only under environmental or metabolic stress. This distinction refines our earlier interpretation by differentiating stress-contingent affective reactivity from baseline behavioral stability.

2. Materials and Methods

This study used a standardized behavioral battery (NORT, OBAT, Y-maze, marble burying, three-chamber, rotarod) with targeted ultra-high-performance liquid chromatography with tandem mass spectrometry (UHPLC–MS/MS) metabolomics across five brain regions. Reporting followed ARRIVE 2.0 guidelines; genotypes were confirmed by a TaqMan allelic discrimination assay on HotSHOT-extracted DNA. Behavioral readouts were acquired with automated video tracking (EthoVision XT14, Noldus Information Technology BV, Wageningen, The Netherlands), and metabolite quantification employed isotope-labeled internal standards and established multiplex panels. Enzyme-activity proxies and oxidative/excitotoxic indices were computed from product–substrate ratios. Statistical analysis prespecified normality testing, variance checks, outlier detection, effect sizes (Hedges g with bootstrap CIs), and post hoc power. Methodological choices align with validated OBAT/NORT protocols, EthoVision reliability, and best practices for UHPLC–MS/MS quantitation and animal reporting.

2.1. Ethical Approval

The Department of Nature Conservation of the Ministry of Agriculture authorized the use of genetically modified organisms in a level 2 biosafety closed system (permit number: TMF/43-20/2015). The import of genetically modified animals was approved by the Department of Biodiversity and Gene Conservation of the Ministry of Agriculture (permit number: BGMF/37-5/2020). The investigations were conducted in accordance with the Ethical Codex for Animal Experiments and were approved by the Ethics Committee of the Faculty of Medicine at the University of Szeged, as well as by the National Food Chain Safety Office, under permission number XI./84/2025. and XI./1008/2025, in accordance with Government Decree 40/2013 (II.14.), and the European Communities Council Directive 2010/63/EU.

2.2. Animals

The C57BL/6N wild-type (WT) strain was originally sourced from Charles River Germany. The *kat2*$^{-/-}$ strain was provided by our collaboration partners at Kyushu University (Fukuoka, Japan). A comprehensive description of the generation of the genetically modified strain can be found in our previously published article [67]. The animals were housed in groups of 4–5 per cage in polycarbonate enclosures (530 cm^2 floor area) under specific pathogen-free conditions at the Animal Facility of the Department of Neurology, University of Szeged. Environmental parameters were stringently controlled, with ambient temperature maintained at 24 ± 1 °C and 45–55% relative humidity under a 12:12 h light–dark cycle. Throughout the duration of the investigation, mice had unrestricted access to standard rodent food and water. Environmental enrichment was provided using paper rolls, gnawing wood, and nesting cotton. In total, 46 WT and 49 *kat2*$^{-/-}$ mice were included in the behavioral assessments, while an additional cohort of 10 WT and 10 *kat2*$^{-/-}$ mice was used for metabolomic analyses. The general condition of the animals was monitored weekly until the start of the experiments, and daily during the experimental period, using a standardized scoring system. This system was applied to assess body weight, general appearance, respiration, mobility, and basic reflexes. If an animal were to reach the predetermined critical score threshold, it would be humanely withdrawn from the study.

2.3. Genotyping with Taqman Allelic Discrimination Assay

All animals were genotyped prior to enrollment. Tail biopsies were collected under 2% isoflurane anesthesia with topical lidocaine and processed by an alkaline lysis protocol adapted from HotSHOT. The extraction yielded DNA suitable for downstream analysis. Concentration and purity were verified by spectrophotometry, and extracts were stored at −20 °C until use [89].

Genotypes were determined with a TaqMan allelic discrimination assay on a CFX Opus 96 real-time PCR system (Bio-Rad Laboratories, Hercules, CA, USA). Reactions were run in singleplex with allele-specific primers and dual-labeled probes. Each plate contained non-template controls together with verified WT and *kat2*$^{-/-}$ controls. Allele calls were assigned from endpoint fluorescence scatter plots and were cross-checked by amplification curves. Ambiguous calls were repeated from the DNA stock.

To improve readability, only the assay overview is retained in the main text. Complete procedural details, including primer and probe sequences, reagent compositions, thermal cycling parameters, plate layout, cluster calling criteria, and representative allelic discrimination plots, are provided in the Supplementary Materials.

2.4. Behavioral Tests

Cognitive, emotional, motor, and social domains were assayed with NORT for recognition memory, OBAT for attention, Y-maze spontaneous alternation for working memory, MBT, the accelerating rotarod for motor coordination, and 3CT for sociability. The behavioral experiments were performed on 8-week-old male mice of the C57BL/6N and *kat2*$^{-/-}$ strains, with n = 10–13 animals included per group. Sample sizes were determined using a power analysis performed with the GPower 3.1 statistical software. A t-test (difference between two independent means, two groups, two-tailed) was applied with the following parameters: significance level (α) = 0.05, power (1–β) = 0.8, effect size d = 1.33, and allocation ratio N2/N1 = 1. Based on these calculations, the required sample size for the behavioral tests was n = 10 per group. After completing the tests, a post hoc analysis was performed to verify whether the sample size was adequate for detecting large effect sizes. The following results were obtained: normality parameter = 2.973, critical t = 2.100, Df = 18, yielding an achieved power of 0.802. Based on these calculations, the resulting statistical power was approximately 0.80, indicating that under the given assumptions, the sample size was sufficient to detect large effect sizes. The animals were habituated to handling by the experimenters for one week prior to testing. all tests were conducted between 8:00 a.m. and 12:00 p.m. Prior to testing, animals were transferred to the experimental laboratory one hour in advance. NORT, OBAT, Y-maze, MBT, and 3CT were recorded using a video tracking system (Basler ace Classic acA1300-60 gm, Basler AG, Ahrensburg, Germany) in combination with behavioral analysis software (EthoVision XT14, Noldus Information Technology BV, Wageningen, The Netherlands). For the rotarod test, we used the TSE RotaRod V4.2.6 system (TSE Laboratory, Ormskirk, UK).

2.4.1. Novel Object Recognition Test (NORT)

For the NORT, we used n = 12 animals per group (total of 24 animals). The behavioral assessments were conducted in a 60 × 60 × 60 cm open-field arena. Three distinct objects—different in color and shape but matched in size and scale relative to the animals—were utilized. The test was carried out across three consecutive days [90–94]. On the habituation day, each animal was placed in the empty arena for a duration of 10 min on the second day (training session), animals were allowed to explore two of the three objects for 10 min, Animals that failed to exhibit any interaction with the object designated as the familiar object during the training phase were excluded from further analysis in the experiment. On the third day (test session), one of the familiar objects from the training phase was substituted with the previously unencountered third object. This unfamiliar item functioned as the novel object, whereas the remaining object served as the familiar object. During NORT, we measured the following parameters: (1) time spent with the training object in the training phase, (2) time spent with the familiar object in the training phase, (3) time spent with the familiar object in the testing phase, (4) time spent with the novel object in the testing phase.

During both NORT and OBAT, the duration of investigation directed toward the novel and familiar objects was systematically recorded. object recognition and novelty preference, two normalized metrics were employed: the discrimination index (DI) and the preference index (PI). The DI quantifies the relative preference for the novel object compared to the familiar one, while the PI expresses the proportion of total exploration time that the animal allocated to the novel object. Both indices account for individual variability in total investigation time and were computed using the following formulas (Equations (1) and (2)).

$$discrimination\ index(DI) = \frac{Tnovel - Tfamiliar}{Tnovel + Tfamiliar} \quad (1)$$

$$preference\ index(PI) = \frac{Tnovel}{Tnovel + Tfamiliar} \times 100 \quad (2)$$

2.4.2. Object-Based Attention Test (OBAT)

The object-based attention test (OBAT), originally developed by Wulaer and colleagues, represents a validated behavioral paradigm for evaluating attentional performance in rodents [95–99]. This method is similar to the NORT; the OBAT leverages the rodent's intrinsic exploratory drive and preference for novelty. A total of 24 animals were used, with 12 assigned to each group (n = 12). The experimental setup comprises a two-compartment arena with dimensions of 40 × 40 × 40 cm (larger compartment) and 20 × 40 × 40 cm (smaller compartment) and utilizes six distinct objects. These objects differ in color and shape but are comparable in size. The procedure consists of two sequential phases: a training phase and a testing phase. During the training phase, the animal is introduced into the larger compartment containing five distinct objects and is allowed a 3 min exploration period. Animals that did not engage in any interaction with the object assigned as the familiar object during the training phase were excluded from subsequent experimental analysis. Subsequently, one of these previously encountered objects, along with a sixth, novel object, is placed in the smaller compartment for the 3 min test phase. The novel item serves as the novel object, while the reintroduced item functions as the familiar object. Animals that did not engage with the object, later serving as the familiar stimulus during the training phase, were systematically excluded from subsequent experimental evaluation.

The following parameters were assessed during the NORT: (1) duration of interaction with the training objects during the training phase, (2) duration of interaction with the familiar object during the training phase, (3) time spent exploring the familiar object during the testing phase, and (4) time spent interacting with the novel object during the testing phase.

2.4.3. Y-Maze Test

Rodents exhibiting intact working memory capacity, and thereby preserved prefrontal cortical function, are capable of recalling which arms have been recently explored and display a preferential inclination to enter the arm that has not been visited in the most recent sequence [100–103]. A total of 24 animals were used, with 12 assigned to each group (n = 12). At the onset of the trial, the animal is positioned at the distal end of the longest arm of the Y-maze, oriented toward the central zone. Thereafter, it is granted an eight-minute period to freely explore the maze. The spontaneous alternation rate was determined according to the following formula (Equation (3)).

$$spontaneous\ alternation(\%) = \frac{number\ of\ spontaneous\ alternations}{total\ number\ of\ arm\ entries - 2} \times 100 \quad (3)$$

During the Y-maze test, we measured spontaneous alternation behavior as well as the total number of entries into all three arms.

2.4.4. Marble Burying Test (MBT)

The marble burying test (MBT) was used to evaluate repetitive and compulsive-like behaviors. Although its interpretation remains debated, several studies suggest that increased marble burying may be associated with enhanced behavioral rigidity and social withdrawal, particularly in animal models displaying impaired sociability [104–108].

The MBT was conducted with 23 animals in total, including 10 WT and 13 $kat2^{-/-}$ mice (n = 10–13 per group). The animals were individually placed in a transparent plastic arena measuring 40 × 24 × 18 cm. The base of the apparatus was filled with a 5 cm deep layer of fresh bedding material. To allow adequate ventilation while preventing escape.

The enclosure was covered with a transparent plastic lid (40 × 24 cm, 1 cm thick) featuring six circular perforations, each 1 cm in diameter. At one end of the arena, sixteen glass marbles (each with dimensions of 1 × 1 × 1 cm^3) were positioned on the bedding in a regular square grid formation. The outermost marbles were placed 3.5 cm from the arena walls, with 5 cm spacing between adjacent marbles. Each mouse was allowed to explore the arena freely for a period of 30 min. The marbles were categorized based on their status: intact, displaced, partially buried (0–75%), or fully buried (75–100%). These measurements were subsequently analyzed and compared across experimental groups.

2.4.5. Three Chamber Test (3CT)

Sociability is operationally defined as the propensity of the test mouse to spend a greater proportion of time in the compartment containing a novel conspecific, as opposed to the compartment housing a novel inanimate object. A supplementary and confirmatory metric involves the quantification of time spent engaging in olfactory investigation of the novel conspecific relative to the novel object, thereby providing an index of direct social interaction. Additionally, the number of transitions between compartments [109–113].

A total of 24 animals were used, with 12 assigned to each group (n = 12). A rectangular three-chambered apparatus was employed for the 3CT. Each compartment measured 20 × 40.5 × 22 cm. The chambers were divided by opaque gray plastic walls, each containing manually operated doors (7.5 × 5 cm) to allow controlled access between compartments. Cylindrical wire-mesh enclosures (15 cm in height, 7 cm in diameter) were positioned in both lateral chambers. The mesh structure, composed of bars spaced 1 cm apart, permitted adequate airflow between the interior and exterior of the cylinder while simultaneously preventing direct physical contact between the test subject and the stimulus animal or object placed within. This configuration allowed for the assessment of social preference and investigatory behavior while minimizing confounding factors related to tactile interaction [109,114–117]. The test protocol consisted of three distinct phases. During the habituation phase, the subject mouse was confined to the center chamber of the apparatus for a period of 10 min with all doors closed, allowing acclimatization to the environment. In the sociability phase, the doors to the lateral chambers were opened, and the test mouse, starting from the center chamber, was allowed to freely explore all three compartments for 10 min. One lateral chamber contained an empty wire-mesh enclosure, while the other housed a wire cage enclosing a novel conspecific that was matched to the test animal in sex, age, and body weight. The social novelty preference phase followed a similar structure: the subject animal started from the center chamber and was given 10 min to explore the entire apparatus. In this phase, the previously encountered conspecific from the sociability phase served as the familiar animal, while a non-familiar, sex-, age-, and weight-matched conspecific was introduced into the formerly empty cage, serving as the novel animal.

During the sociability phase, we quantified (1) time spent in the social chamber, (2) time spent in the non-social chamber, (3) time spent in the center chamber, (4) time spent sniffing the social cage, (5) time spent sniffing the non-social cage, (6) number of entries to the social chamber, (7) number of entries to the non-social chamber, (8) number of entries to both chambers. In the social novelty preference phase, we measured the (1) time spent in the novel chamber, (2) time spent in the familiar chamber, (3) time spent in the center chamber, (4) time spent sniffing the novel animal's cage, (5) time spent sniffing the familiar animal's cage, (6) number of entries to the novel chamber, (7) number of entries to the familiar animal's chamber, (8) number of entries to both chambers.

2.4.6. Rotarod Test

The apparatus comprised a rotating rod equipped with an automated fall-detection system at the base, which interfaced with the TSE RotaRod V4.2.6 system (TSE Laboratory, Berlin, Germany) to automatically terminate the timer upon the animal's fall [118–122]. We used n = 12 animals per group (a total of 24 animals). Animals underwent a two-day habituation and training protocol. On Day 1, each mouse was placed individually on the rotating rod, which was maintained at a constant speed of five revolutions per minute (rpm) for a duration of three minutes. Should the animal have fallen before the allotted time elapses, it was promptly repositioned on the rod. Following the initial session, the animal was returned to its home cage, and the procedure was repeated twice more at 30 min intervals. On Day 2, the training procedure was repeated, with the rotation speed increased to a constant 10 rpm, thereby introducing a higher motoric challenge and reinforcing task familiarity. The testing phase was conducted on Day 3. During this phase, animals were placed on the rod, which now accelerated linearly from 5 to 40 rpm over a 3 min period. Each animal underwent three test trials, with a 30 min inter-trial interval. Unlike during training, animals were not returned to the rod after falling. The latency to fall—defined as the time the animal remained on the rod before falling—was recorded automatically via the tracking software. The average latency across the three test trials served as the composite performance score for each subject, reflecting overall motor coordination and skill retention under increasing demands.

2.5. Ultra-High-Performance Liquid Chromatography with Tandem Mass Spectrometry (UHPLC-MS/MS)

2.5.1. Brain Samples

A total of n = 10 animals per group were included in the metabolomic measurements. Sample sizes were estimated through power analysis using GPower 3.1 statistical software. Calculations were based on a two-tailed t-test comparing two independent means, with the following parameters: significance level (α) = 0.05, power (1–β) = 0.8, effect size (d) = 1.33, and an allocation ratio (N2/N1) of 1. According to these estimates, a sample size of n = 10 animals per group was required for the measurements. Following the completion of the measurements and statistics, a post hoc power analysis was conducted to assess whether the sample size was sufficient to detect large effect sizes. The analysis yielded the following parameters: normality = 2.973, critical t = 2.100, and degrees of freedom (Df) = 18, resulting in an achieved power of 0.802. These findings indicate that, under the given assumptions, the statistical power was approximately 0.80, confirming that the sample size was adequate for detecting large effect sizes.

For tissue collection, mice were anesthetized with 2% isoflurane and then perfused transcardially with artificial cerebrospinal fluid. The brains were subsequently dissected into five distinct regions—striatum, cortex, hippocampus, cerebellum, and brainstem. All tissues were collected on ice and stored at −80 °C until further analysis. Tissue sampling was performed between 8 am and 12 pm local time to limit circadian variability in Trp pathway measures.

We used a randomized, blinded, region-resolved design that integrates targeted liquid chromatography with tandem mass spectrometry (LC-MS/MS) metabolomics with a standardized behavioral battery in *kat2* knockout and WT mice, and we report procedures according to ARRIVE 2.0 to maximize reproducibility. Regarding the brain samples, following the determination of tissue weights, the samples were homogenized using an ultrasonic homogenizer (UP100H, Hielscher Ultrasound Technology, Germany) set to 100% amplitude and a 0.5 cycle setting. Homogenization was performed in threefold volumes of ice-cooled LC-MS grade water relative to tissue mass (e.g., 90 µL of water was added to 30.0 mg of

tissue). Data from any brain regions in which tissue preparation or homogenization did not meet predefined quality standards were excluded from subsequent analyses to ensure methodological consistency and data reliability. We quantified Trp-KYN, serotonergic, and indole metabolites, plus catecholamine intermediates and selected cofactors, using previously published multiplex LC-MS/MS methods and protocols [123,124]. For PA, the MRM transition was 124.0 → 106.0 m/z, with a retention time of 1.21 min, using a declustering potential of 75 V and a collision energy of 13 V. For ICA, the MRM transition was 146.1 → 118.0 m/z, with a retention time of 12.40 min, using a declustering potential of 50 V and a collision energy of 19 V. For IPA, the MRM transition was 190.1 → 130.1 m/z, with a retention time of 13.00 min, using a declustering potential of 50 V and a collision energy of 19 V. For ILA, the MRM transition was 206.1 → 188.1 m/z, with a retention time of 12.00 min, using a declustering potential of 50 V and a collision energy of 13 V. For INS, the MRM transition was 211.9 → 131.9 m/z, with a retention time of 11.80 min, using a declustering potential of −50 V and a collision energy of −25 V. For pCS, the MRM transition was 186.9 → 107.0 m/z, with a retention time of 12.70 min, using a declustering potential of −50 V and a collision energy of −26 V. All reagents and chemicals were of analytical or liquid chromatography–mass spectrometry grade. Trp and its metabolites, and their deuterated forms: d4-serotonin, d5-tryptophan, d4-kynurenine, d5-kynurenic acid, d4-xanthurenic acid, d5-5-hydroxyindole-acetic acid, d3-3-hydroxyanthranilic acid, d4-picolinic acid, and d3-quinolinic acid were purchased from Toronto Research Chemicals (Toronto, ON, Canada). d3-3-hydroxykynurenine was obtained from Buchem B. V. (Apeldoorn, The Netherlands). Acetonitrile (ACN) was provided by Molar Chemicals (Halásztelek, Hungary). Methanol (MeOH) was purchased from LGC Standards (Wesel, Germany). Formic acid (FA) and water were obtained from VWR Chemicals (Monroeville, PA, USA). The UHPLC-MS/MS system consisted of a PerkinElmer Flexar UHPLC system (two FX-10 binary pumps, solvent manager, autosampler, and thermostatic oven; all PerkinElmer Inc. (Waltham, MA, USA)), coupled to an AB SCIEX QTRAP 5500 MS/MS triple quadrupole mass spectrometer and controlled by Analyst 1.7.1 software (both AB Sciex, Framingham, MA, USA).

2.5.2. Plasma and Urine Samples

Plasma and urine samples were collected, prepared, and measured according to previously published methodologies [67,123,124]. The samples were collected between 8 a.m. and 12 p.m. local time to limit circadian variability.

2.6. The Enzyme Activities of Tryptophan (Trp) Metabolism

The enzyme activity of Trp metabolism was estimated by calculating the ratio of the product-to-substrate concentration ratio.

2.7. Oxidative Stress and Excitotoxicity Indices

The oxidative stress index was derived by calculating the ratio between the concentration of the presumed pro-oxidant metabolite 3-HK and the combined concentrations of the putative antioxidant metabolites KYNA, anthranilic acid (AA), and xanthurenic acid (XA) (Equation (4)).

$$Oxidative\ stress\ index\ = \frac{[3-hydroxykynurenine]}{[Kynurenic\ acid]+[Anthranilic\ acid]+[Xanthurenic\ acid]} \quad (4)$$

The excitotoxicity index was determined by computing the ratio of quinolinic acid (QA), an NMDA receptor agonist, to KYNA, an endogenous NMDA receptor antagonist (Equation (5)).

$$Excitotoxicity\ index\ =\ \frac{[Quinolinic\ acid]}{[Kynurenic\ acid]} \quad (5)$$

2.8. Statistical Analysis

All statistical analyses were conducted using IBM SPSS Statistics, version 28.0.0.0 (IBM Corp., Armonk, NY, USA). The normality of data distribution was assessed with the Shapiro–Wilk test, and Q-Q plots were additionally employed to evaluate whether two datasets originated from the same distribution.

In the statistical evaluation of the NORT, OBAT, and Y-maze, 3CT, and rotarod test, inter-strain comparisons were performed using the independent samples *t*-test for normally distributed data, whereas the non-parametric Mann–Whitney U test was employed in cases where the assumption of normality was violated. Intra-strain comparisons of individual parameters were carried out using the paired samples *t*-test when data conformed to a normal distribution, and the Wilcoxon signed-rank test was applied for non-normally distributed datasets.

For the MBT, a mixed ANOVA model was used, followed by the Tamhane post hoc test.

Regarding the UHPLC-MS/MS measurements, the normality of the variables was checked using the Kolmogorov–Smirnov test and visually checked using quantile-quantile plots, and the equality of variances was examined using Welch's F-test. Outliers were identified using Grubbs's test. Comparisons between the two groups were conducted using an independent samples *t*-test.

Values $p < 0.05$ were considered statistically significant. Our data are reported as means ± standard deviations (SD) for all parameters and experimental groups.

3. Results

3.1. Behavioral Tests

3.1.1. Novel Object Recognition Test (NORT)

During the NORT, both WT and *kat2*$^{-/-}$ animals spent significantly more time interacting with the novel object compared to the familiar one. However, no significant differences were detected between the strains (Figure 2, Tables S1 and S2).

3.1.2. Object-Based Attention Test (OBAT)

In the OBAT, no statistically significant differences were detected between the strains in terms of overall object interaction time. Nonetheless, animals from the *kat2*$^{-/-}$ strain exhibited a marked preference for the novel object, spending significantly more time engaging with it compared to the familiar object during the testing phase (Figure 2, Tables S1 and S2).

3.1.3. Three Chamber Test (3CT)

During the 3CT, both examined strains spent significantly less time in the lateral chambers compared to the central starting chamber in both the second and third phases of the test. Apart from this difference, no other significant variations were observed (Figure 2, Tables S1 and S2).

3.1.4. Other Behavioral Tests

No significant differences were observed between the strains or within strains in the Y-maze, MBT, and rotarod tests (Table S1).

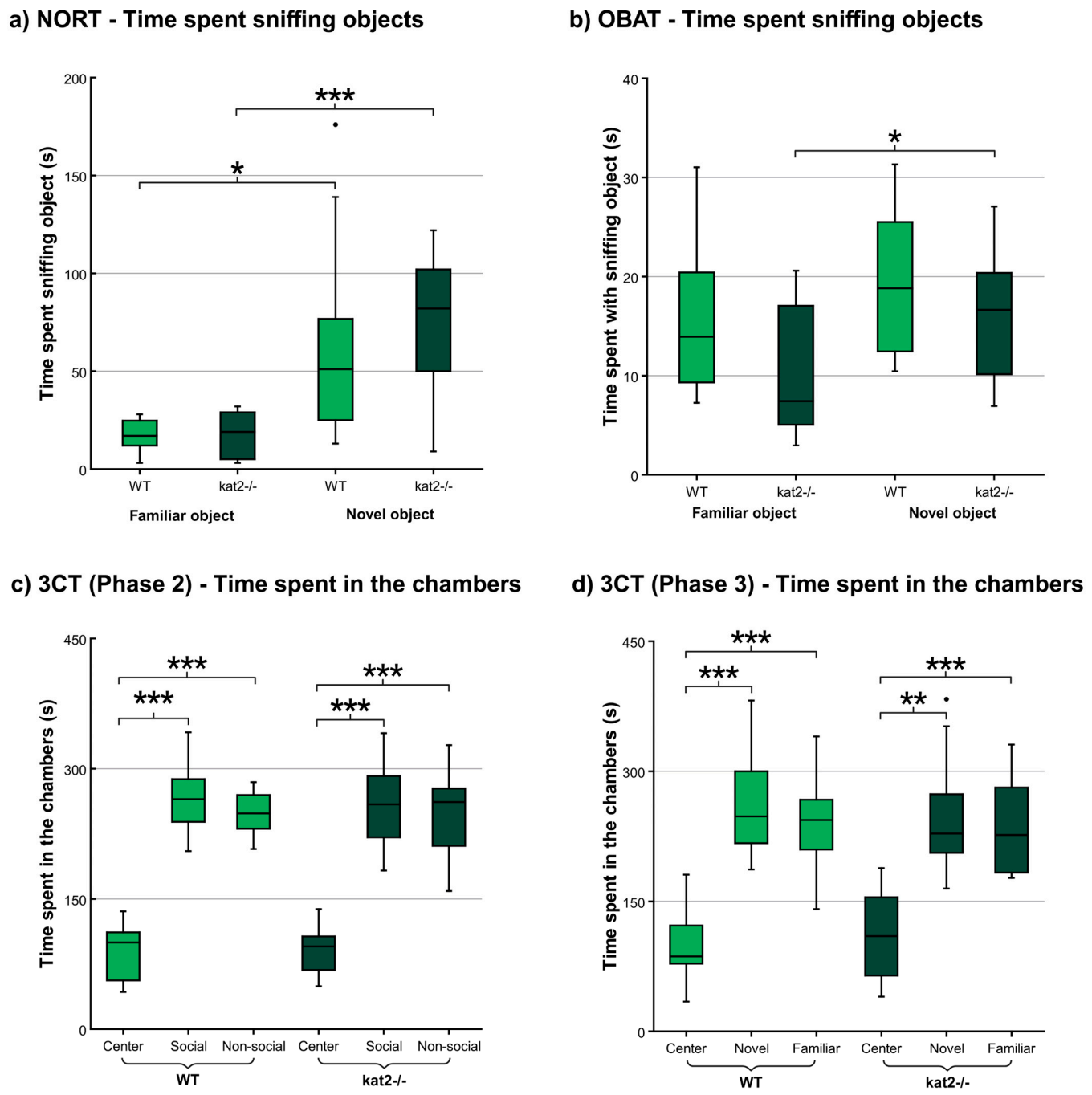

Figure 2. Behavioral assessment of wild-type (WT) and *kat2*$^{-/-}$ mice in object recognition and social interaction paradigms. (**a**) Time spent sniffing familiar vs. novel objects in the novel object recognition test (NORT). During the NORT, both WT and *kat2*$^{-/-}$ animals spent significantly more time exploring the novel object. (**b**) Time spent sniffing familiar vs. novel objects in the object-based attention test (OBAT). In the OBAT, the mutant strain spent more time with the novel object. (**c**) Time spent in the center, social, and non-social chambers during the three-chamber test (3CT, Phase 2). Both WT and *kat2*$^{-/-}$ mice spent more time in the side chambers than in the center chamber. (**d**) Time spent in the center, novel animals, and familiar animals' chambers during the 3CT (Phase 3). Both WT and *kat2*$^{-/-}$ mice spent more time in the side chambers than in the center chamber. Wild-type mice (light green); *kat2*$^{-/-}$ mice (dark green). Data are presented as mean ± SD. •, outlier. *, $p < 0.05$; **, $p < 0.01$; ***, $p < 0.001$. The figure was created with LabPlot 2.9.0 (KDE, Berlin, Germany) and BioRender.com. 3CT, three-chamber test; *kat2*$^{-/-}$, kynurenine aminotransferase II knockout mice; NORT, novel object recognition test; OBAT, object-based attention test; WT, wild-type mice.

3.2. Ultra-High-Performance Liquid Chromatography with Tandem Mass Spectrometry (UHPLC-MS/MS)

Several differences were observed between the WT and mutant strains in the various brain regions examined during the chemical analytical measurements (Figures 3–5, Tables S3 and S4). The most prominent difference was observed in the level of 3-HK, which was uniformly and significantly increased in all examined brain regions of the *kat2*$^{-/-}$ strain compared to the WT. In a similar pattern, xanthurenic acid (XA) levels were reduced across all analyzed regions relative to the WT. In contrast, the concentration of KYNA, whose alteration was most strongly anticipated, exhibited a significant reduction only in the CTX and HIPP; however, the level of KYNA is increased in the STR. Interestingly, the level of its downstream metabolite, quinaldic acid (QAA), remained unaltered in these same areas, while a marked decrease was observed in the CRB and STEM.

In addition to the detailed concentration values presented above, a region- and matrix-integrated overview of metabolite alterations is provided (Table S3). Consistent across all examined brain regions, 3-HK was significantly elevated, whereas XA showed a uniform reduction, underscoring a shift toward an oxidative and excitotoxic milieu. KYNA exhibited a divergent pattern, being decreased in the CTX and HIPP yet elevated in the STR, while QAA was selectively reduced in the CER and STEM. Within the serotonergic pathway, 5-hydroxytryptophan (5-HTP) declined in CTX and CER, whereas 5-HT increased in CTX and urine, indicating altered turnover. Further changes included decreased Tyrin CTX and HIPP and selective reductions in pterins. Peripheral findings in plasma and urine, previously published, are integrated here for comparison, emphasizing the concordance between central and systemic metabolic rewiring.

Complementing our previous measurements of Trp metabolite levels in plasma and urine, we also measured the concentrations of additional metabolites from the indole-pyruvate and TYR-DA pathways; however, we observed significant changes only in 3-methoxy-4-hydroxyphenylglycol sulfate (MHPGS) levels compared to WT (Figure 5, Table S4).

3.3. Enzyme Activities

Enzyme activity ratios revealed pronounced remodeling of tryptophan metabolic fluxes in *kat2*$^{-/-}$ mice (Figure 6, Table S5). As expected, KAT activity (KYN/Trp) displayed a selective reduction in the STR, consistent with the genetic deletion of KAT II. Conversely, KMO activity (3-HK/KYN) was markedly elevated across STR, CTX, HIPP, CER, and STEM, indicating enhanced pro-oxidant pressure through 3-HK production. KYNU activity (3-HAA/3-HK) showed a modest yet significant increase in the HIPP, while KAT III activity (XA/3-HK) was consistently reduced in CTX, HIPP, CER, and STEM, reinforcing the loss of protective XA formation. Within the serotonergic arm, tryptophan hydroxylase (TPH) activity (5-HTP/Trp) was reduced in CTX and CER, whereas aromatic L-amino acid decarboxylase (AADC) activity (5-HT/5-HTP) was elevated in STR, CTX, and HIPP, suggesting compensatory 5-HT turnover. MAO/ALDH activity (5-HIAA/5-HT) was decreased only in CTX, while TMO activity (IAA/Trp) was reduced in CTX, HIPP, and CER. Furthermore, the activity of MAOs (DOPAC/DA) significantly decreased, while the activity of COMT (HVA/DOPAC) increased in CER. Collectively, these shifts highlight a pathway-specific reorganization, with KMO dominance, curtailed XA buffering, and altered 5-HT–indole and Tyr-DA dynamics shaping the *kat2*$^{-/-}$ metabolic phenotype.

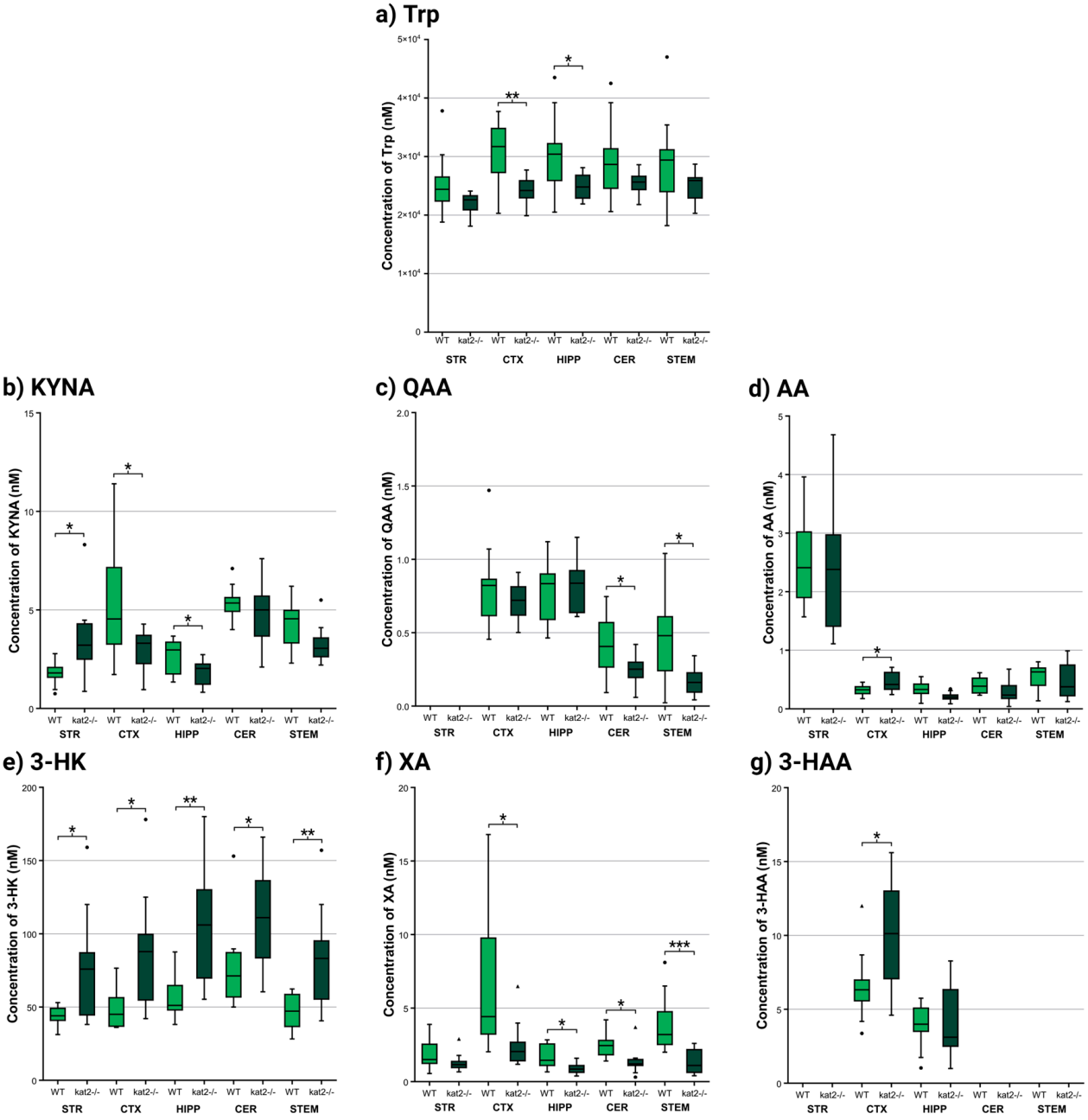

Figure 3. Regional distribution of kynurenine (KYN) pathway metabolites in wild-type (WT) and *kat2*$^{-/-}$ mouse brains. (**a**) Tryptophan (Trp), (**b**) Kynurenic acid (KYNA), (**c**) Quinaldic acid (QAA), (**d**) Anthranilic acid (AA), (**e**) 3-hydroxykynurenine (3-HK), (**f**) Xanthurenic acid (XA), and (**g**) 3-Hydroxyanthranilic acid (3-HAA) concentrations measured in striatum (STR), cortex (CTX), hippocampus (HIPP), cerebellum (CER), and brainstem (STEM). Trp was significantly lower in STR, CTX, and HIPP. While KYNA increased in STR, its concentration lowered in CTX and HIPP. QAA's concentration was significantly lower in CER and STEM. The level of AA was higher in CTX. The concentration of 3-HK increased in every brain region. XA decreased in CTX, HIPP, CER, and STEM. The level of 3-HAA increased in CTX. Wild-type (WT, light green) and *kat2*$^{-/-}$ (dark green) groups are shown. Data are expressed as mean ± SD. •, outlier; ▲, far out. *, $p < 0.05$; **, $p < 0.01$; ***, $p < 0.001$. The figure was created with LabPlot 2.9.0 (KDE, Berlin, Germany) and BioRender.com. 3-HAA, 3-hydroxyanthranilic acid; 3-HK, 3-hydroxykynurenine; AA, anthranilic acid; CER, cerebellum; CTX, cortex; HIPP, hippocampus; KYNA, kynurenic acid; QAA, quinaldic acid; STEM, brainstem; STR, striatum; Trp, tryptophan; WT, wild-type mice; *kat2*$^{-/-}$, kynurenine aminotransferase II knock-out mice; XA, xanthurenic acid.

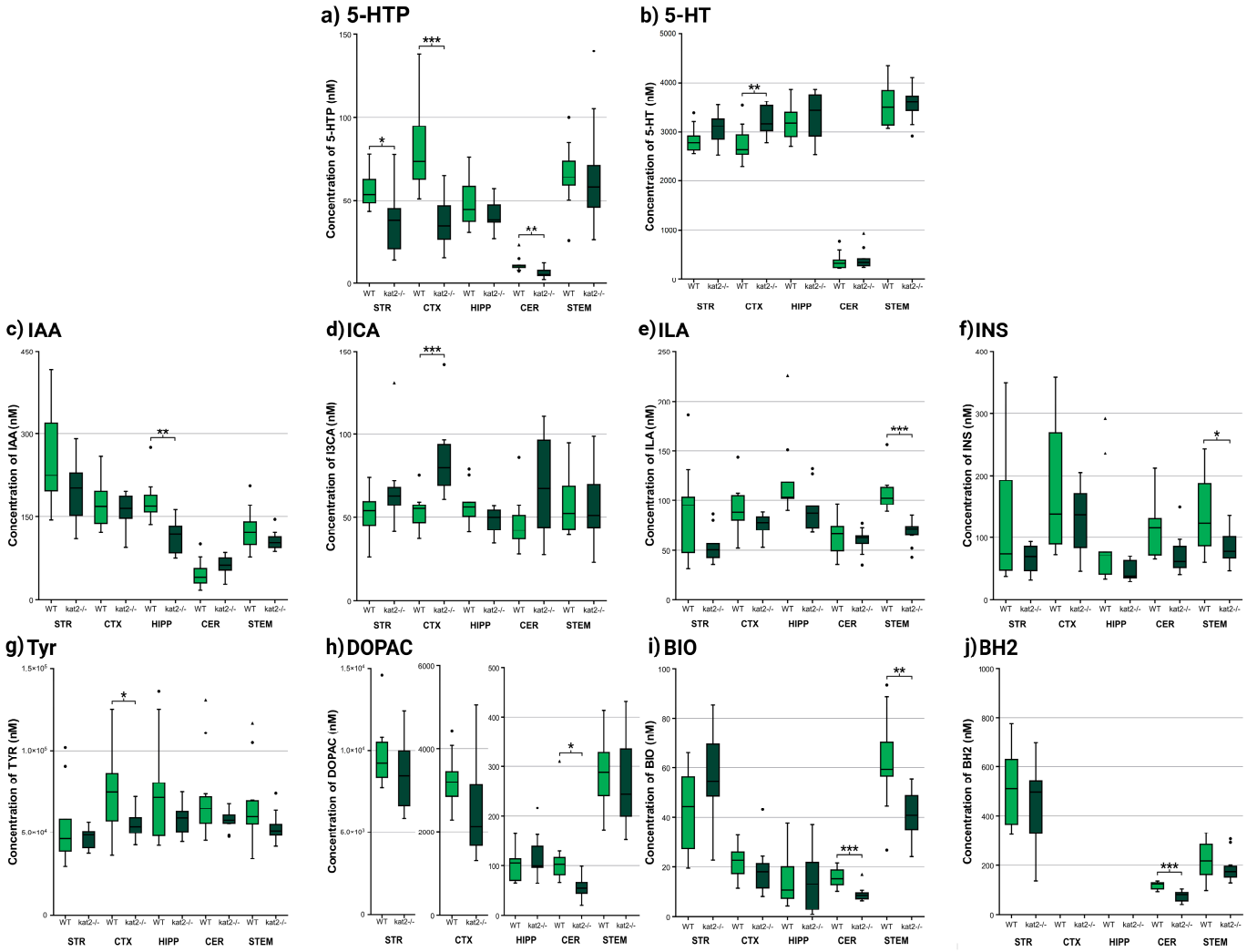

Figure 4. Region-specific alterations in serotonin (5-HT)-, indole-pyruvate-, and tyrosine (Tyr)–dopamine (DA)-derived metabolites in wild-type (WT) and *kat2*$^{-/-}$ mice. Box plots showing concentrations of metabolites across brain regions in wild-type (WT, light green) and *kat2*$^{-/-}$ (dark green) mice. (**a**,**b**) Serotonin pathway: 5-HTP (5-hydroxytryptophan), 5-HT (5-hydroxytryptamine, serotonin). (**c**–**f**) Indole-pyruvate pathway: IAA (indole-3-acetic acid), ICA (indole-3-carboxaldehyde), ILA (indole-3-lactic acid), INS (indoxyl sulfate). (**g**–**j**) Tyrosine-dopamine pathway: Tyr, DOPAC (3,4-dihydroxyphenylacetic acid), BIO (biopterin), BH2 (dihydrobiopterin). Brain regions: STR, striatum; CTX, cortex; HIPP, hippocampus; CER, cerebellum; STEM, brainstem. 5-HTP concentrations were reduced in the STR, CTX, and CER, whereas 5-HT levels were selectively increased in the CTX. IAA concentrations were diminished in the HIPP, ILA, and INS within the STEM, while ICA levels were elevated in the CTX. Tyr levels were reduced in the CTX, and decreases in DOPAC, BIO, and BH2 were detected in the CER. Data are shown as mean ± SD. Symbols: ●, outlier; ▲, far out. Significance: *, $p < 0.05$; **, $p < 0.01$; ***, $p < 0.001$. Figures created with LabPlot 2.9.0 (KDE, Berlin, Germany) and BioRender.com. 5-HT, serotonin (5-hydroxytryptamine); 5-HTP, 5-hydroxytryptophan; BH2, dihydrobiopterin; BIO, biopterin; CER, cerebellum; CTX, cortex; DOPAC, 3,4-dihydroxyphenylacetic acid; HIPP, hippocampus; ICA, indole-3-carboxaldehyde; IAA, indole-3-acetic acid; ILA, indole-3-lactic acid; INS, indoxyl sulfate; *kat2*$^{-/-}$, kynurenine aminotransferase II knockout mice; STEM, brainstem; STR, striatum; Tyr, tyrosine; WT, wild-type mice.

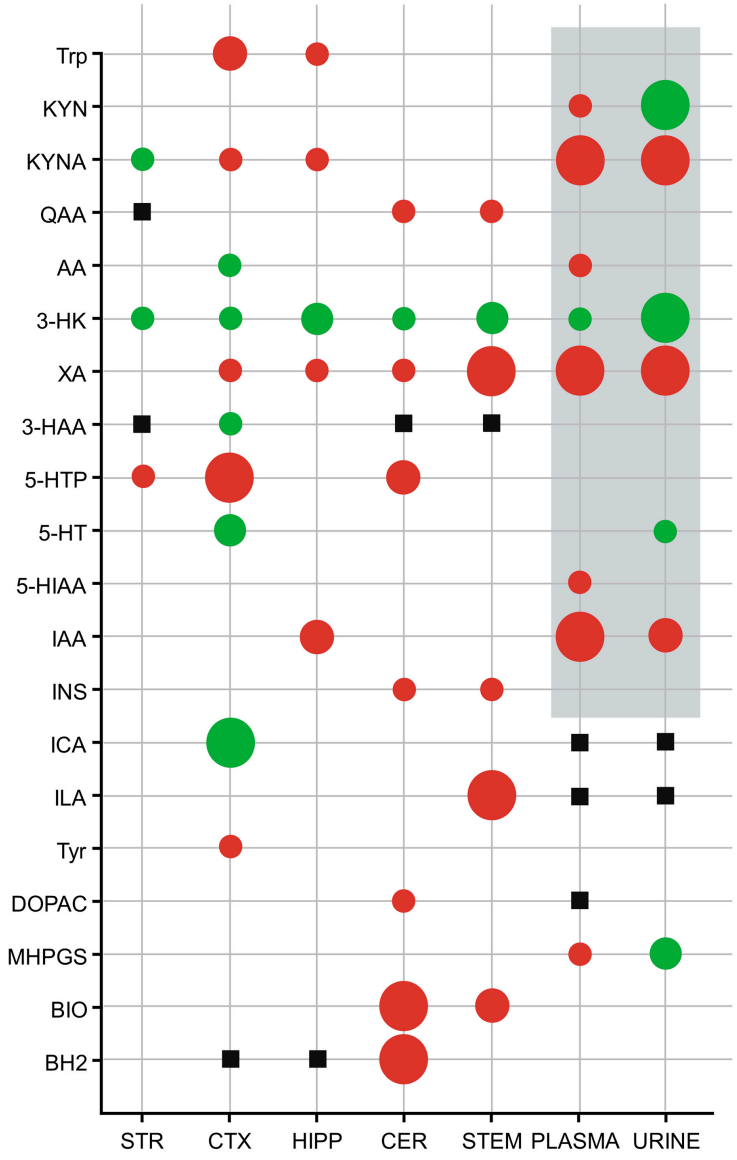

Figure 5. Overview of region- and matrix-specific alterations in tryptophan-derived metabolites in 8-week-old male *kat2*$^{-/-}$ mice compared to wild-type (WT) controls in ultra-high-plasticity liquid chromatography with tandem mass spectrometry. This figure summarizes significant alterations in tryptophan–kynurenine, serotonin, indole-pyruvate, and tyrosine–dopamine pathway metabolites across distinct brain regions (striatum, cortex, hippocampus, cerebellum, brainstem), plasma, and urine in *kat2*$^{-/-}$ mice compared to the WT. Results highlight the region- and pathway-selective metabolic rewiring induced by *kat2* deletion, particularly the consistent increase of 3-hydroxykynurenine and decrease in xanthurenic acid, alongside mixed kynurenic acid responses and downstream shifts in serotonin, indole, and catecholamine derivatives. We marked significant changes with circles. Red circles mean a statistically significant decrease, and green shows a significant increase in the concentration compared to the WT mice. The increasing size of the circles indicates higher levels of significance (small circle: $p < 0.05$; medium circle: $p < 0.01$; large circle: $p < 0.001$). Gray rectangle background: previously published results [67]. Black square: no data. 3-HAA, 3-hydroxyanthranilic acid; 3-HK, 3-hydroxykynurenine; 5-HIAA, 5-hydroxyindole-3-acetic acid; 5-HT, serotonin (5-hydroxytryptamine); 5-HTP, 5-hydroxytryptophan; AA, anthranilic acid; BH2, dihydroxybiopterin; BIO, biopterin; CER, cerebellum; CTX, cortex; DOPAC, 3,4-dihydroxyphenylacetic acid; HIPP, hippocampus; IAA, indole acetic acid; ICA, indole-3-carboxaldehyde; ILA, indole-3-lactic acid; INS, indoxyl sulfate; KYN, kynurenine; KYNA, kynurenic acid; MHPGS, 3-methoxy-4-hydroxyphenylglycol sulfate; QAA, quinaldic acid; Trp, tryptophan; Tyr, tyrosine; STEM, brainstem; STR, striatum; XA, xanthurenic acid.

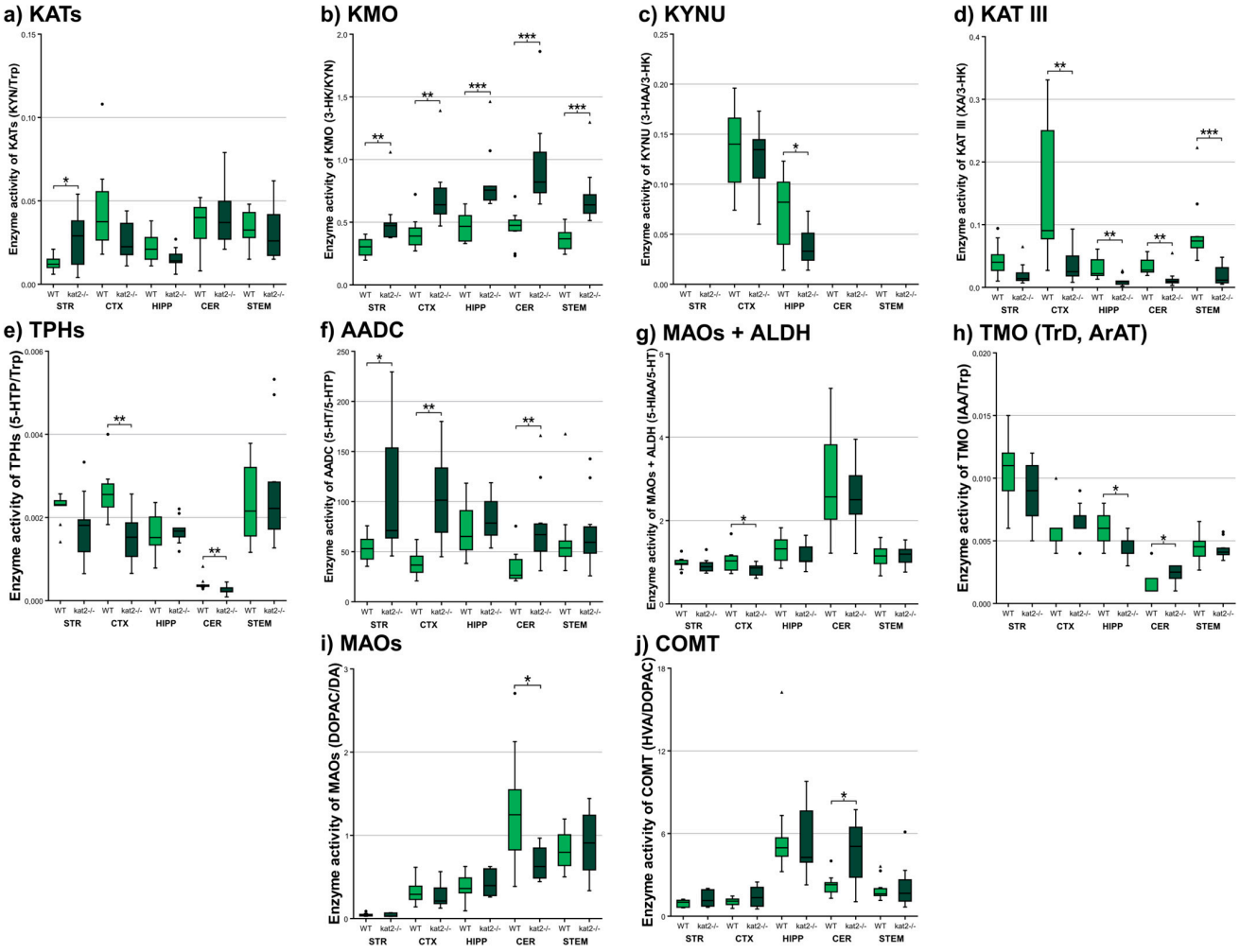

Figure 6. Regional enzyme activity alterations in tryptophan- and serotonin (5-HT)-associated pathways in WT and *kat2*$^{-/-}$ mice. Box plots showing enzyme activities across striatum (STR), cortex (CTX), hippocampus (HIPP), cerebellum (CER), and brainstem (STEM) in wild-type (WT, light green) and *kat2*$^{-/-}$ (dark green) mice. Activities were calculated as product-to-substrate ratios for: (**a**) KATs (KYNA/KYN), (**b**) KMO (3-HK/KYN), (**c**) KYNU (3-HAA/3-HK), (**d**) KAT III (XA/3-HK), (**e**) TPHs (5-HTP/Trp), (**f**) AADC (5-HT/5-HTP), (**g**) MAOs + ALDH (5-HIAA/5-HT), (**h**) TMO [TrD, ArAT] (IAA/Trp), (**i**) MAOs (DOPAC/DA), (**j**) COMT (HVA/DOPAC). Enzyme activity of KATs decreased in STR. KMO's activity significantly increased in every brain region. KYNU's activity decreased in HIPP. KAT III enzyme activity decreased in CTX, HIPP, CER, and STEM. Activity of TPH enzymes decreased in CTX and CER. AADC's activity decreased in STR, CTX, and CER. MAOs + ALDH decreased in CTX. TMO's activity decreased in HIPP and CER. Activity of MAOs in the tyrosine-dopamine pathway significantly decreased in CER. COMT's activity increased in CER. Data are shown as mean ± SD. Symbols: ●, outlier; ▲, far out. Statistical significance: *, $p < 0.05$; **, $p < 0.01$; ***, $p < 0.001$. Figures were created with LabPlot 2.9.0 (KDE, Berlin, Germany) and BioRender.com. 3-HAA, 3-hydroxyanthranilic acid; 3-HK, 3-hydroxykynurenine; 5-HIAA, 5-hydroxyindoleacetic acid; 5-HT, serotonin (5-hydroxytryptamine); 5-HTP, 5-hydroxytryptophan; AADC, aromatic L-amino acid decarboxylase; ALDH, aldehyde dehydrogenase; ArAT, aromatic amino acid aminotransferase; CER, cerebellum; COMT, catechol-O-methyltransferase; CTX, cortex; DA, dopamine; DOPAC, 3,4-dihydroxyphenylacetic acid; HIPP, hippocampus; HVA, homovanillic acid; IAA, indole-3-acetic acid; KAT III, kynurenine aminotransferase III; KATs, kynurenine aminotransferases; *kat2*$^{-/-}$, kynurenine aminotransferase II knockout; KMO, kynurenine-3-monooxygenase; KYN, kynurenine; KYNU, kynureninase; MAOs, monoamine oxidases; STEM, brainstem; STR, striatum; TMO, tryptophan-2-monooxygenase; TPHs, tryptophan hydroxylases; TrD, tryptophan decarboxylase; Trp, tryptophan; WT, wild-type mice; XA, xanthurenic acid.

3.4. Oxidative Stress and Ecitotoxicity Indices

To further evaluate the balance between oxidative pressure and excitotoxic potential, we calculated composite indices from key KYN metabolites (Figure 7, Table S6). The oxidative stress index, defined as 3-HK/(KYNA + AA + XA), was significantly elevated in multiple brain regions of *kat2*$^{-/-}$ mice. Compared to WT controls, the CTX, HIPP, CER, and STEM all exhibited marked increases, with the HIPP and STEM showing the most robust elevations. This pattern reflects the combined impact of increased 3-HK and reduced antioxidant metabolites, underscoring a shift toward pro-oxidant load. In contrast, the excitotoxicity index, measured as QA/KYNA, showed a more selective profile. While values remained unchanged in STR, CTX, and CER, a significant increase emerged in the HIPP, where diminished KYNA coincided with elevated QA. A similar trend, though nonsignificant, was observed in the STEM. Taken together, these data indicate that KAT II deficiency imposes a dual burden of oxidative stress and region-specific excitotoxic vulnerability, with the HIPP emerging as a particularly sensitive locus of metabolic imbalance.

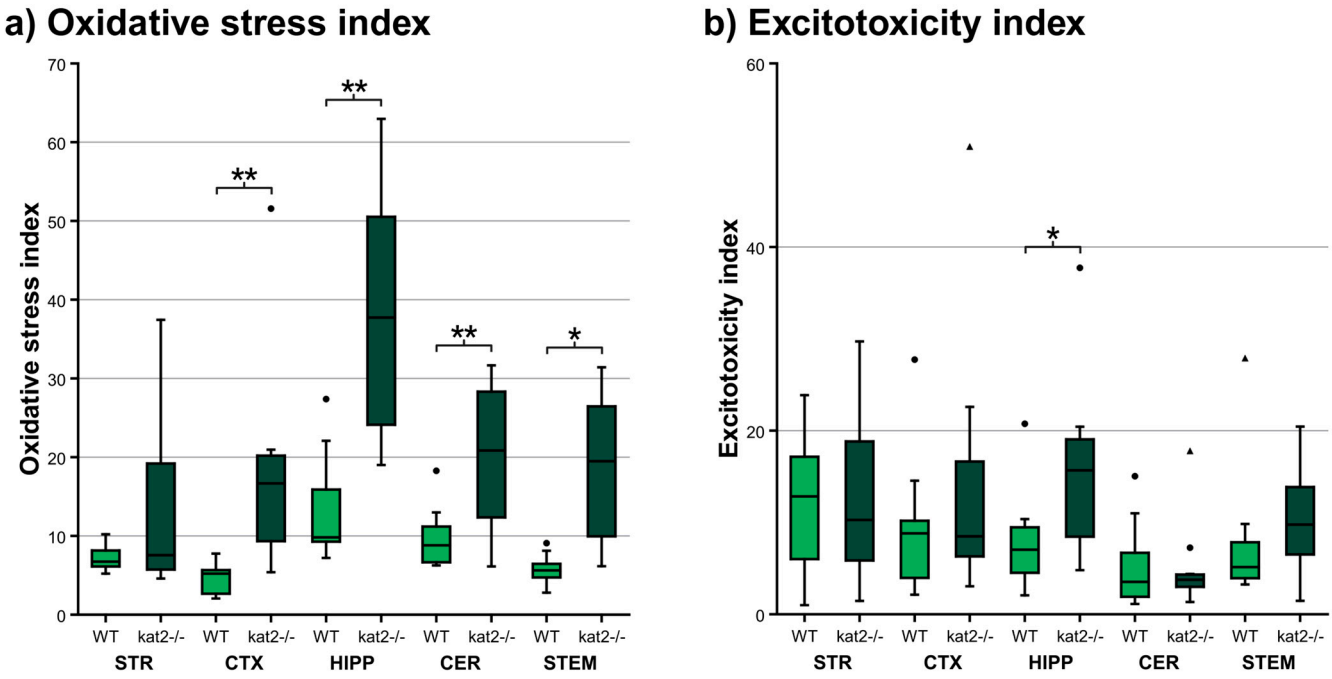

Figure 7. Regional indices of oxidative stress and excitotoxicity in wild-type (WT) and *kat2*$^{-/-}$ mice. Box plots showing oxidative stress and excitotoxicity indices across striatum (STR), cortex (CTX), hippocampus (HIPP), cerebellum (CER), and brainstem (STEM) in WT (light green) and *kat2*$^{-/-}$ (dark green) mice. (**a**) Oxidative stress index, calculated as the ratio 3-HK/(KYNA + AA + XA), reflecting the balance between pro-oxidant and antioxidant metabolites. The oxidative stress index significantly increased in CTX, HIPP, CER, and STEM. (**b**) Excitotoxicity index, calculated as the ratio QA/KYNA, representing the N-methyl-D-aspartate (NMDA) receptor agonist-to-antagonist balance. The excitotoxicity index increased in HIPP. Data are shown as mean ± SD. Symbols: •, outlier; ▲, far out. Statistical significance: *, $p < 0.05$; **, $p < 0.01$. Figures generated with LabPlot 2.9.0 (KDE, Berlin, Germany) and BioRender.com. 3-HK, 3-hydroxykynurenine; AA, anthranilic acid; CER, cerebellum; CTX, cortex; HIPP, hippocampus; *kat2*$^{-/-}$, kynurenine aminotransferase II knockout mice; KYNA, kynurenic acid; QA, quinolinic acid; STEM, brainstem; STR, striatum; WT, wild-type mice; XA, xanthurenic acid.

Results begin with region-resolved metabolomics across STR, CTX, HIPP, CER, and STEM, followed by enzyme-ratio proxies, cofactor mapping, and alignment with behavioral outcomes. A convergent central signature emerges: 3-HK increases and XA decreases pan-regionally, KYNA reduction localizes to CTX and HIPP, KMO activity indices rise while KAT

III flux falls, and oxidative-stress measures increase broadly, with a hippocampal-specific rise in the excitotoxicity index. Cofactor analyses identify BIO depletion in CER and STEM and BH2 loss in CER. Gut–brain and serotonergic markers also shift, with hippocampal IAA reduction, cortical and cerebellar ICA elevation, and reduced cortical 5-HT turnover, yet cognition, sociability, and coordination remain intact. While these preserved functions are reported alongside metabolic profiles, we did not conduct formal correlations linking regional metabolite concentrations to behavioral readouts. This omission reflects the study scope and sample size rather than a conceptual barrier. We now state this as a limitation and outline plans to evaluate specific associations, such as hippocampal KYNA with NORT performance, within a prospectively powered framework. Consistent with region-specific rewiring rather than a uniform KAT II effect, we note a paradoxical pattern: striatal KYNA elevation likely reflects compensatory KAT isoforms or astrocyte-mediated KYN shunting; forebrain bias toward AA aligns with oxidative-stress–driven KMO→KYNU flux that diverts 3-HK from KYNA. In sum, findings delineate a KMO-tilted, pterin-constrained, indole-modulated milieu that selectively burdens affective and motor subdomains while sparing core cognitive and social functions.

4. Discussion

The metabolism of Trp has emerged as a central hub in the neurobiology of cognition, mood, and social behavior, with imbalances along its KYN, 5-HT, indole, and DA branches increasingly linked to neuropsychiatric and neurodegenerative disorders [15,16,22,28,39]. Within this network, KAT II has been considered the dominant enzymatic source of KYNA, a metabolite long viewed as neuroprotective through NMDA, α7-nAChR, AMPA, and kainate antagonism [20,67,125–130]. Yet, earlier reports of global KAT II inhibition or genetic deletion left unresolved how local shifts in KYNA and related metabolites shape functional brain states [20,28,67,126,129,131]. By combining region-resolved metabolomics with behavioral phenotyping, our study addresses this gap, asking whether neurochemical disequilibria in KAT II deficiency necessarily translate into overt cognitive, motor, or social dysfunction [20,22,67,132,133]. To support cross-domain reading, behavioral tasks are mapped to region-specific metabolite indices using shared labels and synchronized panel order, pairing NORT and three chambers with cortical and hippocampal KYNA and 3 HK, and Rotarod with striatal metrics.

Mechanistic bridge linking regional rewiring to behavior. The metabolomic pattern combines KYNA reduction in CTX and HIPP with KYNA elevation in STR, alongside higher oxidative pressure in several regions and a hippocampal rise in the excitotoxicity index. Such spatial heterogeneity can stabilize baseline outputs via compensatory gating while lowering the threshold for deficits when tasks recruit prefrontal hippocampal integration or impose stress. This perspective shifts the focus from global impairment to domain-specific resilience versus vulnerability that depends on region and task demand.

Notably, the lack of inter-strain differences across cognitive, social, and motor tests suggests that *kat2* deletion does not inherently induce depressive-like behavior under baseline conditions. This finding contrasts with our previous report of despair-linked phenotypes under stress paradigms [67], implying that the emotional alterations in *kat2*$^{-/-}$ mice are context-dependent. Rather than manifesting as overt depression-like behavior, the current data support a model in which KAT II deficiency biases affective circuitry through neurochemical disequilibrium, particularly elevated 3-HK and diminished KYNA, thereby establishing a stress-reactive emotional predisposition. Hence, “emotional bias” in this context refers to a neurochemical vulnerability rather than a direct behavioral outcome.

The metabolic profile emerging from *kat2*$^{-/-}$ brains reveals a striking shift toward a pro-oxidant milieu, characterized by pan-regional accumulation of 3-HK and consistent

loss of XA, with an additional region-selective reduction in KYNA in CTX and HIPP. Such changes converge on a biochemical signature that indicates heightened KMO activity alongside impaired KAT II flux, effectively tilting the KYN pathway toward neurotoxic branch products [35,67,134]. The imbalance between reduced antioxidant buffering (XA, KYNA) and sustained excitatory drive amplifies oxidative-stress indices across regions, with the HIPP exhibiting a peak excitotoxicity signal. This constellation suggests that, although behavioral performance remained intact, the HIPP in particular resides in a precarious metabolic state, vulnerable to secondary insults [135]. Thus, the observed disequilibrium highlights a latent central risk architecture, in which KAT II deficiency may predispose selective circuits to degeneration under stress or aging.

The selective decline of KYNA in HIPP and CTX is particularly consequential, as these structures form the backbone of glutamatergic integration underlying memory, attentional control, and affective regulation [126,136–140]. Lower KYNA levels in these regions imply diminished tonic antagonism at NMDA and α7-nicotinic receptors, a state that can facilitate plasticity yet simultaneously heighten vulnerability to excitotoxic cascades. Such changes resonate with the well-documented link between KYN pathway imbalance and affective or cognitive disturbances. In contrast, the cerebellar and STEM pattern, where QAA and related metabolites decline, speaks to circuits subserving motor coordination and arousal [126,136,137,141]. Here, altered metabolic buffering could subtly recalibrate sensorimotor integration and vigilance states, aligning with CER–STEM contributions to motor timing and autonomic tone. Together, these region-specific shifts underscore circuit-level rebalancing rather than global disruption.

The consistent elevation of 3-HK across regions, paralleled by a decline in XA, underscores a shift toward a redox-imbalanced milieu that favors oxidative stress [142–144]. This pro-oxidant tilt is further amplified when considered in the context of derived indices, where the 3-HK–to–antioxidant ratio signals a vulnerability state rather than an immediate injury [142–144]. In parallel, the excitotoxicity index, weighted by QA/KYNA balance, delineates selective windows in which NMDA drive may outweigh intrinsic antagonism [140,142,143,145,146]. These biochemical loads, however, need not manifest uniformly as behavioral deficits at baseline [147–149]. Accordingly, references to depression or post-traumatic stress disorder denote hypothesis-generating convergence on shared metabolic nodes, not confirmation of disorder-specific phenotypes in mice [67,150,151]. Instead, they may represent latent liabilities, poised to surface under developmental, aging, or environmental stressors, thereby marking a hidden susceptibility rather than an overt phenotype [15,143,144].

Region-specific perturbations in the pterin pool highlight a subtle but consequential layer of metabolic vulnerability [152–154]. In *kat2*$^{-/-}$ hindbrain, the concurrent depletion of BIO and loss of BH_2 suggest an erosion of the redox-cycling capacity that normally safeguards BH_4 availability [152–154]. Because BH_4 is indispensable for tyrosine hydroxylase activity, even modest shifts in this cofactor equilibrium may attenuate DA biosynthesis and, secondarily, compromise broader monoaminergic tone [152–155]. These alterations could reverberate into nitric oxide biology, given that endothelial and neuronal nitric oxide synthase (NOS) also require BH_4, thereby coupling monoamine insufficiency to redox imbalance and impaired vasomodulation [152–154].

The neurochemical profile in *kat2*$^{-/-}$ mice suggests that reduced serotonergic turnover in the CTX converges with decreased hippocampal IAA and concomitant elevations of ICA in cortical and cerebellar regions to shape circuit-level excitability [156–158]. Lower 5-HT turnover may weaken cortical inhibitory tone, thereby amplifying the impact of indole-derived signaling [157,158]. The reduction in IAA, a ligand with protective barrier and anti-inflammatory properties, contrasts with the elevation of ICA, a potent AhR agonist capable

of reprogramming microglial states [156–158]. Through this shift, cortical and cerebellar microglia may adopt transcriptional phenotypes that subtly recalibrate glutamatergic drive and synaptic responsiveness [156–158]. Such AhR-mediated modulation, in concert with altered serotonergic dynamics, delineates a mechanism by which KAT II deficiency reshapes microcircuit stability without overtly impairing cognitive or social behaviors.

The parallel remodeling of Trp metabolism across central and peripheral compartments suggests a degree of concordance that greatly enhances translational traction [15,159,160]. When brain signatures mirror those detected in plasma or urine—such as the uniform elevation of 3-HK and the consistent reduction in XA—biomarker feasibility is strengthened because measurements in accessible fluids reliably report on neurochemical states [15,159,160]. This concordance further supports longitudinal monitoring, since repeated peripheral sampling can index dynamic shifts in pathway fluxes without invasive procedures [15,159,160]. Importantly, the pattern of a KMO-tilted, pterin-constrained phenotype provides a stratification handle: individuals or models exhibiting this profile may constitute a distinct subgroup marked by heightened oxidative burden and diminished neuroprotection [15,131,159]. Thus, the central–peripheral alignment not only validates observed signatures but also operationalizes them for precision tracking and targeted intervention [161].

Despite a pervasive biochemical tilt toward oxidative stress and excitotoxic vulnerability, baseline cognition and sociability remain largely preserved in *kat2*$^{-/-}$ mice. This dissociation likely reflects both redundancy within cognitive and social circuits and compensatory plasticity that stabilizes performance until a higher stress threshold is breached [67,162,163]. Cortico-hippocampal KYNA loss may sensitize affective and attentional pathways, but parallel buffering via dopaminergic and indole-linked mechanisms appears sufficient to maintain recognition memory and sociability in standard tasks. In contrast, motor and affective domains, subserved by CER–STEM loops and stress-responsive hippocampal circuits, manifest early pressure, consistent with lower redundancy and higher task sensitivity. These findings underscore that metabolic disequilibria need not uniformly generalize to behavior and that endpoint detectability hinges on domain-specific thresholds. For experimental design, this argues against relying solely on cognition- or sociability-based readouts and instead favors composite panels that capture latent affective or motor liabilities, especially when probing therapeutic interventions or stress challenges.

The paradoxical distribution of metabolites across brain regions points to a region-specific metabolic rewiring rather than a uniform effect of *kat2* loss [125,164]. Striatal KYNA increased, while it declined in CTX and HIPP and remained unchanged in CER and STEM. This striatal KYNA elevation in the absence of *kat2* likely arises from alternative KAT isoform activity or astrocyte-mediated KYN shunting, consistent with the region's dense dopaminergic and glial milieu [165]. In contrast, plasma and urine showed marked KYNA reductions, underscoring that regional enzymatic compensation and astrocytic buffering, rather than systemic availability, govern KYN metabolism within the brain.

Serotonergic metabolism revealed equally complex shifts. 5-HTP fell consistently in STR, CTX, and CER, suggesting precursor depletion, yet cortical 5-HT paradoxically rose. This contrast hints at selective upregulation of decarboxylase activity or altered transporter dynamics in cortical circuits. Importantly, urine samples captured a 5-HT increase, while plasma remained unaltered—underscoring a clear brain–periphery mismatch. Similarly, Trp declined in CTX and HIPP but stayed unchanged peripherally, whereas KYN itself was stable in the brain yet shifted downward in plasma and upward in urine.

Other metabolites highlighted both paradoxical and stable nodes. 3-HK rose broadly across central and peripheral compartments, but its downstream metabolite XA decreased everywhere, revealing a systemic enzymatic bottleneck. AA, however, increased in CTX but decreased in HIPP and STEM, with no peripheral reflection. Several intermediates, in-

cluding Tyr and 3-HAA, remained stable in most regions, pointing to strong compensatory buffering. Taken together, these findings illustrate that *kat2* deletion drives a patchwork of paradoxical imbalances, where regional demands, oxidative stress, and glial density dictate divergent metabolic trajectories, while peripheral readouts capture only a partial, homogenized snapshot of these changes.

Furthermore, the single-gene *kat2* knockout, which markedly reduces KYNA concentrations, exerts consequences that extend far beyond the KYN branch alone. The disruption alters the enzymatic dynamics and metabolite distribution of the Trp–KYN axis and also propagates into parallel domains, such as serotonin biosynthesis, indole-pyruvate flux, and DA turnover. These cross-pathway perturbations likely emerge from shared substrate dependencies and competitive enzymatic hierarchies, wherein the depletion of one metabolic sink amplifies pressure on adjacent routes. In particular, diminished serotonin availability can be interpreted as a direct consequence of altered Trp partitioning, whereas DA irregularities appear linked to secondary changes in redox balance and cofactor utilization. Thus, *kat2* deletion should not be conceptualized merely as a KYNA-specific deficit; rather, it reshapes a broader neurochemical network in which serotonergic, dopaminergic, and indole-derived pathways become entrained into a cascade of adaptive yet destabilizing responses.

A key strength of this study lies in the methodological rigor that enabled reliable mapping of subtle, region-specific metabolic shifts. The UHPLC-MS/MS workflow was not only optimized for brain tissue matrices but was applied in a region-resolved fashion, thereby allowing contrasts across CTX, HIPP, STR, CER, and STEM rather than relying on pooled homogenates [166–168]. Enzyme activities were inferred through calibrated product–substrate ratios, providing functional proxies that extend beyond absolute metabolite abundance [166,168,169]. Importantly, these measurements were embedded in a multi-axis coverage that integrated KYN, serotonergic, indole-derived, and catecholamine pathways. Behavioral assays were performed with a balanced panel that minimizes habituation or training artifacts. Such a design requires a composite technical skill set—ranging from advanced metabolomics and stringent quality control pipelines to expertise in behavioral neuroscience and translational modeling—ensuring robust and reproducible interpretation.

Several limitations should be recognized when interpreting these findings. First, the study design relied on baseline-only testing, which restricts inference on developmental trajectories or dynamic responses to stressors [170–172]. Bulk tissue homogenates were analyzed, inevitably averaging across heterogeneous cell types and masking circuit-specific alterations [170,172,173]. The absence of cell-type resolution is particularly relevant, as astrocytic and neuronal pools may contribute divergently to KYN pathway flux [170,172,173]. Temporal resolution was also limited to a single time point, precluding assessment of circadian phase–dependent or activity-driven fluctuations [170,172,174]. Sex and age effects remain underpowered, raising the possibility that strain differences may emerge in females or in older cohorts [170,172,173]. An important limitation is the absence of microbiome profiling. The microbiome was not systematically characterized, despite its capacity to shape Trp-indole metabolism [175–177]. To establish intestinal origin and systemic distribution, future work will pair brain measurements with quantification of indole derivatives in fecal and plasma samples. This paired design will allow direct assessment of compartmental gradients and transport [178–180]. Without taxonomic or functional data, shifts in ICA, IAA, and INS cannot be assigned to specific microbial pathways or sources, which narrows mechanistic inference regarding gut–brain communication in this dataset [175–177]. To dissect source contributions, we will consider microbiota-targeted interventions, including antibiotic depletion, fecal microbiota transplantation, and probiotic supplementation. These perturbations, combined with fecal and plasma profiling of ICA,

IAA, and related indoles, can distinguish host from microbial activity and probe their interaction, thereby sharpening translational relevance [181–183]. Finally, circadian control was standardized but not manipulated, and phase-dependent metabolic reorganization could shift interpretations [170,172,174].

The neurochemical profile observed in *kat2*$^{-/-}$ mice points toward several therapeutic avenues [67,129,143,184]. Elevated 3-HK alongside reduced XA underscores excessive KMO flux, highlighting selective KMO inhibition as a rational intervention to rebalance the neuroprotective–neurotoxic equilibrium [184,185]. At the same time, the consistent depletion of BH4 and riboflavin-sensitive cofactor pools suggests that restoring the pterin milieu could stabilize DA synthesis and restrain aberrant redox cycling [129,184]. Antioxidant strategies targeting the 3-HK–driven oxidative load may provide additional neuroprotection, particularly in regions where KYNA is diminished [55,129]. Importantly, our data emphasize the need for composite biomarker frameworks that integrate peripheral indices of KYN pathway activity with region-sensitive readouts such as KYNA/QAA ratios, thereby offering translational precision in stratifying patients [55,67,161,184]. For navigation, Table 1 crosswalks behavioral endpoints with regional metabolite and cofactor panels using shared labels and coordinated panel order.

Table 1. Crosswalk of behavioral endpoints and regional metabolic indices. This provides a reader guide that aligns behavioral endpoints with region-specific metabolic indices using shared labels and panel order. Each row lists the task, the regions emphasized in the corresponding metabolite panels, and the indices displayed in figures and Supplementary Tables.

Domain	Behavioral Task	Primary Regions Referenced	Key Indices Listed	Figure Panels
Cognition	NORT	CTX, HIPP	KYNA, 3-HK, XA, QA/KYNA	Figure 2a; Figure 3b,e,f; Figure 5
Attention	OBAT	CTX, HIPP	KYNA, 3-HK, XA	Figure 2b; Figure 3b,e,f; Figure 5
Working memory	Y-maze	HIPP, CTX	KYNA, 3-HK, QA to KYNA	Figure 3b,e; Figure 5
Sociability	3CT sociability	CTX, CER	ICA, IAA, 5-HIAA	Figure 2c,d; Figure 4c,d; Figure 5
Social novelty	3CT novelty preference	CTX, CER, HIPP	ICA, IAA, KYNA	Figure 2c,d; Figure 4c,d; Figure 3b; Figure 5
Motor coordination	Rotarod	STR, CER	KYNA, 3-HK, AA, XA	Figure 3b,d–f; Figure 5
Affective proxy	MBT	HIPP, STEM	3-HK to KYNA plus AA plus XA	Figure 5; Figure 7a
Monoamine milieu	Task-agnostic pairing	CTX, STEM	BH4, BH2, BIO, DA cascade	Figure 4; Figure 5

AA, anthranilic acid; BIO, biopterin; BH2, dihydrobiopterin; BH4, tetrahydrobiopterin; CTX, cortex; DA, dopamine; HIPP, hippocampus; ICA, indole 3 carboxaldehyde; IAA, indole 3 acetic acid; 3-HK, 3 hydroxykynurenine; KYNA, kynurenic acid; QA, quinolinic acid; STR, striatum; CER, cerebellum; STEM, brainstem.

Microbiota-derived indoles may also function as behavior modulators through AhR-dependent signaling, glial state regulation, and serotonergic control of network excitability [156,186,187]. Aligning indole panels with selected behavioral readouts can link peripheral variation to circuit-level outcomes while maintaining conservative inference [52,188]. These convergent insights open the path toward mechanism-guided interventions that cut across psychiatric and neurodegenerative spectra [55,67,184]. Accordingly, microbiota-targeted designs should prespecify behavioral endpoints sensitive to indole tone, including NORT discrimination, three-chamber novelty preference, and open-field indices [161]. Such alignment enables tests of correspondence between ICA, IAA, or INS shifts and measurable changes in performance without reinterpreting existing results [52,189,190]. Furthermore, future work should integrate stool metagenomics or metatranscriptomics with targeted metabolomics to resolve indole biosynthetic routes [177,190,191]. Stable isotope tracing of tryptophan can quantify flux from microbial pathways into circulating indoles and help partition host and microbial contributions [192–194]. Causal designs could include

antibiotic perturbation with recovery, fecal microbiota transfer into gnotobiotic hosts, and longitudinal sampling across clinically relevant transitions [52,190,191]. Joint modeling of taxa, gene families, and indole derivatives will strengthen pathway attribution while maintaining analytic rigor [177,195,196].

Moving forward, the central challenge is to shift from descriptive associations toward mechanistic causation [131,197,198]. Stable-isotope-based in vivo flux tracing could clarify how KMO and KAT activities dynamically shape regional metabolite pools under physiological and stress conditions [197,199]. Complementary pharmacologic or genetic rescue experiments, targeting either KMO suppression or KAT reconstitution, will be critical to determine reversibility and compensatory limits of the pathway [128,131,197]. Behavioral paradigms that introduce stress load or learning demands should be layered on top of biochemical profiling to reveal context-dependent vulnerabilities [198–202].

Assays that tax prefrontal hippocampal control, including attentional set shifting, reversal learning, and contextual extinction, and assays that probe striatal gating under load, including progressive ratio and effort discounting, should be most sensitive to unmask domain-specific vulnerability [203–205]. Coupling these behaviors to region-resolved metabolomics and pathway indices, such as QA to KYNA and 3 HK to KYNA, plus AA, plus XA, will determine whether the cortical and hippocampal KYNA decrease with striatal KYNA increase marks resilience at baseline, yet reduces reserve under demand [139,206,207].

Spatial metabolomics, single-cell resolution analytics, and mesoscale circuit physiology offer the means to connect biochemical imbalances with cellular and network-level adaptations [197,199,202,208,209]. Finally, microbiome manipulation stands as a tractable lever to probe gut–brain indole inputs [131,197,199,210–212]. Integrating these platforms will close the loop from correlation to causation, refining translational targets across psychiatric and neurodegenerative disease contexts [202,213–215].

KAT II loss establishes a distinctive biochemical landscape marked by a KMO-driven tilt, reduced pterin support, and modulation through indole intermediates. This state disproportionately burdens affective and motor circuits, as evidenced by elevated 3-HK, reduced XA, and region-specific KYNA/QAA shifts, while sparing cognition and sociability under baseline conditions. Such dissociation between neurochemical disequilibria and behavioral resilience highlights the selective vulnerability of motor and emotional nodes. Viewed together, region-specific metabolic rewiring offers a parsimonious account of preserved baseline behavior through compensatory stabilization while flagging circuit and task-dependent vulnerability that is predicted to surface during cognitive challenge or stress. Crucially, these pathway imbalances converge into a coherent, biomarker-ready framework that not only clarifies the mechanistic underpinnings of Trp metabolism but also provides a tractable platform for targeted intervention strategies in neuropsychiatric disease contexts.

5. Conclusions

This work integrates region-resolved metabolomics across the STR, CTX, HIPP, CER, and STEM with enzyme-ratio proxies, cofactor mapping, and behavioral readouts. A convergent central signature emerges: 3-HK increases and XA decreases pan-regionally, KYNA reduction localizes to CTX and HIPP, KMO activity indices rise while KAT III flux falls, and oxidative-stress measures increase broadly, with a hippocampal-specific rise in the excitotoxicity index [33]. Cofactor analyses identify BIO depletion in CER and STEM and BH2 loss in CER. Gut–brain and serotonergic markers also shift, with hippocampal IAA reduction, cortical and cerebellar ICA elevation, and reduced cortical 5-HT turnover, yet cognition, sociability, and coordination remain intact. While these preserved functions suggest circuit-level compensation, the current behavioral battery was limited to baseline

conditions. Stress paradigms or cognitively demanding tasks could potentially unmask subtle or latent deficits that remain silent under low-load conditions. Recognizing this limitation refines the interpretation of apparent resilience and underscores the value of incorporating such paradigms in future investigations to delineate compensatory versus genuinely preserved function. Consistent with region-specific rewiring rather than a uniform *kat2* effect, we note a paradoxical pattern: striatal KYNA elevation likely reflects compensatory KAT isoforms or astrocyte-mediated KYN shunting; forebrain bias toward AA aligns with oxidative-stress-driven KMO→KYNU flux that diverts 3-HK from KYNA. Taken together, the KAT II/*kat2* loss establishes a reproducible brain–periphery signature (KYNA↓, 3-HK↑, region-tuned KMO/KAT flux) without broad baseline behavioral deficits—best interpreted as evidence of circuit rewiring that buffers output, i.e., whole-axis metabolic disturbance does not immediately translate into behavior [216]. This framing motivates mechanism-targeted interventions (e.g., KMO inhibition, cofactor restoration, antioxidant support) and argues for biomarker-informed stratification [184]. Finally, because microbiome profiling was outside the present scope, ICA/IAA/INS findings should be viewed as hypothesis-generating for targeted microbiome-manipulation studies. In sum, findings delineate a KMO-tilted, pterin-constrained, indole-modulated milieu that selectively burdens affective and motor subdomains while sparing core cognitive and social functions.

Supplementary Materials: The following supporting information can be downloaded at: https://www.mdpi.com/article/10.3390/cells14211711/s1. Supplement to the description of Section 2.3 Genotyping with TaqMan allelic discrimination assay in the Materials and Methods part of the manuscript; Table S1. Behavioral performance in WT and *kat2*$^{-/-}$ mice across multiple cognitive, social, and motor tests (NORT, OBAT, Y-Maze, MBT, 3CT, and Rotarod). Analyses revealed no significant inter-strain differences. Table S2. Comparative behavioral performance of wild-type (WT) and *kat2*$^{-/-}$ mice in object recognition (NORT, OBAT) and social interaction/novelty preference (3CT). Table S3. Regional brain concentrations of tryptophan (Trp) and its downstream metabolites in wild-type (WT) and *kat2*$^{-/-}$ mice across striatum, cortex, hippocampus, cerebellum, and brainstem. Table S4. Concentrations of indole-pyruvate and tyrosine-dopamine pathway metabolites in wild-type (WT) and *kat2*$^{-/-}$ mice in plasma and urine. Table S5. Ratios of kynurenine (KYN), serotonin (5-HT), indole–pyruvate, and tyrosine (Tyr)–dopamine (DA) metabolites to their precursors and associated enzyme activities across brain regions in wild-type (WT) and *kat2*$^{-/-}$ mice. Activities were estimated using product-to-substrate ratios for key enzymatic steps. Table S6. Ratios of oxidant/antioxidant and N-methyl-D-aspartate (NMDA) agonist/antagonist metabolites across brain regions in wild-type (WT) and *kat2*$^{-/-}$ mice. Regional indices of oxidative stress and excitotoxicity in WT and *kat2*$^{-/-}$ mice.

Author Contributions: Conceptualization, Á.S., Z.G., J.T., E.O., L.V. and M.T.; methodology, Á.S., Z.G., E.S., D.M., M.S., A.F.-S., Á.F., K.T., K.O., H.I., S.Y. and P.M.; software, Á.S., Z.G., E.S., M.S., A.F.-S., Á.F., K.O. and P.M.; validation, Á.S., Z.G., E.S., M.S., A.F.-S., Á.F., K.T., K.O. and P.M.; formal analysis, Á.S., Z.G., E.S., M.S., A.F.-S., Á.F., K.O. and P.M.; investigation, Á.S., Z.G., E.S., D.M., M.S., A.F.-S., Á.F., K.T. and K.O.; resources, Á.S., Z.G., P.M. and E.O.; data curation, Á.S., Z.G., E.S., M.S., A.F.-S., Á.F. and K.O.; writing—original draft preparation, Á.S., Z.G. and M.T.; writing—review and editing, Á.S., Z.G., E.S., D.M., A.F.-S., Á.F., M.S., J.T., E.O., L.V. and M.T.; visualization, Á.S.; supervision, P.M., J.T., E.O., L.V. and M.T.; project administration, P.M., J.T., E.O. and L.V.; funding acquisition, P.M., J.T., E.O., L.V. and M.T. All authors have read and agreed to the published version of the manuscript.

Funding: This work was supported by the National Research, Development, and Innovation Office (NKFIH K138125), SZTE SZAOK-KKA (No: 2022/5S729), the HUN-REN Hungarian Research Network, the JSPS Joint Research Projects under Bilateral Programs (Grant Number JPJSBP120203803), and the University of Szeged Open Access Fund, Grant ID: 7571.

Institutional Review Board Statement: The study was conducted in accordance with the Regulations for Animal Experiments of Kyushu University, the Fundamental Guidelines for Proper Conduct of Animal Experiments and Related Activities in Academic Research Institutions governed by the Ministry of Education, Culture, Sports, Science, and Technology of Japan, and with the approval of the Institutional Animal Experiment Committees of Kyushu University (A29-338-1 (2018), A19-090-1 (2019)), and approved by the National Food Chain Safety Office (XI./1008/2025, approved date: 3 June 2025; XI./84/2025, approved date: 30 March 2025).

Informed Consent Statement: Not applicable.

Data Availability Statement: The original contributions presented in this study are included in the article. Further inquiries can be directed to the corresponding authors.

Acknowledgments: The figures were created with BioRender (https://biorender.com (accessed on 3 September 2025)).

Conflicts of Interest: The authors declare that they have no conflicts of interest and have received no payment for the preparation of their manuscript.

Abbreviations

The following abbreviations are used in this manuscript:

3-HAA	3-hydroxyanthranilic acid
3-HK	3-hydroxykynurenine
3CT	three-chamber test
5-HT	5-hydroxytryptamine (serotonin)
5-HTP	5-hydroxytryptophan
5-HIAA	5-hydroxyindoleacetic acid
AA	anthranilic acid
AADC	aromatic L-amino acid decarboxylase
ALDH	aldehyde dehydrogenase
ARRIVE	animal research: reporting of in vivo experiments
ASD	autism spectrum disorder
BBB	blood–brain barrier
BH2	dihydrobiopterin
BH4	tetrahydrobiopterin
BIO	biopterin
CER	cerebellum
CNS	central nervous system
COMT	catechol-O-methyltransferase
CTX	cortex
DA	dopamine
DI	discrimination index
DOPAC	3,4-dihydroxyphenylacetic acid
GAD	generalized anxiety disorder
HIPP	hippocampus
HVA	homovanillic acid
IAA	indole-3-acetic acid
ICA	indole-3-carboxylic acid
INS	indoxyl sulfate
KAT	kynurenine aminotransferase
KMO	kynurenine 3-monooxygenase
KYN	kynurenine
KYNA	kynurenic acid
KYNU	kynureninase
L-DOPA	dihydroxyphenylalanine/levodopa

LC-MS	liquid chromatography–tandem mass spectrometry
MAO	monoamine oxidase
MBT	marble-burying test
MDD	major depressive disorder
MEL	melatonin
MHPGS	3-methoxy-4-hydroxyphenylglycol sulfate
NMDA	N-methyl-D-aspartate
NORT	novel object recognition test
OBAT	object-based attention test
PI	preference index
QA	quinolinic acid
QAA	quinaldic acid
SCZ	schizophrenia
STEM	brainstem
STR	striatum
Trp	tryptophan
TPH	tryptophan hydroxylase
Tyr	tyrosine
UHPLC-MS	ultra-high-performance liquid chromatography–tandem mass spectrometry
VMA	vanillylmandelic acid
WT	wild-type
XA	xanthurenic acid

References

1. Gupta, R.; Advani, D.; Yadav, D.; Ambasta, R.K.; Kumar, P. Dissecting the Relationship Between Neuropsychiatric and Neurodegenerative Disorders. *Mol. Neurobiol.* **2023**, *60*, 6476–6529. [CrossRef]
2. Grezenko, H.; Rodoshi, Z.N.; Mimms, C.S.; Ahmed, M.; Sabani, A.; Hlaing, M.S.; Batu, B.J.; Hundesa, M.I.; Ayalew, B.D.; Shehryar, A.; et al. From Alzheimer's Disease to Anxiety, Epilepsy to Schizophrenia: A Comprehensive Dive into Neuro-Psychiatric Disorders. *Cureus* **2024**, *16*, e58776. [CrossRef]
3. Nadeem, M.S.; Hosawi, S.; Alshehri, S.; Ghoneim, M.M.; Imam, S.S.; Murtaza, B.N.; Kazmi, I. Symptomatic, Genetic, and Mechanistic Overlaps between Autism and Alzheimer's Disease. *Biomolecules* **2021**, *11*, 1635. [CrossRef]
4. Cummings, J. The Role of Neuropsychiatric Symptoms in Research Diagnostic Criteria for Neurodegenerative Diseases. *Am. J. Geriatr. Psychiatry* **2021**, *29*, 375–383. [CrossRef]
5. Peralta, V.; Cuesta, M.J. Motor Abnormalities: From Neurodevelopmental to Neurodegenerative Through "Functional" (Neuro)Psychiatric Disorders. *Schizophr. Bull.* **2017**, *43*, 956–971. [CrossRef]
6. Wang, S.; Jiang, Y.; Yang, A.; Meng, F.; Zhang, J. The Expanding Burden of Neurodegenerative Diseases: An Unmet Medical and Social Need. *Aging Dis.* **2024**, *16*, 2937–2952. [CrossRef] [PubMed]
7. Aarsland, D.; Batzu, L.; Halliday, G.M.; Geurtsen, G.J.; Ballard, C.; Ray Chaudhuri, K.; Weintraub, D. Parkinson disease-associated cognitive impairment. *Nat. Rev. Dis. Primers* **2021**, *7*, 47. [CrossRef] [PubMed]
8. de Lima, E.P.; Tanaka, M.; Lamas, C.B.; Quesada, K.; Detregiachi, C.R.P.; Araújo, A.C.; Guiguer, E.L.; Catharin, V.; de Castro, M.V.M.; Junior, E.B.; et al. Vascular Impairment, Muscle Atrophy, and Cognitive Decline: Critical Age-Related Conditions. *Biomedicines* **2024**, *12*, 2096. [CrossRef]
9. Morella, I.M.; Brambilla, R.; Morè, L. Emerging roles of brain metabolism in cognitive impairment and neuropsychiatric disorders. *Neurosci. Biobehav. Rev.* **2022**, *142*, 104892. [CrossRef]
10. de Lima, E.P.; Laurindo, L.F.; Catharin, V.C.S.; Direito, R.; Tanaka, M.; Jasmin Santos German, I.; Lamas, C.B.; Guiguer, E.L.; Araújo, A.C.; Fiorini, A.M.R.; et al. Polyphenols, Alkaloids, and Terpenoids Against Neurodegeneration: Evaluating the Neuroprotective Effects of Phytocompounds Through a Comprehensive Review of the Current Evidence. *Metabolites* **2025**, *15*, 124. [CrossRef]
11. Li, D.; Yu, S.; Long, Y.; Shi, A.; Deng, J.; Ma, Y.; Wen, J.; Li, X.; Liu, S.; Zhang, Y.; et al. Tryptophan metabolism: Mechanism-oriented therapy for neurological and psychiatric disorders. *Front. Immunol.* **2022**, *13*, 985378. [CrossRef]
12. Davidson, M.; Rashidi, N.; Nurgali, K.; Apostolopoulos, V. The Role of Tryptophan Metabolites in Neuropsychiatric Disorders. *Int. J. Mol. Sci.* **2022**, *23*, 9968. [CrossRef]
13. Muneer, A. Kynurenine Pathway of Tryptophan Metabolism in Neuropsychiatric Disorders: Pathophysiologic and Therapeutic Considerations. *Clin Psychopharmacol. Neurosci.* **2020**, *18*, 507–526. [CrossRef] [PubMed]

14. Gostner, J.M.; Geisler, S.; Stonig, M.; Mair, L.; Sperner-Unterweger, B.; Fuchs, D. Tryptophan Metabolism and Related Pathways in Psychoneuroimmunology: The Impact of Nutrition and Lifestyle. *Neuropsychobiology* **2020**, *79*, 89–99. [CrossRef] [PubMed]
15. Huang, Y.; Zhao, M.; Chen, X.; Zhang, R.; Le, A.; Hong, M.; Zhang, Y.; Jia, L.; Zang, W.; Jiang, C.; et al. Tryptophan Metabolism in Central Nervous System Diseases: Pathophysiology and Potential Therapeutic Strategies. *Aging Dis.* **2023**, *14*, 858–878. [CrossRef] [PubMed]
16. Xue, C.; Li, G.; Zheng, Q.; Gu, X.; Shi, Q.; Su, Y.; Chu, Q.; Yuan, X.; Bao, Z.; Lu, J.; et al. Tryptophan metabolism in health and disease. *Cell Metab.* **2023**, *35*, 1304–1326. [CrossRef]
17. Hestad, K.; Alexander, J.; Rootwelt, H.; Aaseth, J.O. The Role of Tryptophan Dysmetabolism and Quinolinic Acid in Depressive and Neurodegenerative Diseases. *Biomolecules* **2022**, *12*, 998. [CrossRef]
18. Cervenka, I.; Agudelo, L.Z.; Ruas, J.L. Kynurenines: Tryptophan's metabolites in exercise, inflammation, and mental health. *Science* **2017**, *357*, eaaf9794. [CrossRef]
19. Kennedy, P.J.; Cryan, J.F.; Dinan, T.G.; Clarke, G. Kynurenine pathway metabolism and the microbiota-gut-brain axis. *Neuropharmacology* **2017**, *112*, 399–412. [CrossRef]
20. Lovelace, M.D.; Varney, B.; Sundaram, G.; Lennon, M.J.; Lim, C.K.; Jacobs, K.; Guillemin, G.J.; Brew, B.J. Recent evidence for an expanded role of the kynurenine pathway of tryptophan metabolism in neurological diseases. *Neuropharmacology* **2017**, *112*, 373–388. [CrossRef]
21. Maddison, D.C.; Giorgini, F. The kynurenine pathway and neurodegenerative disease. *Semin. Cell Dev. Biol.* **2015**, *40*, 134–141. [CrossRef]
22. Tanaka, M.; Tóth, F.; Polyák, H.; Szabó, Á.; Mándi, Y.; Vécsei, L. Immune Influencers in Action: Metabolites and Enzymes of the Tryptophan-Kynurenine Metabolic Pathway. *Biomedicines* **2021**, *9*, 734. [CrossRef] [PubMed]
23. Dehhaghi, M.; Kazemi Shariat Panahi, H.; Guillemin, G.J. Microorganisms, Tryptophan Metabolism, and Kynurenine Pathway: A Complex Interconnected Loop Influencing Human Health Status. *Int. J. Tryptophan Res.* **2019**, *12*, 1178646919852996. [CrossRef]
24. Stone, T.W.; Williams, R.O. Tryptophan metabolism as a 'reflex' feature of neuroimmune communication: Sensor and effector functions for the indoleamine-2, 3-dioxygenase kynurenine pathway. *J. Neurochem.* **2024**, *168*, 3333–3357. [CrossRef]
25. Badawy, A.A. Kynurenine Pathway of Tryptophan Metabolism: Regulatory and Functional Aspects. *Int. J. Tryptophan Res.* **2017**, *10*, 1178646917691938. [CrossRef]
26. Sathyasaikumar, K.V.; Notarangelo, F.M.; Kelly, D.L.; Rowland, L.M.; Hare, S.M.; Chen, S.; Mo, C.; Buchanan, R.W.; Schwarcz, R. Tryptophan Challenge in Healthy Controls and People with Schizophrenia: Acute Effects on Plasma Levels of Kynurenine, Kynurenic Acid and 5-Hydroxyindoleacetic Acid. *Pharmaceuticals* **2022**, *15*, 1003. [CrossRef]
27. Hasegawa, M.; Kunisawa, K.; Wulaer, B.; Kubota, H.; Kurahashi, H.; Sakata, T.; Ando, H.; Fujigaki, S.; Fujigaki, H.; Yamamoto, Y.; et al. Chronic stress induces behavioural changes through increased kynurenic acid by downregulation of kynurenine-3-monooxygenase with microglial decline. *Br. J. Pharmacol.* **2025**, *182*, 1466–1486. [CrossRef]
28. Fujigaki, H.; Yamamoto, Y.; Saito, K. L-Tryptophan-kynurenine pathway enzymes are therapeutic target for neuropsychiatric diseases: Focus on cell type differences. *Neuropharmacology* **2017**, *112*, 264–274. [CrossRef]
29. Martos, D.; Tuka, B.; Tanaka, M.; Vécsei, L.; Telegdy, G. Memory Enhancement with Kynurenic Acid and Its Mechanisms in Neurotransmission. *Biomedicines* **2022**, *10*, 849. [CrossRef]
30. Stone, T.W. Does kynurenic acid act on nicotinic receptors? An assessment of the evidence. *J. Neurochem.* **2020**, *152*, 627–649. [CrossRef] [PubMed]
31. Rossi, F.; Miggiano, R.; Ferraris, D.M.; Rizzi, M. The Synthesis of Kynurenic Acid in Mammals: An Updated Kynurenine Aminotransferase Structural KATalogue. *Front. Mol. Biosci.* **2019**, *6*, 7. [CrossRef]
32. Nematollahi, A.; Sun, G.; Jayawickrama, G.S.; Church, W.B. Kynurenine Aminotransferase Isozyme Inhibitors: A Review. *Int. J. Mol. Sci.* **2016**, *17*, 946. [CrossRef]
33. Mor, A.; Tankiewicz-Kwedlo, A.; Krupa, A.; Pawlak, D. Role of Kynurenine Pathway in Oxidative Stress during Neurodegenerative Disorders. *Cells* **2021**, *10*, 1603. [CrossRef]
34. Castellano-Gonzalez, G.; Jacobs, K.R.; Don, E.; Cole, N.J.; Adams, S.; Lim, C.K.; Lovejoy, D.B.; Guillemin, G.J. Kynurenine 3-Monooxygenase Activity in Human Primary Neurons and Effect on Cellular Bioenergetics Identifies New Neurotoxic Mechanisms. *Neurotox. Res.* **2019**, *35*, 530–541. [CrossRef]
35. Juhász, L.; Spisák, K.; Szolnoki, B.Z.; Nászai, A.; Szabó, Á.; Rutai, A.; Tallósy, S.P.; Szabó, A.; Toldi, J.; Tanaka, M.; et al. The Power Struggle: Kynurenine Pathway Enzyme Knockouts and Brain Mitochondrial Respiration. *J. Neurochem.* **2025**, *169*, e70075. [CrossRef]
36. Tanaka, M.; Szabó, Á.; Vécsei, L. Redefining Roles: A Paradigm Shift in Tryptophan-Kynurenine Metabolism for Innovative Clinical Applications. *Int. J. Mol. Sci.* **2024**, *25*, 12767. [CrossRef]
37. Comai, S.; Bertazzo, A.; Brughera, M.; Crotti, S. Tryptophan in health and disease. *Adv. Clin. Chem.* **2020**, *95*, 165–218. [CrossRef]
38. Roth, W.; Zadeh, K.; Vekariya, R.; Ge, Y.; Mohamadzadeh, M. Tryptophan Metabolism and Gut-Brain Homeostasis. *Int. J. Mol. Sci.* **2021**, *22*, 2973. [CrossRef] [PubMed]

39. Höglund, E.; Øverli, Ø.; Winberg, S. Tryptophan Metabolic Pathways and Brain Serotonergic Activity: A Comparative Review. *Front. Endocrinol.* **2019**, *10*, 158. [CrossRef] [PubMed]
40. Platten, M.; Nollen, E.A.A.; Röhrig, U.F.; Fallarino, F.; Opitz, C.A. Tryptophan metabolism as a common therapeutic target in cancer, neurodegeneration and beyond. *Nat. Rev. Drug Discov.* **2019**, *18*, 379–401. [CrossRef]
41. Correia, A.S.; Vale, N. Tryptophan Metabolism in Depression: A Narrative Review with a Focus on Serotonin and Kynurenine Pathways. *Int. J. Mol. Sci.* **2022**, *23*, 8493. [CrossRef] [PubMed]
42. Gibson, E.L. Tryptophan supplementation and serotonin function: Genetic variations in behavioural effects. *Proc. Nutr. Soc.* **2018**, *77*, 174–188. [CrossRef]
43. Ribeiro, R.F.N.; Santos, M.R.; Aquino, M.; de Almeida, L.P.; Cavadas, C.; Silva, M.M.C. The Therapeutic Potential of Melatonin and Its Novel Synthetic Analogs in Circadian Rhythm Sleep Disorders, Inflammation-Associated Pathologies, and Neurodegenerative Diseases. *Med. Res. Rev.* **2025**, *45*, 1515–1539. [CrossRef]
44. Vasey, C.; McBride, J.; Penta, K. Circadian Rhythm Dysregulation and Restoration: The Role of Melatonin. *Nutrients* **2021**, *13*, 3480. [CrossRef]
45. Kholghi, G.; Eskandari, M.; Shokouhi Qare Saadlou, M.S.; Zarrindast, M.R.; Vaseghi, S. Night shift hormone: How does melatonin affect depression? *Physiol. Behav.* **2022**, *252*, 113835. [CrossRef]
46. Kałużna-Czaplińska, J.; Gątarek, P.; Chirumbolo, S.; Chartrand, M.S.; Bjørklund, G. How important is tryptophan in human health? *Crit. Rev. Food Sci. Nutr.* **2019**, *59*, 72–88. [CrossRef]
47. Zhou, Y.; Chen, Y.; He, H.; Peng, M.; Zeng, M.; Sun, H. The role of the indoles in microbiota-gut-brain axis and potential therapeutic targets: A focus on human neurological and neuropsychiatric diseases. *Neuropharmacology* **2023**, *239*, 109690. [CrossRef]
48. Generoso, J.S.; Giridharan, V.V.; Lee, J.; Macedo, D.; Barichello, T. The role of the microbiota-gut-brain axis in neuropsychiatric disorders. *Braz. J. Psychiatry* **2021**, *43*, 293–305. [CrossRef]
49. Tran, S.M.; Mohajeri, M.H. The Role of Gut Bacterial Metabolites in Brain Development, Aging and Disease. *Nutrients* **2021**, *13*, 732. [CrossRef]
50. Gao, K.; Mu, C.L.; Farzi, A.; Zhu, W.Y. Tryptophan Metabolism: A Link Between the Gut Microbiota and Brain. *Adv. Nutr.* **2020**, *11*, 709–723. [CrossRef] [PubMed]
51. Ma, Q.; Xing, C.; Long, W.; Wang, H.Y.; Liu, Q.; Wang, R.F. Impact of microbiota on central nervous system and neurological diseases: The gut-brain axis. *J. Neuroinflamm.* **2019**, *16*, 53. [CrossRef]
52. Jaglin, M.; Rhimi, M.; Philippe, C.; Pons, N.; Bruneau, A.; Goustard, B.; Daugé, V.; Maguin, E.; Naudon, L.; Rabot, S. Indole, a Signaling Molecule Produced by the Gut Microbiota, Negatively Impacts Emotional Behaviors in Rats. *Front. Neurosci.* **2018**, *12*, 216. [CrossRef]
53. Ahmed, H.; Leyrolle, Q.; Koistinen, V.; Kärkkäinen, O.; Layé, S.; Delzenne, N.; Hanhineva, K. Microbiota-derived metabolites as drivers of gut-brain communication. *Gut Microbes* **2022**, *14*, 2102878. [CrossRef]
54. Giau, V.V.; Wu, S.Y.; Jamerlan, A.; An, S.S.A.; Kim, S.Y.; Hulme, J. Gut Microbiota and Their Neuroinflammatory Implications in Alzheimer's Disease. *Nutrients* **2018**, *10*, 1765. [CrossRef]
55. Chen, C.Y.; Wang, Y.F.; Lei, L.; Zhang, Y. Impacts of microbiota and its metabolites through gut-brain axis on pathophysiology of major depressive disorder. *Life Sci.* **2024**, *351*, 122815. [CrossRef]
56. Wang, Q.; Yang, Q.; Liu, X. The microbiota-gut-brain axis and neurodevelopmental disorders. *Protein Cell* **2023**, *14*, 762–775. [CrossRef] [PubMed]
57. Figueiredo Godoy, A.C.; Frota, F.F.; Araújo, L.P.; Valenti, V.E.; Pereira, E.; Detregiachi, C.R.P.; Galhardi, C.M.; Caracio, F.C.; Haber, R.S.A.; Fornari Laurindo, L.; et al. Neuroinflammation and Natural Antidepressants: Balancing Fire with Flora. *Biomedicines* **2025**, *13*, 1129. [CrossRef] [PubMed]
58. Ichinose, H.; Aida, R.; Nago-Iwashita, Y.; Moriya, Y.; Ide, S.; Ikeda, K. Modulation of The Dopaminergic Neurotransmission by Controlling The Activity Of Tyrosine Hydroxylase. *Int. J. Neuropsychopharmacol.* **2025**, *28*, i9. [CrossRef]
59. Speranza, L.; di Porzio, U.; Viggiano, D.; de Donato, A.; Volpicelli, F. Dopamine: The Neuromodulator of Long-Term Synaptic Plasticity, Reward and Movement Control. *Cells* **2021**, *10*, 735. [CrossRef]
60. Oakes, M.; Law, W.J.; Komuniecki, R. Cannabinoids Stimulate the TRP Channel-Dependent Release of Both Serotonin and Dopamine to Modulate Behavior in C. elegans. *J. Neurosci.* **2019**, *39*, 4142–4152. [CrossRef]
61. Marcos, J.; Renau, N.; Valverde, O.; Aznar-Laín, G.; Gracia-Rubio, I.; Gonzalez-Sepulveda, M.; Pérez-Jurado, L.A.; Ventura, R.; Segura, J.; Pozo, O.J. Targeting tryptophan and tyrosine metabolism by liquid chromatography tandem mass spectrometry. *J. Chromatogr. A* **2016**, *1434*, 91–101. [CrossRef] [PubMed]
62. Ney, D.M.; Murali, S.G.; Stroup, B.M.; Nair, N.; Sawin, E.A.; Rohr, F.; Levy, H.L. Metabolomic changes demonstrate reduced bioavailability of tyrosine and altered metabolism of tryptophan via the kynurenine pathway with ingestion of medical foods in phenylketonuria. *Mol. Genet. Metab.* **2017**, *121*, 96–103. [CrossRef] [PubMed]
63. Ma, Z.; Stork, T.; Bergles, D.E.; Freeman, M.R. Neuromodulators signal through astrocytes to alter neural circuit activity and behaviour. *Nature* **2016**, *539*, 428–432. [CrossRef]

64. Baik, J.H. Stress and the dopaminergic reward system. *Exp. Mol. Med.* **2020**, *52*, 1879–1890. [CrossRef]
65. Maleeva, G.; Matera, C.; Roda, S.; Colleoni, A.; De Amici, M.; Gorostiza, P. Molecular Tools to Study and Control Dopaminergic Neurotransmission With Light. *Med. Res. Rev.* **2025**, *45*, 1407–1422. [CrossRef]
66. Tanaka, M.; He, Z.; Han, S.; Battaglia, S. Editorial: Noninvasive brain stimulation: A promising approach to study and improve emotion regulation. *Front. Behav. Neurosci.* **2025**, *19*, 1633936. [CrossRef]
67. Szabó, Á.; Galla, Z.; Spekker, E.; Szűcs, M.; Martos, D.; Takeda, K.; Ozaki, K.; Inoue, H.; Yamamoto, S.; Toldi, J.; et al. Oxidative and Excitatory Neurotoxic Stresses in CRISPR/Cas9-Induced Kynurenine Aminotransferase Knockout Mice: A Novel Model for Despair-Based Depression and Post-Traumatic Stress Disorder. *Front. Biosci. Landmark* **2025**, *30*, 25706. [CrossRef]
68. Li, Y.T.; Zhang, C.; Han, J.C.; Shang, Y.X.; Chen, Z.H.; Cui, G.B.; Wang, W. Neuroimaging features of cognitive impairments in schizophrenia and major depressive disorder. *Ther. Adv. Psychopharmacol.* **2024**, *14*, 20451253241243290. [CrossRef]
69. Luo, W.; Luo, L.; Wang, Q.; Li, Y.; Zhang, Y.; Hu, Y.; Yu, Y.; Yu, S.; Lu, F.; Chen, J.; et al. Disorder-specific impaired neurocognitive function in major depression and generalized anxiety disorder. *J. Affect. Disord.* **2022**, *318*, 123–129. [CrossRef]
70. Rhee, T.G.; Shim, S.R.; Manning, K.J.; Tennen, H.A.; Kaster, T.S.; d'Andrea, G.; Forester, B.P.; Nierenberg, A.A.; McIntyre, R.S.; Steffens, D.C. Neuropsychological Assessments of Cognitive Impairment in Major Depressive Disorder: A Systematic Review and Meta-Analysis with Meta-Regression. *Psychother. Psychosom.* **2024**, *93*, 8–23. [CrossRef]
71. Bora, E. Peripheral inflammatory and neurotrophic biomarkers of cognitive impairment in schizophrenia: A meta-analysis. *Psychol. Med.* **2019**, *49*, 1971–1979. [CrossRef]
72. MacQueen, G.M.; Memedovich, K.A. Cognitive dysfunction in major depression and bipolar disorder: Assessment and treatment options. *Psychiatry Clin. Neurosci.* **2017**, *71*, 18–27. [CrossRef]
73. Martin, D.M.; Wollny-Huttarsch, D.; Nikolin, S.; McClintock, S.M.; Alonzo, A.; Lisanby, S.H.; Loo, C.K. Neurocognitive subgroups in major depressive disorder. *Neuropsychology* **2020**, *34*, 726–734. [CrossRef]
74. Ramos-Chávez, L.A.; Roldán-Roldán, G.; García-Juárez, B.; González-Esquivel, D.; Pérez de la Cruz, G.; Pineda, B.; Ramírez-Ortega, D.; García Muñoz, I.; Jiménez Herrera, B.; Ríos, C.; et al. Low Serum Tryptophan Levels as an Indicator of Global Cognitive Performance in Nondemented Women over 50 Years of Age. *Oxid. Med. Cell Longev.* **2018**, *2018*, 8604718. [CrossRef] [PubMed]
75. Hammar, Å.; Ronold, E.H.; Rekkedal, G. Cognitive Impairment and Neurocognitive Profiles in Major Depression-A Clinical Perspective. *Front. Psychiatry* **2022**, *13*, 764374. [CrossRef]
76. Barbalho, S.M.; Laurindo, L.F.; de Oliveira Zanuso, B.; da Silva, R.M.S.; Gallerani Caglioni, L.; Nunes Junqueira de Moraes, V.B.F.; Fornari Laurindo, L.; Dogani Rodrigues, V.; da Silva Camarinha Oliveira, J.; Beluce, M.E.; et al. AdipoRon's Impact on Alzheimer's Disease-A Systematic Review and Meta-Analysis. *Int. J. Mol. Sci.* **2025**, *26*, 484. [CrossRef]
77. Nunes, Y.C.; Mendes, N.M.; Pereira de Lima, E.; Chehadi, A.C.; Lamas, C.B.; Haber, J.F.S.; Dos Santos Bueno, M.; Araújo, A.C.; Catharin, V.C.S.; Detregiachi, C.R.P.; et al. Curcumin: A Golden Approach to Healthy Aging: A Systematic Review of the Evidence. *Nutrients* **2024**, *16*, 2721. [CrossRef]
78. Gebreegziabhere, Y.; Habatmu, K.; Mihretu, A.; Cella, M.; Alem, A. Cognitive impairment in people with schizophrenia: An umbrella review. *Eur. Arch. Psychiatry Clin. Neurosci.* **2022**, *272*, 1139–1155. [CrossRef]
79. van Hal, R.; Geurts, D.; van Eijndhoven, P.; Kist, J.; Collard, R.M.; Tendolkar, I.; Vrijsen, J.N. A transdiagnostic view on MDD and ADHD: Shared cognitive characteristics? *J. Psychiatr. Res.* **2023**, *165*, 315–324. [CrossRef] [PubMed]
80. Martos, D.; Lőrinczi, B.; Szatmári, I.; Vécsei, L.; Tanaka, M. Decoupling Behavioral Domains via Kynurenic Acid Analog Optimization: Implications for Schizophrenia and Parkinson's Disease Therapeutics. *Cells* **2025**, *14*, 973. [CrossRef]
81. Dounay, A.B.; Tuttle, J.B.; Verhoest, P.R. Challenges and Opportunities in the Discovery of New Therapeutics Targeting the Kynurenine Pathway. *J. Med. Chem.* **2015**, *58*, 8762–8782. [CrossRef]
82. Li, S.; Chen, Y.; Chen, G. Cognitive disorders: Potential astrocyte-based mechanism. *Brain Res. Bull.* **2025**, *220*, 111181. [CrossRef]
83. Tanaka, M.; Szatmári, I.; Vécsei, L. Quinoline Quest: Kynurenic Acid Strategies for Next-Generation Therapeutics via Rational Drug Design. *Pharmaceuticals* **2025**, *18*, 607. [CrossRef]
84. Yang, W.; Chen, X.; Li, S.; Li, X.J. Genetically modified large animal models for investigating neurodegenerative diseases. *Cell Biosci.* **2021**, *11*, 218. [CrossRef]
85. Verbitsky, A.; Dopfel, D.; Zhang, N. Rodent models of post-traumatic stress disorder: Behavioral assessment. *Transl. Psychiatry* **2020**, *10*, 132. [CrossRef]
86. Pan, M.-T.; Zhang, H.; Li, X.-J.; Guo, X.-Y. Genetically modified non-human primate models for research on neurodegenerative diseases. *Zool. Res.* **2024**, *45*, 263. [CrossRef] [PubMed]
87. Tanaka, M. From Serendipity to Precision: Integrating AI, Multi-Omics, and Human-Specific Models for Personalized Neuropsychiatric Care. *Biomedicines* **2025**, *13*, 167. [CrossRef]
88. Tanaka, M. Beyond the boundaries: Transitioning from categorical to dimensional paradigms in mental health diagnostics. *Adv. Clin. Exp. Med.* **2024**, *33*, 1295–1301. [CrossRef] [PubMed]
89. Tanaka, M.; Battaglia, S. From Biomarkers to Behavior: Mapping the Neuroimmune Web of Pain, Mood, and Memory. *Biomedicines* **2025**, *13*, 2226. [CrossRef]

90. Lueptow, L.M. Novel Object Recognition Test for the Investigation of Learning and Memory in Mice. *J. Vis. Exp.* **2017**, *126*, e55718. [CrossRef]
91. Grayson, B.; Leger, M.; Piercy, C.; Adamson, L.; Harte, M.; Neill, J.C. Assessment of disease-related cognitive impairments using the novel object recognition (NOR) task in rodents. *Behav. Brain Res.* **2015**, *285*, 176–193. [CrossRef]
92. Cohen, S.J.; Stackman, R.W., Jr. Assessing rodent hippocampal involvement in the novel object recognition task. A review. *Behav. Brain Res.* **2015**, *285*, 105–117. [CrossRef] [PubMed]
93. Denninger, J.K.; Smith, B.M.; Kirby, E.D. Novel Object Recognition and Object Location Behavioral Testing in Mice on a Budget. *J. Vis. Exp.* **2018**, *141*, e58593. [CrossRef] [PubMed]
94. Chao, O.Y.; Nikolaus, S.; Yang, Y.M.; Huston, J.P. Neuronal circuitry for recognition memory of object and place in rodent models. *Neurosci. Biobehav. Rev.* **2022**, *141*, 104855. [CrossRef]
95. Wulaer, B.; Kunisawa, K.; Kubota, H.; Suento, W.J.; Saito, K.; Mouri, A.; Nabeshima, T. Prefrontal cortex, dorsomedial striatum, and dentate gyrus are necessary in the object-based attention test in mice. *Mol. Brain* **2020**, *13*, 171. [CrossRef]
96. Wulaer, B.; Kunisawa, K.; Tanabe, M.; Yanagawa, A.; Saito, K.; Mouri, A.; Nabeshima, T. Pharmacological blockade of dopamine D1- or D2-receptor in the prefrontal cortex induces attentional impairment in the object-based attention test through different neuronal circuits in mice. *Mol. Brain* **2021**, *14*, 43. [CrossRef]
97. Thiele, A.; Bellgrove, M.A. Neuromodulation of Attention. *Neuron* **2018**, *97*, 769–785. [CrossRef]
98. Věchetová, G.; Nikolai, T.; Slovák, M.; Forejtová, Z.; Vranka, M.; Straková, E.; Teodoro, T.; Růžička, E.; Edwards, M.J.; Serranová, T. Attention impairment in motor functional neurological disorders: A neuropsychological study. *J. Neurol.* **2022**, *269*, 5981–5990. [CrossRef]
99. Barone, V.; van Dijk, J.P.; Debeij-van Hall, M.; van Putten, M. A Potential Multimodal Test for Clinical Assessment of Visual Attention in Neurological Disorders. *Clin. EEG Neurosci.* **2023**, *54*, 512–521. [CrossRef]
100. Yoon, T.; Okada, J.; Jung, M.W.; Kim, J.J. Prefrontal cortex and hippocampus subserve different components of working memory in rats. *Learn. Mem.* **2008**, *15*, 97–105. [CrossRef]
101. Kraeuter, A.K.; Guest, P.C.; Sarnyai, Z. The Y-Maze for Assessment of Spatial Working and Reference Memory in Mice. *Methods Mol. Biol.* **2019**, *1916*, 105–111. [CrossRef] [PubMed]
102. Prieur, E.A.K.; Jadavji, N.M. Assessing Spatial Working Memory Using the Spontaneous Alternation Y-maze Test in Aged Male Mice. *Bio Protoc.* **2019**, *9*, e3162. [CrossRef]
103. Melbiarta, R.R.; Kalanjati, V.P.; Herawati, L.; Salim, Y.; Othman, Z. Analysis of spatial working memory using the Y-maze on rodents treated with high-calorie diet and moderate-intensity exercise. *Folia Med. Indones.* **2022**, *59*, 40–45. [CrossRef]
104. Dixit, P.V.; Sahu, R.; Mishra, D.K. Marble-burying behavior test as a murine model of compulsive-like behavior. *J. Pharmacol. Toxicol. Methods* **2020**, *102*, 106676. [CrossRef]
105. Thomas, A.; Burant, A.; Bui, N.; Graham, D.; Yuva-Paylor, L.A.; Paylor, R. Marble burying reflects a repetitive and perseverative behavior more than novelty-induced anxiety. *Psychopharmacology* **2009**, *204*, 361–373. [CrossRef]
106. Taylor, G. Marble burying as compulsive behaviors in male and female mice. *Acta Neurobiol. Exp.* **2017**, *77*, 254–260. [CrossRef]
107. De Brouwer, G.; Wolmarans, W. Back to basics: A methodological perspective on marble-burying behavior as a screening test for psychiatric illness. *Behav. Process.* **2018**, *157*, 590–600. [CrossRef]
108. Langer, E.; Einat, H.; Stukalin, Y. Similarities and dissimilarities in the effects of benzodiazepines and specific serotonin reuptake inhibitors (SSRIs) in the defensive marble burying test: A systematic review and meta-analysis. *Eur. Neuropsychopharmacol.* **2020**, *36*, 38–49. [CrossRef]
109. Yang, M.; Silverman, J.L.; Crawley, J.N. Automated three-chambered social approach task for mice. *Curr. Protoc. Neurosci.* **2011**, *56*, 8–26. [CrossRef] [PubMed]
110. Oliver, L.D.; Moxon-Emre, I.; Lai, M.C.; Grennan, L.; Voineskos, A.N.; Ameis, S.H. Social Cognitive Performance in Schizophrenia Spectrum Disorders Compared with Autism Spectrum Disorder: A Systematic Review, Meta-analysis, and Meta-regression. *JAMA Psychiatry* **2021**, *78*, 281–292. [CrossRef]
111. Fernandes, J.M.; Cajão, R.; Lopes, R.; Jerónimo, R.; Barahona-Corrêa, J.B. Social Cognition in Schizophrenia and Autism Spectrum Disorders: A Systematic Review and Meta-Analysis of Direct Comparisons. *Front. Psychiatry* **2018**, *9*, 504. [CrossRef]
112. Morrison, K.E.; Pinkham, A.E.; Penn, D.L.; Kelsven, S.; Ludwig, K.; Sasson, N.J. Distinct profiles of social skill in adults with autism spectrum disorder and schizophrenia. *Autism Res.* **2017**, *10*, 878–887. [CrossRef]
113. Pinkham, A.E.; Morrison, K.E.; Penn, D.L.; Harvey, P.D.; Kelsven, S.; Ludwig, K.; Sasson, N.J. Comprehensive comparison of social cognitive performance in autism spectrum disorder and schizophrenia. *Psychol. Med.* **2020**, *50*, 2557–2565. [CrossRef]
114. Arakawa, H. Revisiting Sociability: Factors facilitating approach and avoidance during the three-chamber test. *Physiol. Behav.* **2023**, *272*, 114373. [CrossRef] [PubMed]
115. Kaidanovich-Beilin, O.; Lipina, T.; Vukobradovic, I.; Roder, J.; Woodgett, J.R. Assessment of social interaction behaviors. *J. Vis. Exp.* **2011**, *48*, e2473. [CrossRef] [PubMed]

116. Rein, B.; Ma, K.; Yan, Z. A standardized social preference protocol for measuring social deficits in mouse models of autism. *Nat. Protoc.* **2020**, *15*, 3464–3477. [CrossRef] [PubMed]
117. Moy, S.S.; Nadler, J.J.; Perez, A.; Barbaro, R.P.; Johns, J.M.; Magnuson, T.R.; Piven, J.; Crawley, J.N. Sociability and preference for social novelty in five inbred strains: An approach to assess autistic-like behavior in mice. *Genes Brain Behav.* **2004**, *3*, 287–302. [CrossRef]
118. Lubrich, C.; Giesler, P.; Kipp, M. Motor behavioral deficits in the cuprizone model: Validity of the rotarod test paradigm. *Int. J. Mol. Sci.* **2022**, *23*, 11342. [CrossRef]
119. Shan, H.M.; Maurer, M.A.; Schwab, M.E. Four-parameter analysis in modified Rotarod test for detecting minor motor deficits in mice. *BMC Biol.* **2023**, *21*, 177. [CrossRef] [PubMed]
120. Widjaja, J.H.; Sloan, D.C.; Hauger, J.A.; Muntean, B.S. Customizable Open-Source Rotating Rod (Rotarod) Enables Robust Low-Cost Assessment of Motor Performance in Mice. *eNeuro* **2023**, *10*, ENEURO.0123-23.2023. [CrossRef]
121. Keane, S.P.; Chadman, K.K.; Gomez, A.R.; Hu, W. Pros and cons of narrow- versus wide-compartment rotarod apparatus: An experimental study in mice. *Behav. Brain Res.* **2024**, *463*, 114901. [CrossRef]
122. Cording, K.R.; Bateup, H.S. Altered motor learning and coordination in mouse models of autism spectrum disorder. *Front. Cell Neurosci.* **2023**, *17*, 1270489. [CrossRef]
123. Galla, Z.; Rajda, C.; Rácz, G.; Grecsó, N.; Baráth, Á.; Vécsei, L.; Bereczki, C.; Monostori, P. Simultaneous determination of 30 neurologically and metabolically important molecules: A sensitive and selective way to measure tyrosine and tryptophan pathway metabolites and other biomarkers in human serum and cerebrospinal fluid. *J. Chromatogr. A* **2021**, *1635*, 461775. [CrossRef]
124. Galla, Z.; Rácz, G.; Grecsó, N.; Baráth, Á.; Kósa, M.; Bereczki, C.; Monostori, P. Improved LC-MS/MS method for the determination of 42 neurologically and metabolically important molecules in urine. *J. Chromatogr. B Analyt. Technol. Biomed. Life. Sci.* **2021**, *1179*, 122846. [CrossRef]
125. Fathi, M.; Vakili, K.; Yaghoobpoor, S.; Tavasol, A.; Jazi, K.; Hajibeygi, R.; Shool, S.; Sodeifian, F.; Klegeris, A.; McElhinney, A.; et al. Dynamic changes in metabolites of the kynurenine pathway in Alzheimer's disease, Parkinson's disease, and Huntington's disease: A systematic Review and meta-analysis. *Front. Immunol.* **2022**, *13*, 997240. [CrossRef]
126. Tanaka, M.; Bohár, Z.; Vécsei, L. Are Kynurenines Accomplices or Principal Villains in Dementia? Maintenance of Kynurenine Metabolism. *Molecules* **2020**, *25*, 564. [CrossRef] [PubMed]
127. Kim, Y.K.; Jeon, S.W. Neuroinflammation and the Immune-Kynurenine Pathway in Anxiety Disorders. *Curr. Neuropharmacol.* **2018**, *16*, 574–582. [CrossRef]
128. Imbeault, S.; Gubert Olivé, M.; Jungholm, O.; Erhardt, S.; Wigström, H.; Engberg, G.; Jardemark, K. Blockade of KAT II Facilitates LTP in Kynurenine 3-Monooxygenase Depleted Mice. *Int. J. Tryptophan Res.* **2021**, *14*, 11786469211041368. [CrossRef]
129. Blanco Ayala, T.B.; Ramírez Ortega, D.R.; Ovalle Rodríguez, P.O.; Pineda, B.; Pérez de la Cruz, G.P.; González Esquivel, D.G.; Schwarcz, R.; Sathyasaikumar, K.V.; Jiménez Anguiano, A.J.; Pérez de la Cruz, V.P. Subchronic N-acetylcysteine Treatment Decreases Brain Kynurenic Acid Levels and Improves Cognitive Performance in Mice. *Antioxidants* **2021**, *10*, 2035. [CrossRef]
130. Ovalle Rodríguez, P.; Ramírez Ortega, D.; Blanco Ayala, T.; Roldán Roldán, G.; Pérez de la Cruz, G.; González Esquivel, D.F.; Gómez-Manzo, S.; Sánchez Chapul, L.; Salazar, A.; Pineda, B.; et al. Modulation of Kynurenic Acid Production by N-acetylcysteine Prevents Cognitive Impairment in Adulthood Induced by Lead Exposure during Lactation in Mice. *Antioxidants* **2023**, *12*, 2035. [CrossRef] [PubMed]
131. Bai, M.Y.; Lovejoy, D.B.; Guillemin, G.J.; Kozak, R.; Stone, T.W.; Koola, M.M. Galantamine-Memantine Combination and Kynurenine Pathway Enzyme Inhibitors in the Treatment of Neuropsychiatric Disorders. *Complex Psychiatry* **2021**, *7*, 19–33. [CrossRef]
132. Nikolaus, S.; Fazari, B.; Chao, O.Y.; Almeida, F.R.; Abdel-Hafiz, L.; Beu, M.; Henke, J.; Antke, C.; Hautzel, H.; Mamlins, E.; et al. 2,5-Dimethoxy-4-iodoamphetamine and altanserin induce region-specific shifts in dopamine and serotonin metabolization pathways in the rat brain. *Pharmacol. Biochem. Behav.* **2024**, *242*, 173823. [CrossRef] [PubMed]
133. Tanaka, M.; Battaglia, S.; Liloia, D. Navigating Neurodegeneration: Integrating Biomarkers, Neuroinflammation, and Imaging in Parkinson's, Alzheimer's, and Motor Neuron Disorders. *Biomedicines* **2025**, *13*, 1045. [CrossRef]
134. Qin, Y.; Hu, X.; Zhao, H.-L.; Kurban, N.; Chen, X.; Yi, J.-K.; Zhang, Y.; Cui, S.-Y.; Zhang, Y.-H. Inhibition of indoleamine 2, 3-dioxygenase exerts antidepressant-like effects through distinct pathways in prelimbic and infralimbic cortices in rats under intracerebroventricular injection with streptozotocin. *Int. J. Mol. Sci.* **2024**, *25*, 7496. [CrossRef] [PubMed]
135. Barbalho, S.M.; Leme Boaro, B.; da Silva Camarinha Oliveira, J.; Patočka, J.; Barbalho Lamas, C.; Tanaka, M.; Laurindo, L.F. Molecular Mechanisms Underlying Neuroinflammation Intervention with Medicinal Plants: A Critical and Narrative Review of the Current Literature. *Pharmaceuticals* **2025**, *18*, 133. [CrossRef] [PubMed]
136. Nicosia, N.; Giovenzana, M.; Misztak, P.; Mingardi, J.; Musazzi, L. Glutamate-Mediated Excitotoxicity in the Pathogenesis and Treatment of Neurodevelopmental and Adult Mental Disorders. *Int. J. Mol. Sci.* **2024**, *25*, 6521. [CrossRef]
137. Pastor, V.; Medina, J.H. α7 nicotinic acetylcholine receptor in memory processing. *Eur. J. Neurosci.* **2024**, *59*, 2138–2154. [CrossRef]

138. Pocivavsek, A.; Baratta, A.M.; Mong, J.A.; Viechweg, S.S. Acute Kynurenine Challenge Disrupts Sleep-Wake Architecture and Impairs Contextual Memory in Adult Rats. *Sleep* **2017**, *40*, zsx141. [CrossRef]
139. Young, K.D.; Drevets, W.C.; Dantzer, R.; Teague, T.K.; Bodurka, J.; Savitz, J. Kynurenine pathway metabolites are associated with hippocampal activity during autobiographical memory recall in patients with depression. *Brain Behav. Immun.* **2016**, *56*, 335–342. [CrossRef]
140. Savitz, J.; Dantzer, R.; Wurfel, B.E.; Victor, T.A.; Ford, B.N.; Bodurka, J.; Bellgowan, P.S.; Teague, T.K.; Drevets, W.C. Neuroprotective kynurenine metabolite indices are abnormally reduced and positively associated with hippocampal and amygdalar volume in bipolar disorder. *Psychoneuroendocrinology* **2015**, *52*, 200–211. [CrossRef]
141. Chmiel-Perzyńska, I.; Perzyński, A.; Olajossy, B.; Gil-Kulik, P.; Kocki, J.; Urbańska, E.M. Losartan Reverses Hippocampal Increase of Kynurenic Acid in Type 1 Diabetic Rats: A Novel Procognitive Aspect of Sartan Action. *J. Diabetes Res.* **2019**, *2019*, 4957879. [CrossRef] [PubMed]
142. Sánchez Chapul, L.; Pérez de la Cruz, G.; Ramos Chávez, L.A.; Valencia León, J.F.; Torres Beltrán, J.; Estrada Camarena, E.; Carillo Mora, P.; Ramírez Ortega, D.; Baños Vázquez, J.U.; Martínez Nava, G. Characterization of redox environment and tryptophan catabolism through kynurenine pathway in military divers' and swimmers' serum samples. *Antioxidants* **2022**, *11*, 1223. [CrossRef]
143. Ostapiuk, A.; Urbanska, E.M. Kynurenic acid in neurodegenerative disorders—Unique neuroprotection or double-edged sword? *CNS Neurosci. Ther.* **2022**, *28*, 19–35. [CrossRef] [PubMed]
144. Jomova, K.; Raptova, R.; Alomar, S.Y.; Alwasel, S.H.; Nepovimova, E.; Kuca, K.; Valko, M. Reactive oxygen species, toxicity, oxidative stress, and antioxidants: Chronic diseases and aging. *Arch. Toxicol.* **2023**, *97*, 2499–2574. [CrossRef]
145. Kubota, H.; Kunisawa, K.; Niijima, M.; Hirakawa, M.; Mori, Y.; Hasegawa, M.; Fujigaki, S.; Fujigaki, H.; Yamamoto, Y.; Saito, K. Deficiency of kynurenine 3-monooxygenase exacerbates impairment of prepulse inhibition induced by phencyclidine. *Biochem. Biophys. Res. Commun.* **2022**, *629*, 142–151. [CrossRef]
146. Wurfel, B.E.; Drevets, W.C.; Bliss, S.A.; McMillin, J.R.; Suzuki, H.; Ford, B.N.; Morris, H.M.; Teague, T.K.; Dantzer, R.; Savitz, J.B. Serum kynurenic acid is reduced in affective psychosis. *Transl. Psychiatry* **2017**, *7*, e1115. [CrossRef]
147. Parrott, J.M.; Redus, L.; Santana-Coelho, D.; Morales, J.; Gao, X.; O'Connor, J.C. Neurotoxic kynurenine metabolism is increased in the dorsal hippocampus and drives distinct depressive behaviors during inflammation. *Transl. Psychiatry* **2016**, *6*, e918. [CrossRef]
148. Paul, E.R.; Schwieler, L.; Erhardt, S.; Boda, S.; Trepci, A.; Kämpe, R.; Asratian, A.; Holm, L.; Yngve, A.; Dantzer, R.; et al. Peripheral and central kynurenine pathway abnormalities in major depression. *Brain Behav. Immun.* **2022**, *101*, 136–145. [CrossRef]
149. Brown, S.J.; Huang, X.F.; Newell, K.A. The kynurenine pathway in major depression: What we know and where to next. *Neurosci. Biobehav. Rev.* **2021**, *127*, 917–927. [CrossRef]
150. Savitz, J. Role of Kynurenine Metabolism Pathway Activation in Major Depressive Disorders. *Curr. Top. Behav. Neurosci.* **2017**, *31*, 249–267. [CrossRef] [PubMed]
151. Meier, T.B.; Savitz, J. The Kynurenine Pathway in Traumatic Brain Injury: Implications for Psychiatric Outcomes. *Biol. Psychiatry* **2022**, *91*, 449–458. [CrossRef]
152. Fanet, H.; Capuron, L.; Castanon, N.; Calon, F.; Vancassel, S. Tetrahydrobioterin (BH4) pathway: From metabolism to neuropsychiatry. *Curr. Neuropharmacol.* **2021**, *19*, 591–609. [PubMed]
153. Vasquez-Vivar, J.; Shi, Z.; Tan, S. Tetrahydrobiopterin in cell function and death mechanisms. *Antioxid. Redox Signal.* **2022**, *37*, 171–183. [CrossRef]
154. Feng, Y.; Feng, Y.; Gu, L.; Liu, P.; Cao, J.; Zhang, S. The critical role of tetrahydrobiopterin (BH4) metabolism in modulating radiosensitivity: BH4/NOS axis as an angel or a devil. *Front. Oncol.* **2021**, *11*, 720632. [CrossRef] [PubMed]
155. Tanaka, M.; Battaglia, S. Dualistic Dynamics in Neuropsychiatry: From Monoaminergic Modulators to Multiscale Biomarker Maps. *Biomedicines* **2025**, *13*, 1456. [CrossRef]
156. Sun, J.; Zhang, Y.; Kong, Y.; Ye, T.; Yu, Q.; Kumaran Satyanarayanan, S.; Su, K.P.; Liu, J. Microbiota-derived metabolite Indoles induced aryl hydrocarbon receptor activation and inhibited neuroinflammation in APP/PS1 mice. *Brain Behav. Immun.* **2022**, *106*, 76–88. [CrossRef]
157. Czapski, G.A.; Strosznajder, J.B. Glutamate and GABA in Microglia-Neuron Cross-Talk in Alzheimer's Disease. *Int. J. Mol. Sci.* **2021**, *22*, 11677. [CrossRef]
158. Basilico, B.; Ferrucci, L.; Ratano, P.; Golia, M.T.; Grimaldi, A.; Rosito, M.; Ferretti, V.; Reverte, I.; Sanchini, C.; Marrone, M.C.; et al. Microglia control glutamatergic synapses in the adult mouse hippocampus. *Glia* **2022**, *70*, 173–195. [CrossRef]
159. Li, C.C.; Jiang, N.; Gan, L.; Zhao, M.J.; Chang, Q.; Liu, X.M.; Pan, R.L. Peripheral and cerebral abnormalities of the tryptophan metabolism in the depression-like rats induced by chronic unpredicted mild stress. *Neurochem. Int.* **2020**, *138*, 104771. [CrossRef]
160. Peng, Y.; Gao, P.; Shi, L.; Chen, L.; Liu, J.; Long, J. Central and Peripheral Metabolic Defects Contribute to the Pathogenesis of Alzheimer's Disease: Targeting Mitochondria for Diagnosis and Prevention. *Antioxid. Redox. Signal.* **2020**, *32*, 1188–1236. [CrossRef] [PubMed]
161. Tanaka, M. Parkinson's Disease: Bridging Gaps, Building Biomarkers, and Reimagining Clinical Translation. *Cells* **2025**, *14*, 1161. [CrossRef]

162. Correia, A.S.; Cardoso, A.; Vale, N. Oxidative Stress in Depression: The Link with the Stress Response, Neuroinflammation, Serotonin, Neurogenesis and Synaptic Plasticity. *Antioxidants* **2023**, *12*, 470. [CrossRef]
163. Ferreira, A.; Harter, A.; Afreen, S.; Kanai, K.; Batori, S.; Redei, E.E. The WMI Rat of Premature Cognitive Aging Presents Intrinsic Vulnerability to Oxidative Stress in Primary Neurons and Astrocytes Compared to Its Nearly Isogenic WLI Control. *Int. J. Mol. Sci.* **2024**, *25*, 1692. [CrossRef]
164. Sathyasaikumar, K.V.; Pérez de la Cruz, V.; Pineda, B.; Vázquez Cervantes, G.I.; Ramírez Ortega, D.; Donley, D.W.; Severson, P.L.; West, B.L.; Giorgini, F.; Fox, J.H.; et al. Cellular Localization of Kynurenine 3-Monooxygenase in the Brain: Challenging the Dogma. *Antioxidants* **2022**, *11*, 315. [CrossRef]
165. Brown, S.J.; Brown, A.M.; Purves-Tyson, T.D.; Huang, X.F.; Shannon Weickert, C.; Newell, K.A. Alterations in the kynurenine pathway and excitatory amino acid transporter-2 in depression with and without psychosis: Evidence of a potential astrocyte pathology. *J. Psychiatr. Res.* **2022**, *147*, 203–211. [CrossRef] [PubMed]
166. Wu, P.; Wang, W.; Huang, C.; Sun, L.; Wu, X.; Xu, L.; Xiao, P. A rapid and reliable targeted LC-MS/MS method for quantitative analysis of the Tryptophan-NAD metabolic network disturbances in tissues and blood of sleep deprivation mice. *Anal. Chim. Acta* **2024**, *1328*, 343125. [CrossRef]
167. Bellot, M.; Espinosa-Velasco, M.; López-Arnau, R.; Escubedo, E.; Gómez-Canela, C. Characterization of monoaminergic neurochemicals in cortex and striatum of mouse brain. *J. Pharm. Biomed. Anal.* **2022**, *217*, 114844. [CrossRef]
168. Gomez-Gomez, A.; Olesti, E.; Montero-San-Martin, B.; Soldevila, A.; Deschamps, T.; Pizarro, N.; de la Torre, R.; Pozo, O.J. Determination of up to twenty carboxylic acid containing compounds in clinically relevant matrices by o-benzylhydroxylamine derivatization and liquid chromatography-tandem mass spectrometry. *J. Pharm. Biomed. Anal.* **2022**, *208*, 114450. [CrossRef] [PubMed]
169. Patel, V.D.; Shamsi, S.A.; Miller, A.; Liu, A.; Powell, M. Simultaneous separation and detection of nine kynurenine pathway metabolites by reversed-phase liquid chromatography-mass spectrometry: Quantitation of inflammation in human cerebrospinal fluid and plasma. *Anal. Chim. Acta* **2023**, *1278*, 341659. [CrossRef] [PubMed]
170. Herb, B.R.; Glover, H.J.; Bhaduri, A.; Colantuoni, C.; Bale, T.L.; Siletti, K.; Hodge, R.; Lein, E.; Kriegstein, A.R.; Doege, C.A.; et al. Single-cell genomics reveals region-specific developmental trajectories underlying neuronal diversity in the human hypothalamus. *Sci. Adv.* **2023**, *9*, eadf6251. [CrossRef]
171. Pokhilko, A.; Handel, A.E.; Curion, F.; Volpato, V.; Whiteley, E.S.; Bøstrand, S.; Newey, S.E.; Akerman, C.J.; Webber, C.; Clark, M.B.; et al. Targeted single-cell RNA sequencing of transcription factors enhances the identification of cell types and trajectories. *Genome Res.* **2021**, *31*, 1069–1081. [CrossRef]
172. Steyn, C.; Mishi, R.; Fillmore, S.; Verhoog, M.B.; More, J.; Rohlwink, U.K.; Melvill, R.; Butler, J.; Enslin, J.M.N.; Jacobs, M.; et al. A temporal cortex cell atlas highlights gene expression dynamics during human brain maturation. *Nat. Genet.* **2024**, *56*, 2718–2730. [CrossRef]
173. Zhang, P.; Omanska, A.; Ander, B.P.; Gandal, M.J.; Stamova, B.; Schumann, C.M. Neuron-specific transcriptomic signatures indicate neuroinflammation and altered neuronal activity in ASD temporal cortex. *Proc. Natl. Acad. Sci. USA* **2023**, *120*, e2206758120. [CrossRef]
174. Swift, J.; Greenham, K.; Ecker, J.R.; Coruzzi, G.M.; Robertson McClung, C. The biology of time: Dynamic responses of cell types to developmental, circadian and environmental cues. *Plant. J.* **2022**, *109*, 764–778. [CrossRef] [PubMed]
175. Gheorghe, C.E.; Martin, J.A.; Manriquez, F.V.; Dinan, T.G.; Cryan, J.F.; Clarke, G. Focus on the essentials: Tryptophan metabolism and the microbiome-gut-brain axis. *Curr. Opin. Pharmacol.* **2019**, *48*, 137–145. [CrossRef] [PubMed]
176. Hou, Y.; Li, J.; Ying, S. Tryptophan Metabolism and Gut Microbiota: A Novel Regulatory Axis Integrating the Microbiome, Immunity, and Cancer. *Metabolites* **2023**, *13*, 1166. [CrossRef]
177. Lu, Y.; Chong, J.; Shen, S.; Chammas, J.B.; Chalifour, L.; Xia, J. TrpNet: Understanding Tryptophan Metabolism across Gut Microbiome. *Metabolites* **2021**, *12*, 10. [CrossRef]
178. Lai, Y.; Liu, C.W.; Yang, Y.; Hsiao, Y.C.; Ru, H.; Lu, K. High-coverage metabolomics uncovers microbiota-driven biochemical landscape of interorgan transport and gut-brain communication in mice. *Nat. Commun.* **2021**, *12*, 6000. [CrossRef]
179. Dong, F.; Hao, F.; Murray, I.A.; Smith, P.B.; Koo, I.; Tindall, A.M.; Kris-Etherton, P.M.; Gowda, K.; Amin, S.G.; Patterson, A.D.; et al. Intestinal microbiota-derived tryptophan metabolites are predictive of Ah receptor activity. *Gut Microbes* **2020**, *12*, 1788899. [CrossRef]
180. Kunevičius, A.; Sadauskas, M.; Raudytė, J.; Meškys, R.; Burokas, A. Unraveling the Dynamics of Host-Microbiota Indole Metabolism: An Investigation of Indole, Indolin-2-one, Isatin, and 3-Hydroxyindolin-2-one. *Molecules* **2024**, *29*, 993. [CrossRef]
181. Loh, J.S.; Mak, W.Q.; Tan, L.K.S.; Ng, C.X.; Chan, H.H.; Yeow, S.H.; Foo, J.B.; Ong, Y.S.; How, C.W.; Khaw, K.Y. Microbiota-gut-brain axis and its therapeutic applications in neurodegenerative diseases. *Signal Transduct. Target Ther.* **2024**, *9*, 37. [CrossRef] [PubMed]
182. Eslami, M.; Adampour, Z.; Fadaee Dowlat, B.; Yaghmayee, S.; Motallebi Tabaei, F.; Oksenych, V.; Naderian, R. A Novel Frontier in Gut-Brain Axis Research: The Transplantation of Fecal Microbiota in Neurodegenerative Disorders. *Biomedicines* **2025**, *13*, 915. [CrossRef]

183. Kim, C.S.; Jung, S.; Hwang, G.S.; Shin, D.M. Gut microbiota indole-3-propionic acid mediates neuroprotective effect of probiotic consumption in healthy elderly: A randomized, double-blind, placebo-controlled, multicenter trial and in vitro study. *Clin. Nutr.* **2023**, *42*, 1025–1033. [CrossRef]
184. Pocivavsek, A.; Schwarcz, R.; Erhardt, S. Neuroactive Kynurenines as Pharmacological Targets: New Experimental Tools and Exciting Therapeutic Opportunities. *Pharmacol. Rev.* **2024**, *76*, 978–1008. [CrossRef]
185. Cheng, D.; Qin, Z.S.; Zheng, Y.; Xie, J.Y.; Liang, S.S.; Zhang, J.L.; Feng, Y.B.; Zhang, Z.J. Minocycline, a classic antibiotic, exerts psychotropic effects by normalizing microglial neuroinflammation-evoked tryptophan-kynurenine pathway dysregulation in chronically stressed male mice. *Brain Behav. Immun.* **2023**, *107*, 305–318. [CrossRef] [PubMed]
186. Wei, G.Z.; Martin, K.A.; Xing, P.Y.; Agrawal, R.; Whiley, L.; Wood, T.K.; Hejndorf, S.; Ng, Y.Z.; Low, J.Z.Y.; Rossant, J.; et al. Tryptophan-metabolizing gut microbes regulate adult neurogenesis via the aryl hydrocarbon receptor. *Proc. Natl. Acad. Sci. USA* **2021**, *118*, e2021091118. [CrossRef]
187. Wang, X.; Hu, M.; Wu, W.; Lou, X.; Gao, R.; Ma, T.; Dheen, S.T.; Cheng, J.; Xiong, J.; Chen, X.; et al. Indole derivatives ameliorated the methamphetamine-induced depression and anxiety via aryl hydrocarbon receptor along "microbiota-brain" axis. *Gut Microbes* **2025**, *17*, 2470386. [CrossRef]
188. Yu, W.; Xiao, Y.; Jayaraman, A.; Yen, Y.C.; Lee, H.U.; Pettersson, S.; Je, H.S. Microbial metabolites tune amygdala neuronal hyperexcitability and anxiety-linked behaviors. *EMBO Mol. Med.* **2025**, *17*, 249–264. [CrossRef]
189. Jabarin, R.; Netser, S.; Wagner, S. Beyond the three-chamber test: Toward a multimodal and objective assessment of social behavior in rodents. *Mol. Autism* **2022**, *13*, 41. [CrossRef]
190. Wang, G.; Fan, Y.; Zhang, G.; Cai, S.; Ma, Y.; Yang, L.; Wang, Y.; Yu, H.; Qiao, S.; Zeng, X. Microbiota-derived indoles alleviate intestinal inflammation and modulate microbiome by microbial cross-feeding. *Microbiome* **2024**, *12*, 59. [CrossRef] [PubMed]
191. Heumel, S.; de Rezende Rodovalho, V.; Urien, C.; Specque, F.; Brito Rodrigues, P.; Robil, C.; Delval, L.; Sencio, V.; Descat, A.; Deruyter, L.; et al. Shotgun metagenomics and systemic targeted metabolomics highlight indole-3-propionic acid as a protective gut microbial metabolite against influenza infection. *Gut Microbes* **2024**, *16*, 2325067. [CrossRef]
192. Nemet, I.; Li, X.S.; Haghikia, A.; Li, L.; Wilcox, J.; Romano, K.A.; Buffa, J.A.; Witkowski, M.; Demuth, I.; König, M.; et al. Atlas of gut microbe-derived products from aromatic amino acids and risk of cardiovascular morbidity and mortality. *Eur. Heart J.* **2023**, *44*, 3085–3096. [CrossRef]
193. Ahmad, S.; Mohammed, M.; Mekala, L.P.; Anusha, R.; Sasikala, C.; Ramana, C.V. Stable isotope-assisted metabolite profiling reveals new insights into L-tryptophan chemotrophic metabolism of Rubrivivax benzoatilyticus. *World J. Microbiol. Biotechnol.* **2023**, *39*, 98. [CrossRef]
194. Han, S.; Van Treuren, W.; Fischer, C.R.; Merrill, B.D.; DeFelice, B.C.; Sanchez, J.M.; Higginbottom, S.K.; Guthrie, L.; Fall, L.A.; Dodd, D.; et al. A metabolomics pipeline for the mechanistic interrogation of the gut microbiome. *Nature* **2021**, *595*, 415–420. [CrossRef]
195. Pascal Andreu, V.; Augustijn, H.E.; Chen, L.; Zhernakova, A.; Fu, J.; Fischbach, M.A.; Dodd, D.; Medema, M.H. gutSMASH predicts specialized primary metabolic pathways from the human gut microbiota. *Nat. Biotechnol.* **2023**, *41*, 1416–1423. [CrossRef] [PubMed]
196. Zampieri, G.; Campanaro, S.; Angione, C.; Treu, L. Metatranscriptomics-guided genome-scale metabolic modeling of microbial communities. *Cell Rep. Methods* **2023**, *3*, 100383. [CrossRef] [PubMed]
197. Chen, Y.; Zhang, J.; Yang, Y.; Xiang, K.; Li, H.; Sun, D.; Chen, L. Kynurenine-3-monooxygenase (KMO): From its biological functions to therapeutic effect in diseases progression. *J. Cell Physiol.* **2022**, *237*, 4339–4355. [CrossRef] [PubMed]
198. Mouri, A.; Hasegawa, M.; Kunisawa, K.; Saito, K.; Nabeshima, T. [Diagnoses and new therapeutic strategy focused on physiological alteration of tryptophan metabolism]. *Nihon Yakurigaku Zasshi* **2023**, *158*, 233–237. [CrossRef]
199. Ramirez Ortega, D.; Ovalle Rodríguez, P.; Pineda, B.; González Esquivel, D.F.; Ramos Chávez, L.A.; Vázquez Cervantes, G.I.; Roldán Roldán, G.; Pérez de la Cruz, G.; Díaz Ruiz, A.; Méndez Armenta, M.; et al. Kynurenine Pathway as a New Target of Cognitive Impairment Induced by Lead Toxicity During the Lactation. *Sci. Rep.* **2020**, *10*, 3184. [CrossRef]
200. Milosavljevic, S.; Piroli, M.V.; Sandago, E.J.; Piroli, G.G.; Smith, H.H.; Beggiato, S.; Frizzell, N.; Pocivavsek, A. Parental kynurenine 3-monooxygenase genotype in mice directs sex-specific behavioral outcomes in offspring. *Biol. Sex Differ.* **2025**, *16*, 22. [CrossRef]
201. Leigh, S.J.; Uhlig, F.; Wilmes, L.; Sanchez-Diaz, P.; Gheorghe, C.E.; Goodson, M.S.; Kelley-Loughnane, N.; Hyland, N.P.; Cryan, J.F.; Clarke, G. The impact of acute and chronic stress on gastrointestinal physiology and function: A microbiota-gut-brain axis perspective. *J. Physiol.* **2023**, *601*, 4491–4538. [CrossRef]
202. Kuijer, E.J.; Steenbergen, L. The microbiota-gut-brain axis in hippocampus-dependent learning and memory: Current state and future challenges. *Neurosci. Biobehav. Rev.* **2023**, *152*, 105296. [CrossRef]
203. Heisler, J.M.; Morales, J.; Donegan, J.J.; Jett, J.D.; Redus, L.; O'Connor, J.C. The attentional set shifting task: A measure of cognitive flexibility in mice. *J. Vis. Exp.* **2015**, *96*, e51944. [CrossRef]
204. Robbins, T.W. Shifting and stopping: Fronto-striatal substrates, neurochemical modulation and clinical implications. *Philos. Trans. R Soc. Lond. B Biol. Sci.* **2007**, *362*, 917–932. [CrossRef]

205. Cernotova, D.; Stuchlik, A.; Svoboda, J. Roles of the ventral hippocampus and medial prefrontal cortex in spatial reversal learning and attentional set-shifting. *Neurobiol. Learn. Mem.* **2021**, *183*, 107477. [CrossRef]
206. Savitz, J.; Dantzer, R.; Meier, T.B.; Wurfel, B.E.; Victor, T.A.; McIntosh, S.A.; Ford, B.N.; Morris, H.M.; Bodurka, J.; Teague, T.K.; et al. Activation of the kynurenine pathway is associated with striatal volume in major depressive disorder. *Psychoneuroendocrinology* **2015**, *62*, 54–58. [CrossRef]
207. Potter, M.C.; Elmer, G.I.; Bergeron, R.; Albuquerque, E.X.; Guidetti, P.; Wu, H.Q.; Schwarcz, R. Reduction of endogenous kynurenic acid formation enhances extracellular glutamate, hippocampal plasticity, and cognitive behavior. *Neuropsychopharmacology* **2010**, *35*, 1734–1742. [CrossRef] [PubMed]
208. Huang, T.T.; Tseng, L.M.; Chen, J.L.; Chu, P.Y.; Lee, C.H.; Huang, C.T.; Wang, W.L.; Lau, K.Y.; Tseng, M.F.; Chang, Y.Y.; et al. Kynurenine 3-monooxygenase upregulates pluripotent genes through β-catenin and promotes triple-negative breast cancer progression. *EBioMedicine* **2020**, *54*, 102717. [CrossRef] [PubMed]
209. Rutsch, A.; Kantsjö, J.B.; Ronchi, F. The Gut-Brain Axis: How Microbiota and Host Inflammasome Influence Brain Physiology and Pathology. *Front. Immunol* **2020**, *11*, 604179. [CrossRef] [PubMed]
210. Interino, N.; Vitagliano, R.; D'Amico, F.; Lodi, R.; Porru, E.; Turroni, S.; Fiori, J. Microbiota-Gut-Brain Axis: Mass-Spectrometry-Based Metabolomics in the Study of Microbiome Mediators-Stress Relationship. *Biomolecules* **2025**, *15*, 243. [CrossRef]
211. Deng, Y.; Zhou, M.; Wang, J.; Yao, J.; Yu, J.; Liu, W.; Wu, L.; Wang, J.; Gao, R. Involvement of the microbiota-gut-brain axis in chronic restraint stress: Disturbances of the kynurenine metabolic pathway in both the gut and brain. *Gut Microbes* **2021**, *13*, 1863134. [CrossRef] [PubMed]
212. Góralczyk-Bińkowska, A.; Szmajda-Krygier, D.; Kozłowska, E. The Microbiota-Gut-Brain Axis in Psychiatric Disorders. *Int. J. Mol. Sci.* **2022**, *23*, 11245. [CrossRef]
213. Tanaka, M.; Vécsei, L. Revolutionizing our understanding of Parkinson's disease: Dr. Heinz Reichmann's pioneering research and future research direction. *J. Neural. Transm.* **2024**, *131*, 1367–1387. [CrossRef]
214. Verma, A.; Inslicht, S.S.; Bhargava, A. Gut-Brain Axis: Role of Microbiome, Metabolomics, Hormones, and Stress in Mental Health Disorders. *Cells* **2024**, *13*, 1436. [CrossRef]
215. Heidari, H.; Lawrence, D.A. An integrative exploration of environmental stressors on the microbiome-gut-brain axis and immune mechanisms promoting neurological disorders. *J. Toxicol. Environ. Health B Crit. Rev.* **2024**, *27*, 233–263. [CrossRef] [PubMed]
216. Skorobogatov, K.; De Picker, L.; Verkerk, R.; Coppens, V.; Leboyer, M.; Müller, N.; Morrens, M. Brain Versus Blood: A Systematic Review on the Concordance Between Peripheral and Central Kynurenine Pathway Measures in Psychiatric Disorders. *Front. Immunol.* **2021**, *12*, 716980. [CrossRef] [PubMed]

cells

Supplement to the description of section 2.3 Genotyping with TaqMan allelic discrimination assay in the Materials and Methods part of the manuscript.

All animals were genotyped in advance, ensuring verification before the subsequent experimental studies. Mice were anesthetized with 2% isoflurane, and following local analgesia with 5% lidocaine ointment, a 3 mm fragment of the tail was excised using sterile instruments under aseptic conditions. Tissue samples were stored at -80°C until further processing. For DNA extraction, 75 µl of a freshly prepared lysis buffer containing equal volumes of 25 mM NaOH and 0.2 mM disodium EDTA was added to each sample. After incubation at 95°C for 30 minutes, the suspension was cooled to 4°C and then neutralized with 75 µl of 40 mM TRIS-HCl buffer. This method was adapted from the HotSHOT protocol and consistently yields DNA suitable for reliable genotyping, as previously demonstrated by Truett et al. DNA concentration and purity were assessed using a NanoDrop spectrophotometer (MaestroGen, Taipei, Taiwan). The resulting DNA extracts were stored at -20°C until analysis.

Genotyping was performed using a fluorescence-labeled TaqMan allelic discrimination assay. The forward primer sequence was 5′–TAACAGTGCATCCCGAGTGA–3′, the reverse primer sequence was 5′–GAGGGCTCTGGCTTTGTTTT–3′, while probe 1 and probe 2 sequences were 5′–6-FAM-CAACGAGCCTGGCCAGAA-BHQ-1–3′ and 5′–HEX-TGCAACGACTGGCCAGAAAG-BHQ-1–3′, respectively (Metabion, Steinkirchen / Planegg, Germany). For each reaction, the PCR was assembled using the following reagents: PCR Master Mix (5 µl; PCRBiosystems, London, UK), forward primer (1 µl), reverse primer (1 µl), probe 1 (0.5 µl), probe 2 (0.5 µl), DNA template (1 µl), and water (1 µl). Non-template control reactions contained water instead of DNA. Reaction mixtures were aliquoted into 96-well plates. PCR amplification and allelic discrimination were performed in single-plex reactions using a CFX Opus 96 Real-Time PCR System (Bio-Rad Laboratories, Hercules, California, USA) according to the manufacturer's instructions. The amplification protocol consisted of an initial denaturation at 95°C for 10 min, followed by 40 cycles of 92°C for 15 sec and 60°C for 1 min. Fluorescence data were analyzed with CFX Maestro software.

This approach ensured that all mutant animals included in the experiments were confirmed to carry the targeted genetic modification, and wild-type mice were correctly identified as controls.

Table S1. Behavioral performance in WT and *kat2*$^{-/-}$ mice across multiple cognitive, social, and motor tests (NORT, OBAT, Y-Maze, MBT, 3CT, and Rotarod). Analyses revealed no significant inter-strain differences.

Behavioral Test Type	Number of Animals (WT/*kat2*$^{-/-}$)	Phase of the Test	Parameter of the Test	WT Mean ± SD	*kat2*$^{-/-}$ Mean ± SD	*p*-Value
NORT	12/12	Testing phase	Time spent with familiar object (s)	17.500 ± 8.635	18.556 ± 11.886	$p < 0.839$
			Time spent with novel object (s)	66.250 ± 59.461	72.444 ± 38.730	$p < 0.596$
			Discrimination index	0.455 ± 0.321	0.592 ± 0.141	$p < 0.294$
			Preference	72.760	79.604	$p < 0.293$

			index	± 16.032	± 7.061	
OBAT	12/12	Testing phase	Time spent with familiar object (s)	15.362 ± 7.437	10.729 ± 6.786	$p < 0.905$
			Time spent with novel object (s)	19.747 ± 7.820	15.796 ± 6.372	$p < 0.268$
			Discrimination index	0.136 ± 0.239	0.239 ± 0.287	$p < 0.428$
			Preference index (%)	56.802 ± 11.943	61.944 ± 14.355	$p < 0.428$
Y-maze	12/12	-	Spontaneous alternations (%)	52.833 ± 27.996	66.500 ± 18.880	$p < 0.175$
			Number of total entries	15.583 ± 11.579	18.000 ± 15.788	$p < 0.954$
MBT	10/13	-	Buried marbles	5.467 ± 4.207	6.133 ± 4.121	$p < 0.738$
			Partially buried marbles	4.267 ± 2.344	4.533 ± 2.326	$p < 0.757$
			Displaced marbles	1.733 ± 1.870	1.333 ± 1.345	$p < 0.731$
			Intact marbles	4.533 ± 3.248	4.000 ± 2.976	$p < 0.643$
3CT	12/12	Testing sociability	Time in social chamber (s)	265.717 ± 40.368	260.658 ± 54.993	$p < 0.799$
			Time in non-social chamber (s)	247.748 ± 25.751	247.988 ± 56.056	$p < 0.989$
			Time in center chamber (s)	86.536 ± 32.148	91.355 ± 28.005	$p < 0.699$
			Sniffing social cage (s)	145.955 ± 39.690	136.336 ± 37.149	$p < 0.546$
			Sniffing non-social cage (s)	114.603 ± 33.637	117.447 ± 33.452	$p < 0.837$
			Total sniffing time (s)	260.558 ± 38.784	253.783 ± 47.129	$p < 0.704$
			Social chamber entries (number)	12.667 ± 3.725	13.417 ± 4.621	$p < 0.666$
			Non-social chamber entries (number)	13.167 ± 4.174	12.833 ± 4.687	$p < 0.855$
			Total entries (number)	25.833 ± 7.673	26.250 ± 9.245	$p < 0.905$
		Testing novelty preference	Time in novel chamber (s)	263.188 ± 60.124	253.058 ± 68.641	$p < 0.704$
			Time in familiar chamber (s)	238.687 ± 55.961	237.654 ± 56.502	$p < 0.964$
			Time in center chamber (s)	98.126 ± 40.008	109.288 ± 53.470	$p < 0.568$
			Sniffing novel animal's cage (s)	129.261 ± 50.164	109.373 ± 44.085	$p < 0.313$
			Sniffing familiar animal's cage (s)	95.015 ± 51.306	92.903 ± 62.090	$p < 0.928$
			Total sniffing time (s)	224.276 ± 75.342	202.276 ± 79.270	$p < 0.493$

			Novel chamber entries (number)	9.917 ± 3.450	11.083 ± 3.679	$p < 0.431$
			Familiar chamber entries (number)	10.250 ± 3.279	11.167 ± 4.764	$p < 0.589$
			Total entries (number)	20.167 ± 6.548	22.250 ± 7.979	$p < 0.492$
Rotarod	12/12	-	Mean time spent on the rod	100.428 ± 35.017	89.708 ± 41.453	$p < 0.501$

Mean ± SD. 3CT, three-chamber test; MBT, marble burying test; NORT, novel object recognition test; OBAT, object-based attention test.

Table S2. Comparative behavioral performance of wild-type (WT) and *kat2*$^{-/-}$ mice in object recognition (NORT, OBAT) and social interaction/novelty preference (3CT). In the NORT, both WT and *kat2*$^{-/-}$ mice demonstrated a significant preference for the novel object. In the OBAT, the mutant strain exhibited greater exploration of the novel object. In the 3CT, both genotypes spent more time in the side chambers than in the center chamber during both the sociability and novelty preference phases.

Test Type	**Phase of the Test**	**WT**			***kat2*$^{-/-}$**		
NORT	Testing phase	**Sniffing familiar object (s)**	**Sniffing novel object (s)**	***p*-value**	**Sniffing familiar object (s)**	**Sniffing novel object (s)**	***p*-value**
		17.500 ± 8.635	66.250 ± 59.461	$p < 0.018$ *	18.556 ± 11.886	72.444 ± 38.730	$p < 0.001$ ***
OBAT	Testing phase	**Sniffing familiar object (s)**	**Sniffing novel object (s)**		**Sniffing familiar object (s)**	**Sniffing novel object (s)**	
		15.362 ± 7.437	19.747 ± 7.820	$p < 0.081$	10.729 ± 6.786	15.796 ± 6.372	$p < 0.039$ *
3CT	Testing sociability	**Time in social chamber (s)**	**Time in center chamber (s)**		**Time in social chamber (s)**	**Time in center chamber (s)**	
		265.717 ± 40.368	86.536 ± 32.148	$p < 0.001$ ***	260.658 ± 54.993	91.355 ± 28.005	$p < 0.001$ ***
		Time in non-social chamber (s)	**Time in center chamber (s)**		**Time in non-social chamber (s)**	**Time in center chamber (s)**	
		247.748 ± 25.751	86.536 ± 32.148	$p < 0.001$ ***	247.988 ± 56.056	91.355 ± 28.005	$p < 0.001$ ***
		Time in social chamber (s)	**Time in non-social chamber (s)**		**Time in social chamber (s)**	**Time in non-social chamber (s)**	
		265.717 ± 40.368	247.748 ± 25.751	$p < 0.319$	260.658 ± 54.993	247.988 ± 56.056	$p < 0.691$
		Sniffing social cage (s)	**Sniffing non-social cage (s)**		**Sniffing social cage (s)**	**Sniffing non-social cage (s)**	
		145.955 ± 39.690	114.603 ± 33.637	$p < 0.110$	136.336 ± 37.149	117.447 ± 33.452	$p < 0.240$
		Social chamber entries	**Non-social chamber entries**		**Social chamber entries**	**Non-social chamber entries**	

	(number)	**(number)**		**(number)**	**(number)**	
	12.667 ± 3.725	13.167 ± 4.174	$p < 0.389$	13.417 ± 4.621	12.833 ± 4.687	$p < 0.089$
	Time in novel chamber (s)	**Time in center chamber (s)**		**Time in novel chamber (s)**	**Time in center chamber (s)**	
	263.188 ± 60.124	98.126 ± 40.008	$p < 0.001$ ***	253.058 ± 68.641	109.288 ± 53.470	$p < 0.002$ **
	Time in familiar chamber (s)	**Time in center chamber (s)**		**Time in familiar chamber (s)**	**Time in center chamber (s)**	
	238.687 ± 55.961	98.126 ± 40.008	$p < 0.001$ ***	237.654 ± 56.502	109.288 ± 53.470	$p < 0.001$ ***
	Time in novel chamber (s)	**Time in familiar chamber (s)**		**Time in novel chamber (s)**	**Time in familiar chamber (s)**	
Testing novelty preference	263.188 ± 60.124	238.687 ± 55.961	$p < 0.453$	253.058 ± 68.641	237.654 ± 56.502	$p < 0.754$
	Sniffing novel animal's cage (s)	**Sniffing familiar animal's cage (s)**		**Sniffing novel animal's cage (s)**	**Sniffing familiar animal's cage (s)**	
	129.261 ± 50.164	95.015 ± 51.306	$p < 0.109$	109.373 ± 44.085	92.903 ± 62.090	$p < 0.530$
	Novel chamber entries (number)	**Familiar chamber entries (number)**		**Novel chamber entries (number)**	**Familiar chamber entries (number)**	
	9.917 ± 3.450	10.250 ± 3.279	$p < 0.474$	11.083 ± 3.679	11.167 ± 4.764	$p < 0.681$

Statistical significance was assessed for within-group contrasts (familiar vs. novel; social vs. non-social; chamber comparisons), and p-values are reported. Mean ± SD. Asterisks denote significance levels: *, $p < 0.05$, **, $p < 0.01$, ***, $p < 0.001$. 3CT, three-chamber test; *kat2*$^{-/-}$, kynurenine aminotransferase II knockout mice; NORT, novel object recognition test; OBAT, object-based attention test; WT, wild-type mice.

Table S3. Regional brain concentrations of tryptophan (Trp) and its downstream metabolites in wild-type (WT) and *kat2*$^{-/-}$ mice across striatum, cortex, hippocampus, cerebellum, and brainstem.

Metabolite	Striatum (nM)			Cortex (nM)			Hippocampus (nM)			Cerebellum (nM)			Brainstem (nM)		
	Mean ± SD		*p*-Value	Mean ± SD		*p*-Value	Mean ± SD		*p*-Value	Mean ± SD		*p*-Value	Mean ± SD		*p*-Value
	WT	*kat2*$^{-/-}$		WT	*kat2*$^{-/-}$		WT	*kat2*$^{-/-}$		WT	*kat2*$^{-/-}$		WT	*kat2*$^{-/-}$	
Trp	25511.111 ± 5688.243	21988.889 ± 1940.647	$p < 0.098$	30780.000 ± 5921.674	24090.000 ± 2431.026	$p < 0.004$ **	30433.333 ± 7230.664	25000.000 ± 2256.103	$p < 0.047$ *	29530.000 ± 6997.468	25410.000 ± 2154.814	$p < 0.092$	29210.000 ± 8273.579	24730.000 ± 2685.786	$p < 0.121$
KYN	146.444 ± 32.423	152.000 ± 45.031	$p < 0.768$	123.880 ± 27.763	121.230 ± 40.829	$p < 0.867$	126.822 ± 25.699	124.600 ± 38.033	$p < 0.886$	204.000 ± 173.369	129.880 ± 56.356	$p < 0.215$	132.130 ± 37.311	119.560 ± 41.100	$p < 0.483$
KYNA	1.757 ± 0.623	3.561 ± 2.124	$p < 0.026$ *	5.428 ± 3.032	2.963 ± 1.108	$p < 0.027$ *	2.683 ± 0.885	1.787 ± 0.647	$p < 0.026$ *	5.347 ± 0.925	4.832 ± 1.728	$p < 0.417$	4.315 ± 1.303	3.273 ± 0.974	$p < 0.058$
QAA	no data	no data	no data	0.812 ± 0.298	0.714 ± 0.127	$p < 0.349$	0.765 ± 0.216	0.807 ± 0.188	$p < 0.671$	0.416 ± 0.210	0.249 ± 0.113	$p < 0.040$ *	0.469 ± 0.323	0.171 ± 0.102	$p < 0.012$ *
AA	2.534 ± 0.771	2.431 ± 1.145	$p < 0.825$	0.320 ± 0.089	0.461 ± 0.176	$p < 0.036$ *	0.323 ± 0.136	0.213 ± 0.077	$p < 0.050$	0.400 ± 0.148	0.296 ± 0.193	$p < 0.192$	0.554 ± 0.209	0.477 ± 0.308	$p < 0.523$
3-HK	43.078 ± 7.418	78.644 ± 40.163	$p < 0.019$ *	50.230 ± 15.967	87.210 ± 42.381	$p < 0.019$ *	57.667 ± 15.585	104.467 ± 41.026	$p < 0.006$ **	77.460 ± 30.378	118.100 ± 51.104	$p < 0.044$ *	47.070 ± 12.161	83.740 ± 35.505	$p < 0.006$ **
XA	1.906 ± 1.161	1.342 ± 0.662	$p < 0.224$	7.316 ± 5.644	2.516 ± 1.631	$p < 0.019$ *	1.698 ± 0.800	0.885 ± 0.406	$p < 0.015$ *	2.402 ± 0.838	1.349 ± 0.903	$p < 0.015$ *	3.945 ± 2.037	1.324 ± 0.854	$p < 0.001$ ***
3-HAA	no data	no data	no data	6.581 ± 2.409	10.128 ± 3.732	$p < 0.021$ *	3.820 ± 1.574	3.994 ± 2.532	$p < 0.863$	no data	no data	no data	no data	no data	no data
QA	20.337 ± 11.449	32.537 ± 15.421	$p < 0.075$	35.650 ± 11.656	32.946 ± 20.266	$p < 0.719$	18.296 ± 7.872	24.667 ± 11.260	$p < 0.183$	27.057 ± 21.057	20.015 ± 12.182	$p < 0.372$	28.390 ± 16.309	30.201 ± 13.870	$p < 0.792$
PA	223.877 ± 45.544	233.296 ± 67.819	$p < 0.734$	146.707 ± 43.541	171.643 ± 46.369	$p < 0.231$	165.885 ± 81.710	146.251 ± 46.419	$p < 0.540$	213.970 ± 57.567	291.345 ± 135.202	$p < 0.152$	220.273 ± 63.283	246.122 ± 89.874	$p < 0.467$
Serotonin pathway															
5-HTP	55.689 ± 11.051	37.989 ± 20.492	$p < 0.037$ *	80.070 ± 26.609	37.490 ± 15.897	$p < 0.001$ ***	48.167 ± 15.514	42.011 ± 9.346	$p < 0.323$	11.708 ± 4.638	6.451 ± 2.871	$p < 0.007$ **	65.120 ± 19.882	65.200 ± 34.451	$p < 0.995$
5-HT	2854.444 ± 281.741	3087.778 ± 318.856	$p < 0.119$	2780.000 ± 364.722	3238.000 ± 304.478	$p < 0.007$ **	3162.222 ± 368.571	3316.667 ± 482.519	$p < 0.457$	382.600 ± 182.449	423.500 ± 218.472	$p < 0.655$	3542.000 ± 426.375	3554.000 ± 334.006	$p < 0.945$
5-HIAA	2771.111 ± 232.886	2825.556 ± 493.739	$p < 0.769$	2816.000 ± 511.147	2634.000 ± 333.340	$p < 0.358$	3984.444 ± 640.666	3618.889 ± 412.566	$p < 0.169$	952.300 ± 165.692	954.100 ± 216.632	$p < 0.984$	3998.000 ± 733.664	4076.000 ± 651.804	$p < 0.804$
Indole-pyruvate pathway															

IAA	263.000 ± 94.166	196.111 ± 59.711	$p < 0.091$	174.300 ± 46.294	160.100 ± 32.385	$p < 0.437$	179.000 ± 41.985	113.767 ± 30.709	$p < 0.002$ **	47.260 ± 26.084	62.300 ± 18.091	$p < 0.151$	126.790 ± 38.684	106.450 ± 17.163	$p < 0.146$
ICA	52.522 ± 15.104	67.000 ± 25.999	$p < 0.168$	53.590 ± 10.768	85.520 ± 23.399	$p < 0.001$ ***	58.078 ± 12.274	48.344 ± 7.459	$p < 0.059$	46.850 ± 16.225	70.060 ± 31.928	$p < 0.055$	57.430 ± 18.870	56.190 ± 21.972	$p < 0.894$
IPA	no data	no data	no data	no data	no data	no data	no data	no data	no data	14.509 ± 7.547	12.995 ± 6.244	$p < 0.631$	29.370 ± 14.081	19.479 ± 5.821	$p < 0.055$
ILA	88.656 ± 49.392	54.078 ± 17.784	$p < 0.066$	91.820 ± 24.495	74.690 ± 11.764	$p < 0.062$	122.067 ± 43.164	91.444 ± 23.630	$p < 0.080$	62.750 ± 18.591	59.500 ± 12.143	$p < 0.649$	106.910 ± 19.352	68.030 ± 12.774	$p < 0.001$ ***
INS	136.444 ± 124.642	66.144 ± 22.154	$p < 0.115$	181.320 ± 108.171	129.140 ± 54.474	$p < 0.190$	102.700 ± 93.846	48.411 ± 15.970	$p < 0.106$	114.680 ± 46.885	73.380 ± 32.000	$p < 0.034$ *	135.570 ± 66.490	86.080 ± 27.670	$p < 0.043$ *
pCS	22.863 ± 45.643	6.428 ± 3.057	$p < 0.297$	13.201 ± 15.641	6.452 ± 6.191	$p < 0.221$	11.421 ± 14.434	2.932 ± 1.870	$p < 0.099$	28.415 ± 45.171	4.284 ± 2.878	$p < 0.109$	5.987 ± 5.293	4.280 ± 4.371	$p < 0.442$
Tyrosine-dopamine pathway															
Tyr	55533.333 ± 25146.620	47200.000 ± 66.11.354	$p < 0.351$	74760.000 ± 27036.856	55710.000 ± 9047.216	$p < 0.049$ *	76522.222 ± 33835.513	57944.444 ± 10032.337	$p < 0.134$	72320.000 ± 27354.983	57480.000 ± 6273.542	$p < 0.112$	67800.000 ± 25030.026	53600.000 ± 9267.026	$p < 0.110$
L-DOPA	no data	no data	no data	130.840 ± 71.182	119.180 ± 91.862	$p < 0.755$	147.389 ± 60.587	122.400 ± 31.455	$p < 0.288$	97.580 ± 16.040	103.530 ± 54.909	$p < 0.746$	144.090 ± 139.318	118.740 ± 19.909	$p < 0.576$
3OMD	43.067 ± 11.017	48.467 ± 22.082	$p < 0.521$	42.010 ± 7.379	46.620 ± 10.305	$p < 0.265$	42.867 ± 13.189	41.678 ± 9.240	$p < 0.828$	44.220 ± 8.036	38.350 ± 6.488	$p < 0.089$	36.990 ± 11.834	35.540 ± 8.342	$p < 0.755$
DA	238805.321 ± 62124.925	226596.946 ± 85742.994	$p < 0.734$	11460.000 ± 4415.938	9733.000 ± 1997.838	$p < 0.265$	327.778 ± 184.660	301.556 ± 119.914	$p < 0.726$	126.260 ± 129.803	90.500 ± 32.822	$p < 0.409$	373.800 ± 137.416	320.700 ± 78.006	$p < 0.302$
3-MT	12277.778 ± 3429.001	15417.778 ± 7109.386	$p < 0.250$	2637.000 ± 1213.370	3510.000 ± 2184.272	$p < 0.284$	72.811 ± 27.012	76.333 ± 42.626	$p < 0.837$	48.360 ± 51.290	39.780 ± 27.131	$p < 0.646$	108.990 ± 55.943	100.420 ± 45.985	$p < 0.713$
DOPAC	9731.111 ± 2098.681	8508.889 ± 2173.571	$p < 0.243$	3231.000 ± 662.528	2604.000 ± 1298.026	$p < 0.190$	99.844 ± 31.080	119.122 ± 46.575	$p < 0.317$	118.510 ± 70.272	58.230 ± 22.991	$p < 0.019$ *	286.600 ± 83.187	269.700 ± 90.096	$p < 0.668$
HVA	8845.556 ± 1621.983	9957.778 ± 2933.235	$p < 0.334$	3219.000 ± 465.271	2994.000 ± 815.383	$p < 0.458$	563.667 ± 249.747	622.000 ± 272.426	$p < 0.642$	241.000 ± 72.399	235.410 ± 110.270	$p < 0.895$	512.900 ± 142.529	479.100 ± 199.441	$p < 0.668$
VMA	no data	no data	no data	6.815 ± 4.531	9.876 ± 7.149	$p < 0.268$	4.113 ± 2.537	7.131 ± 3.580	$p < 0.056$	23.772 ± 34.420	34.862 ± 38.254	$p < 0.504$	7.121 ± 4.828	8.801 ± 6.926	$p < 0.537$
MHPGS	31.467 ± 15.193	33.022 ± 10.663	$p < 0.805$	42.420 ± 20.320	47.070 ± 7.532	$p < 0.506$	49.722 ± 16.118	46.011 ± 9.992	$p < 0.565$	23.668 ± 27.307	17.066 ± 6.494	$p < 0.467$	21.700 ± 9.295	22.040 ± 5.288	$p < 0.921$
BIO	43.611 ± 16.815	55.533 ± 18.984	$p < 0.178$	22.410 ± 7.193	18.823 ± 10.159	$p < 0.374$	15.201 ± 11.095	14.789 ± 12.229	$p < 0.941$	15.690 ± 3.897	9.233 ± 3.056	$p < 0.001$ ***	62.380 ± 19.428	41.020 ± 9.643	$p < 0.006$ **
BH2	514.956 ± 164.623	441.378 ± 173.194	$p < 0.369$	no data	no data	no data	no data	no data	no data	117.947 ± 16.544	76.528 ± 22.014	$p < 0.001$ ***	222.409 ± 82.207	192.147 ± 59.659	$p < 0.359$

Mean ± SD. Asterisks indicate significance levels: *, $p < 0.05$; **, $p < 0.01$; ***, $p < 0.001$. 3-HAA, 3-hydroxyanthranilic acid; 3-HK, 3-hydroxykynurenine; 3-MT, 3-methoxytyramine; 5-HIAA, 5-hydroxyindoleacetic acid; 5-HT, serotonin (5-hydroxytryptamine); 5-HTP, 5-hydroxytryptophan; AA, anthranilic acid; BH2, dihydrobiopterin; BIO, biopterin; DA, dopamine; DOPAC, 3,4-dihydroxyphenylacetic acid; HVA, homovanillic acid; ICA, indole-3-carboxaldehyde; IAA, indole-3-acetic acid; ILA, indole-3-lactic acid; INS, indoxyl sulfate; IPA, indole-3-propionic acid; KYN, kynurenine; KYNA, kynurenic acid; L-DOPA, levodopa; 3OMD, 3-O-methyldopa; MHPGS, 3-methoxy-4-hydroxyphenylglycol sulfate; PA, picolinic acid; pCS, p-Cresyl sulfate; QA, quinolinic acid; QAA, quinaldic acid; Trp, tryptophan; Tyr, tyrosine; VMA, vanillylmandelic acid; XA, xanthurenic acid.

Table S4. Concentrations of indole-pyruvate and tyrosine-dopamine pathway metabolites in wild-type (WT) and *kat2*$^{-/-}$ mice in plasm and urine.

Metabolite	Plasm (nM)			Urine (nM)		
	Mean ± SD		*p*-Value	Mean ± SD		*p*-Value
	WT	*kat2*$^{-/-}$		WT	*kat2*$^{-/-}$	
Indole-pyruvate pathway						
ICA	no data	no data	no data	no data	no data	no data
IPA	no data	no data	no data	no data	no data	no data
ILA	no data	no data	no data	no data	no data	no data
pCS	853.520 ± 961.663	1097.193 ± 1196.572	$p < 0.622$	9683.873 ± 15558.939	7429.639 ± 12598.662	$p < 0.726$
Tyrosine-dopamine pathway						
Tyr	50824.432 ± 20811.617	35775.857 ±16975.863	$p < 0.093$	9411.420 ± 2214.266	8789.288 ± 1547.575	$p < 0.476$
L-DOPA	36.800 ± 15.606	35.109 ± 13.708	$p < 0.800$	no data	no data	no data
3OMD	36.340 ± 5.556	31.128 ± 5.595	$p < 0.051$	41.828 ± 21.255	40.299 ± 17.829	$p < 0.864$
DA	no data	no data	no data	671.105 ± 320.951	779.887 ± 193.877	$p < 0.371$
3-MT	2.653 ± 1.315	1.796 ± 0.655	$p < 0.082$	241.517 ± 93.336	235.939 ± 50.578	$p < 0.870$
DOPAC	no data	no data	no data	370.196 ± 224.797	301.471 ± 108.291	$p < 0.395$
HVA	no data	no data	no data	1120.520 ± 890.606	731.657 ± 173.621	$p < 0.192$
VMA	no data	no data	no data	820.064 ± 567.571	760.459 ± 124.132	$p < 0.749$
MHPGS	27.657 ± 12.496	15.392 ± 6.886	$p < 0.014$ *	8533.153 ± 3929.104	14639.178 ± 3364.617	$p < 0.002$ **
BIO	68.419 ± 23.013	82.535 ± 17.725	$p < 0.142$	231.328 ± 80.142	221.133 ± 88.018	$p < 0.790$
BH2	588.898 ± 122.352	577.701 ± 178.965	$p < 0.872$	4508.851 ± 2655.882	4488.304 ± 2298.353	$p < 0.985$

Mean ± SD. Asterisks indicate significance levels: *, $p < 0.05$; **, $p < 0.01$. 3OMD, 3-O-methyldopa; 3-MT, 3-methoxytyramine; BH2, dihydroxybiopterin; BIO, biopterin; DA, dopamine; DOPAC, 3,4-dihydroxyphenylacetic acid; HVA, homovanillic acid; ICA, indole-3-carboxaldehyde; ILA, indole-3-lactic acid; IPA, 3-indolepropionic acid; *kat2*$^{-/-}$, kynurenine aminotransferase II knockout mice; L-DOPA, levodopa; MHPGS, 3-methoxy-4-hydroxyphenylglycol sulphate; pCS, para-Cresol sulphate; SD, standard deviance; Tyr, tyrosine; VMA, vanillylmandelic acid; WT, wild-type mice.

Table S5. Ratios of kynurenine (KYN), serotonin (5-HT), indole-pyruvate and tyrosine (Tyr)-dopamine (DA) metabolites to their precursors and associated enzyme activities across brain regions in wild-type (WT) and *kat2*$^{-/-}$ mice. Activities were estimated using product-to-substrate ratios for key enzymatic steps.

Enzyme	Product/Substrate	Striatum			Cortex			Hippocampus			Cerebellum			Brainstem		
		Mean ± SD		*p*-Value	Mean ± SD		*p*-Value	Mean ± SD		*p*-Value	Mean ± SD		*p*-Value	Mean ± SD		*p*-Value
		WT	*kat2*$^{-/-}$		WT	*kat2*$^{-/-}$		WT	*kat2*$^{-/-}$		WT	*kat2*$^{-/-}$		WT	*kat2*$^{-/-}$	
TDO/IDOs	KYN/Trp	0.006 ± 0.001	0.007 ± 0.002	$p < 0.188$	0,004 ± 0,001	0.005 ± 0.001	$p < 0.212$	0.004 ± 0.001	0.005 ± 0.001	$p < 0.245$	0.006 ± 0.004	0.005 ± 0.002	$p < 0.349$	0.005 ± 0.001	0.005 ± 0.002	$p < 0.907$
KATs	KYNA/KYN	0.012 ± 0.005	0.026 ± 0.017	$p < 0.035$ *	0.045 ± 0.027	0.026 ± 0.012	$p < 0.063$	0.022 ± 0.010	0.015 ± 0.007	$p < 0.099$	0.036 ± 0.015	0.041 ± 0.019	$p < 0.487$	0.034 ± 0.011	0.032 ± 0.017	$p < 0.696$
KMO	3-HK/KYN	0.305 ± 0.075	0.510 ± 0.216	$p < 0.002$ **	0.413 ± 0.131	0.714 ± 0.262	$p < 0.001$ **	0.463 ± 0.121	0.844 ± 0.264	$p < 0.001$ ***	0.458 ± 0.139	0.957 ± 0.365	$p < 0.001$ ***	0.365 ± 0.087	0.709 ± 0.230	$p < 0.001$ ***
KYNU	AA/KYN	0.018 ± 0.006	0.018 ± 0.009	$p < 0.951$	0.003 ± 0.001	0.004 ± 0.003	$p < 0.208$	0.003 ± 0.001	0.002 ± 0.001	$p < 0.301$	0.003 ± 0.001	0.003 ± 0.002	$p < 0.913$	0.004 ± 0.002	0.005 ± 0.004	$p < 0.651$
KYNU	3-HAA/3-HK	no data	no data	no data	0.135 ± 0.040	0.125 ± 0.034	$p < 0.540$	0.072 ± 0.036	0.038 ± 0.020	$p < 0.026$ *	no data	no data	no data	no data	no data	no data
KAT III	XA/3-HK	0.045 ± 0.027	0.022 ± 0.018	$p < 0.052$	0.151 ± 0.106	0.035 ± 0.027	$p < 0.001$ **	0.031 ± 0.017	0.011 ± 0.009	$p < 0.007$ **	0.034 ± 0.015	0.014 ± 0.015	$p < 0.001$ **	0.088 ± 0.054	0.020 ± 0.017	$p < 0.001$ ***
3-HAO	QA/3-HAA	no data	no data	no data	5.910 ± 2.878	3.693 ± 2.022	$p < 0.112$	6.125 ± 4.070	10.220 ± 9.885	$p < 0.508$	no data	no data	no data	no data	no data	no data
3-HAO + ACMSD	PA/3-HAA	no data	no data	no data	23.688 ± 7.982	20.024 ± 13.316	$p < 0.082$	66.477 ± 82.924	51.852 ± 33.947	$p < 0.895$	no data	no data	no data	no data	no data	no data
TPHs	5-HTP/Trp	0.002 ± 0.000	0.002 ± 0.001	$p < 0.313$	0.003 ± 0.001	0.002 ± 0.001	$p < 0.005$ **	0.002 ± 0.000	0.002 ± 0.000	$p < 0.331$	0.000 ± 0.000	0.000 ± 0.000	$p < 0.003$ **	0.002 ± 0.001	0.003 ± 0.001	$p < 1.000$
AADC	5-HT/5-HTP	53.246 ± 12.810	110.941 ± 73.047	$p < 0.015$ *	37.833 ± 12.360	102.426 ± 43.532	$p < 0.001$ **	72.470 ± 26.437	82.603 ± 22.339	$p < 0.393$	34.597 ± 17.138	74.676 ± 41.567	$p < 0.004$ **	63.557 ± 38.662	68.894 ± 37.313	$p < 0.496$
MAOs + ALDH	5-HIAA/5-HT	0.982 ± 0.148	0.922 ± 0.180	$p < 0.453$	1.036 ± 0.280	0.822 ± 0.141	$p < 0.044$ *	1.290 ± 0.327	1.126 ± 0.285	$p < 0.274$	2.905 ± 1.239	2.539 ± 0.796	$p < 0.442$	1.150 ± 0.271	1.160 ± 0.232	$p < 0.926$
TMO (TrD, ArAT)	IAA/Trp	0.010 ± 0.003	0.009 ± 0.002	$p < 0.212$	0.006 ± 0.002	0.007 ± 0.001	$p < 0.054$	0.006 ± 0.001	0.005 ± 0.001	$p < 0.021$ *	0.002 ± 0.001	0.002 ± 0.001	$p < 0.026$ *	0.004 ± 0.001	0.004 ± 0.001	$p < 0.597$
TNA	INS/Trp	0.005 ± 0.003	0.003 ± 0.001	$p < 0.554$	0.006 ± 0.003	0.005 ± 0.002	$p < 0.624$	0.003 ± 0.002	0.002 ± 0.001	$p < 0.161$	0.004 ± 0.002	0.003 ± 0.001	$p < 0.170$	0.005 ± 0.003	0.003 ± 0.001	$p < 0.147$
TH	L-DOPA/Tyr	no data	no data	no data	0.002 ± 0.001	0.002 ± 0.002	$p < 0.968$	0.002 ± 0.001	0.002 ± 0.001	$p < 0.555$	0.001 ± 0.000	0.002 ± 0.001	$p < 0.126$	0.002 ± 0.001	0.002 ± 0.001	$p < 0.132$

AADC	DA/L-DOPA	no data	no data	no data	110.049 ± 70.406	132.849 ± 107.738	$p < 0.880$	2.583 ± 1.810	2.556 ± 1.048	$p < 0.969$	1.370 ± 1.513	1.101 ± 0.682	$p < 0.821$	3.589 ± 1.777	2.775 ± 0.933	$p < 0.216$
MAOs	DOPAC/DA	0.044 ± 0.020	0.043 ± 0.020	$p < 0.452$	0.320 ± 0.142	0.274 ± 0.140	$p < 0.290$	0.376 ± 0.178	0.427 ± 0.156	$p < 0.532$	1.324 ± 0.697	0.669 ± 0.210	$p < 0.023$ *	0.810 ± 0.238	0.909 ± 0.393	$p < 0.500$
COMT	HVA/DOPAC	0.944 ± 0.256	1.279 ± 0.584	$p < 0.143$	1.045 ± 0.290	1.444 ± 0.799	$p < 0.165$	6.137 ± 3.971	5.665 ± 2.558	$p < 0.895$	2.271 ± 0.755	4.685 ± 2.395	$p < 0.012$ *	1.933 ± 0.850	2.145 ± 1.626	$p < 0.791$
MAOs + COMT	HVA/DA	0.039 ± 0.010	0.046 ± 0.009	$p < 0.141$	0.309 ± 0.094	0.314 ± 0.094	$p < 0.892$	1.821 ± 0.365	2.140 ± 0.577	$p < 0.181$	2.849 ± 1.324	2.763 ± 1.020	$p < 0.872$	1.453 ± 0.413	1.469 ± 0.320	$p < 0.922$

Mean ± SD. Asterisks indicate significance levels: *, $p < 0.05$; **, $p < 0.01$; ***, $p < 0.001$. 3-HAA, 3-hydroxyanthranilic acid; 3-HAO, 3-hydroxyanthranilate oxidase; 3-HK, 3-hydroxykynurenine; AA, anthranilic acid; AADC, aromatic L-amino acid decarboxylase; ACMSD, aminocarboxymuconate-semialdehyde decarboxylase; ALDH, aldehyde dehydrogenase; COMT, catechol-O-methyltransferase; DA, dopamine; DOPAC, 3,4-dihydroxyphenylacetic acid; HVA, homovanillic acid; IAA, indole-3-acetic acid; IDOs, indoleamine 2,3-dioxygenases; INS, indoxyl sulfate; *kat2*$^{-/-}$, kynurenine aminotransferase II knockout mice; KATs, kynurenine aminotransferases; KMO, kynurenine 3-monooxygenase; KYNA, kynurenic acid; KYNU, kynureninase; L-DOPA, dihydroxyphenylalanine/levodopa; MAOs, monoamine oxidases; PA, picolinic acid; QA, quinolinic acid; QAA, quinolinic acid analog; TDO, tryptophan 2,3-dioxygenase; TH, tyrosine hydroxylase; TMO, tryptophan monooxygenase; TNA, tryptophan N-acetyltransferase; TrD, tryptophan deaminase; Trp, tryptophan; Tyr, tyrosine; 5-HIAA, 5-hydroxyindoleacetic acid; 5-HT, serotonin (5-hydroxytryptamine); 5-HTP, 5-hydroxytryptophan; WT, wild-type mice; XA, xanthurenic acid.

Table S6. Ratios of oxidant/antioxidant and N-methyl-D-aspartate (NMDA) agonist/antagonist metabolites across brain regions in wild-type (WT) and *kat2*$^{-/-}$ mice. Regional indices of oxidative stress and excitotoxicity in WT and *kat2*$^{-/-}$ mice.

Oxidant/antioxidant metabolites	**Striatum**			**Cortex**			**Hippocampus**			**Cerebellum**			**Brainstem**		
	Mean ± SD		***p*-Value**	**Mean ± SD**		***p*-Value**	**Mean ± SD**		***p*-Value**	**Mean ± SD**		***p*-Value**	**Mean ± SD**		***p*-Value**
	WT	***kat2*$^{-/-}$**		**WT**	***kat2*$^{-/-}$**		**WT**	***kat2*$^{-/-}$**		**WT**	***kat2*$^{-/-}$**		**WT**	***kat2*$^{-/-}$**	
3-HK/(KYNA+AA+XA)	6.951 ± 2.904	10.723 ± 10.215	$p < 0.627$	4.700 ± 2.112	17.670 ± 13.315	$p < 0.001$ **	13.509 ± 6.992	37.148 ± 15.859	$p < 0.002$ **	9.667 ± 3.839	20.311 ± 9.275	$p < 0.006$ **	5.740 ± 1.892	18.705 ± 9.300	$p < 0.002$ **
NMDA agonist/antagonist metabolites	**Striatum**			**Cortex**			**Hippocampus**			**Cerebellum**			**Brainstem**		
	Mean ± SD		***p*-value**	**Mean ± SD**		***p*-value**	**Mean ± SD**		***p*-value**	**Mean ± SD**		***p*-value**	**Mean ± SD**		***p*-value**
	WT	***kat2*$^{-/-}$**		**WT**	***kat2*$^{-/-}$**		**WT**	***kat2*$^{-/-}$**		**WT**	***kat2*$^{-/-}$**		**WT**	***kat2*$^{-/-}$**	
QA/KYNA	11.575 ± 18.379	9.138 ± 7.260	$p < 0.923$	9.263 ± 7.574	14.235 ± 14.254	$p < 0.597$	7.957 ± 5.478	16.120 ± 9.907	$p < 0.046$ *	5.306 ± 4.601	4.998 ± 4.789	$p < 0.880$	7.724 ± 7.414	10.224 ± 5.544	$p < 0.096$

Mean ± SD. Asterisks indicate significance levels: *, $p < 0.05$; **, $p < 0.01$; ***, $p < 0.001$. 3-HK, 3-hydroxykynurenine; AA, anthranilic acid; *kat2*$^{-/-}$, kynurenine aminotransferase II knockout mice; KYNA, kynurenic acid; NMDA. N-methyl-D-aspartate; QA, quinolinic acid; WT, wild-type mice; XA, xanthurenic acid.